MULTIPLE TIME SCALE DYNAMICS WITH TWO FAST VARIABLES AND ONE SLOW VARIABLE

A Dissertation

Presented to the Faculty of the Graduate School

of Cornell University

in Partial Fulfillment of the Requirements for the Degree of

Doctor of Philosophy

by

Christian Kuehn

May 2010

MULTIPLE TIME SCALE DYNAMICS WITH TWO FAST VARIABLES AND ONE SLOW VARIABLE

Christian Kuehn, Ph.D.

Cornell University 2010

This thesis considers dynamical systems that have multiple time scales. The focus lies on systems with two fast variables and one slow variable. The two-parameter bifurcation structure of the FitzHugh-Nagumo (FHN) equation is analyzed in detail. A singular bifurcation diagram is constructed and invariant manifolds of the problem are computed. A boundary-value approach to compute slow manifolds of saddle-type is developed. Interactions of classical invariant manifolds and slow manifolds explain the exponentially small turning of a homoclinic bifurcation curve in parameter space. Mixed-mode oscillations and maximal canards are detected in the FHN equation. An asymptotic formula to find maximal canards is proved which is based on the first Lyapunov coefficient at a singular Hopf bifurcation.

BIOGRAPHICAL SKETCH

Christian Kuehn was born in Bremen, Germany. He completed the Abitur at the Cato Bontjes van Beek-Gymnasium Achim in 2001. After a year of community service he began undergraduate studies at Jacobs University Bremen. He obtained a Bachelor of Science in Mathematics in 2005. The following year he finished the Certificate of Advanced Study in Cambridge and then joined the Center for Applied Mathematics at Cornell University in 2006.

To my family.

ACKNOWLEDGEMENTS

First and foremost, I would like to thank John Guckenheimer, who has been a fantastic thesis adviser. This view does not only apply to my graduate student years but is shared by all of John's doctoral students. Hence I decided to compile parts of different acknowledgments of theses that John supervised. The quotes provide a collage that describes the many aspects that make John a special adviser, teacher and colleague.

"John has been a very patient teacher over these many years." [B.D. Bond, 1993]

"I would like to thank my adviser John Guckenheimer for all this guidance and support which has been invaluable to me.", [P.A. Worfolk, 1993]

"John was always able to provide me with a 'big picture', yet he allowed me the freedom to pursue my own ideas.", [F.J. Wicklin, 1993]

"I would like to thank my adviser John Guckenheimer for his excellent coaching and support, as well as being eager to listen to all of my ideas - both good and bad.", [S. Malo, 1994]

"To begin, I would like to thank my adviser, Dr. John Guckenheimer, a man of many hats who nonetheless found sufficient time to answer my questions and gently prod my thinking along productive paths.", [A.R. Willms, 1997]

"He has been a tremendous source of inspiration and guidance, and has provided invaluable insights into the mathematics underpinning numerical methods for simulat-

ing mechanical systems.", [E.T. Phipps, 2003]

"First and foremost, I would like to thank my adviser, Professor John Guckenheimer, for his support and encouragement, and for setting an inspirational example as a mathematician and scientist.", [R.J. Casey, 2004]

"His door was ever open and conversations with him were always illuminating, but most of all highly motivating. His company would invariably restore the faith I would sometimes lose.", [R. Haiduc, 2005]

"He has encouraged independence and patiently indulged my tangential interests. It has been a thoroughly edifying apprenticeship.", [W.E. Sherwood, 2008]

I would also like to thank Richard Rand and John Smillie for serving on my committee and for teaching graduate courses that I have followed with great interest. John Guckenheimer, Tim Healey and Yulij Ilyashenko have taught excellent dynamical systems courses as well from which I learned a lot. The "Cornell Dynamics School" has not only shaped how I view the subject today but also provided tremendous inspiration for my work as a graduate student.

I also had many interesting discussions with fellow multiple-time-scales-graduate-students at Cornell. Chris Scheper, Mike Cortez and Phillip Meerkamp have tolerated my unnecessarily exuberant approach in discussions more than once. A similar remark applies to Dolores Pendell and Selene Cammer who have taken care of any administrative hurdles that the Cornell bureaucracy tried to put in my way. Overall, the support of CAM was great.

I would also like to acknowledge several professors at Jacobs University Bremen that have influenced my mathematical undergraduate education before coming to Cornell. Without them I would not have found the interest or acquired the knowledge to pursue a PhD [in alphabetical order]: Nikolai Krylov, Marcel Oliver, Peter Oswald, Götz Pfander, Dierk Schleicher, Des Sheiham, Michael Stoll and Rein van der Hout. Their thoughtful approach, combined with the broad mathematical view provided in my year in Cambridge, have provided me with tremendous foundations that I really came to appreciate during my time as a PhD student.

TABLE OF CONTENTS

LIST OF TABLES

LIST OF FIGURES

CHAPTER 1

INTRODUCTION

1.1 Fast-Slow systems

The subject of this dissertation is the theory of multiple time scale dynamical systems. If only two time scales are present the term fast-slow system is commonly used. Note that several viewpoints have influenced the development of the subject starting with asymptotic analysis [93, 37] using techniques like matched asymptotic expansions [75, 89]. A geometric theory focusing on invariant manifolds was developed [42, 71, 73, 1, 106] which is now commonly known as Fenichel theory due to Fenichel's seminal work [42]. There was also significant influence by a group using nonstandard analysis [29, 28, 8, 6, 9, 7].

1.1.1 Basic Terminology

We shall focus on the geometric viewpoint which played a significant role in understanding bifurcation phenomena. The term "Geometric Singular Perturbation Theory" (GSPT) is used to encompass Fenichel theory and further geometric methods developed over the last three decades in the context of multiple time scale problems. The general formulation of a fast-slow system of ordinary differential equations (ODEs) is:

$$\begin{aligned} \epsilon \dot{x} &= \epsilon \frac{dx}{d\tau} = f(x, y, \lambda, \epsilon) \\ \dot{y} &= \frac{dy}{d\tau} = g(x, y, \lambda, \epsilon) \end{aligned} \tag{1.1}$$

where $(x, y) \in \mathbb{R}^m \times \mathbb{R}^n$ are variables, $\lambda \in \mathbb{R}^p$ are system parameters and ϵ is a small parameter $0 < \epsilon \ll 1$ representing the ratio of time scales. The functions $f : \mathbb{R}^m \times \mathbb{R}^n \times \mathbb{R}^p \times \mathbb{R} \to \mathbb{R}^m$ and $g : \mathbb{R}^m \times \mathbb{R}^n \times \mathbb{R}^p \times \mathbb{R} \to \mathbb{R}^n$ are usually assumed to be sufficiently smooth. The variables x are fast and the variables y are slow and we can change in (1.1) from the slow time scale τ to the fast time scale $t = \tau/\epsilon$ which yields:

$$\begin{aligned} x' &= \frac{dx}{dt} = f(x, y, \lambda, \epsilon) \\ y' &= \frac{dy}{dt} = \epsilon g(x, y, \lambda, \epsilon) \end{aligned} \tag{1.2}$$

To illustrate the definitions and concepts to be introduced we use the classical example of Van der Pol's equation [23, 24, 25] with constant forcing $\lambda \in \mathbb{R}$:

$$\begin{aligned} \epsilon \dot{x} &= y - \frac{x^3}{3} + x \\ \dot{y} &= \lambda - x \end{aligned} \tag{1.3}$$

Although (1.3) is one of simplest fast-slow systems with a one fast and one slow variable it exhibits complicated dynamics that can be analyzed using the fast-slow structure. The first major idea to analyze (1.1)-(1.2) is to consider the singular limit as $\epsilon \to 0$. From equation (1.2) we obtain

$$\begin{aligned} x' &= f(x, y, \lambda, 0) \\ y' &= 0 \end{aligned} \tag{1.4}$$

which is system of ODEs parametrized by the slow variables y. We call (1.4) the fast subsystem or layer equations. Considering the singular limit for (1.1) we get:

$$\begin{aligned} 0 &= f(x, y, \lambda, 0) \\ \dot{y} &= g(x, y, \lambda, 0) \end{aligned} \tag{1.5}$$

System (1.5) is a differential-algebraic equation (DAE) called slow subsystem or reduced system. The flow of the slow subsystem will be called slow flow and analogously we also have the fast flow for the fast subsystem. One goal of GSPT is to use the fast and slow subsystems to understand the dynamics of the full system (1.1)-(1.2) for $\epsilon > 0$.

1.1.2 Fenichel Theory

The algebraic constraint of (1.5) defines the critical manifold:

$$C = \{(x, y) \in \mathbb{R}^m \times \mathbb{R}^n | f(x, y, \lambda, 0) = 0\}$$

Note that it is possible that C is not an actual manifold [84] but we shall not consider this case here. Points in C are equilibrium points for the fast subsystem (1.4). In Van der Pol's equation (1.3) the critical manifold is a cubic curve

$$C^{\mathrm{VdP}} = \{(x, y) \in \mathbb{R}^2 | y = x^3/3 - x =: c(x)\} \tag{1.6}$$

A subset $S \subset C$ is called normally hyperbolic if the $m \times m$ matrix $(D_x f)(p)$ of first partial derivatives with respect to the fast variables has eigenvalues with nonzero real parts for all $p \in S$; this condition is equivalent to requiring that points $p \in S$ are hyperbolic equilibria of the fast subsystem (1.4). We call a normally hyperbolic subset S attracting if all eigenvalues of $(D_x f)(p)$ have negative real parts for $p \in S$; similarly S is called repelling if all eigenvalues have positive real parts. If S is normally hyperbolic and neither attracting nor repelling we say it is of saddle-type.

Remark: Normal hyperbolicity can be developed in the more general context [39, 40, 41, 64] of normally hyperbolic invariant manifolds M. Intuitively

the general definition of normal hyperbolicity of M requires that the flow in the tangential directions to M ("slow") is dominated by the flow transverse to it ("fast").

In Van der Pol's equation the critical manifold C^{VdP} is normally hyperbolic away from the local maximum and minimum of the cubic. These two special points are defined by $c'(x) = 0$ and given by $p_\pm = (\pm 1, \mp 2/3)$. At $p_\pm$ normal hyperbolicity fails and we call these points fold points. Note that the fold points are saddle-node bifurcation (i.e. fold bifurcation) points of the fast subsystem (1.4). The fold points naturally decompose the critical manifold

$$C^{\mathrm{VdP}} = S^{a,-} \cup \{p_-\} \cup S^r \cup \{p_+\} \cup S^{a,+}$$

where the three branches of C^{VdP} are

$$S^{a,-} = C \cap \{x < -1\}, \quad S^r = C \cap \{-1 < x < 1\}, \quad S^{a,+} = C \cap \{x > 1\}$$

Observe that $C^{a,\pm}$ are attracting whereas S^r is repelling since

$$\frac{\partial}{\partial x} f(x, y, \lambda, 0) = 1 - x^2 = \begin{cases} < 0 & \text{for } |x| > 1 \\ > 0 & \text{for } |x| < 1 \end{cases}$$

The general definition of a fold point p_* is to require that the critical manifold C is locally parabolic i.e. $f(p_*, \lambda, 0) = 0$, $(D_x f)(p_*, \lambda, 0)$ has rank $m - 1$ with left and right null vectors w and v, $w \cdot [(D_{xx} f)(p)(v, v)] \neq 0$ and $w \cdot [(D_y f)(p)] \neq 0$. For Van der Pol's equation this just means that $f(p_*, \lambda, 0) = 0$, $f_x(p_*, \lambda, 0) = 0$, $f_{xx}(p_*, \lambda, 0) \neq 0$ and $f_y(p_*, \lambda, 0) \neq 0$. In principle, the critical manifold can have more degenerate non-normally hyperbolic points which we shall not consider here.

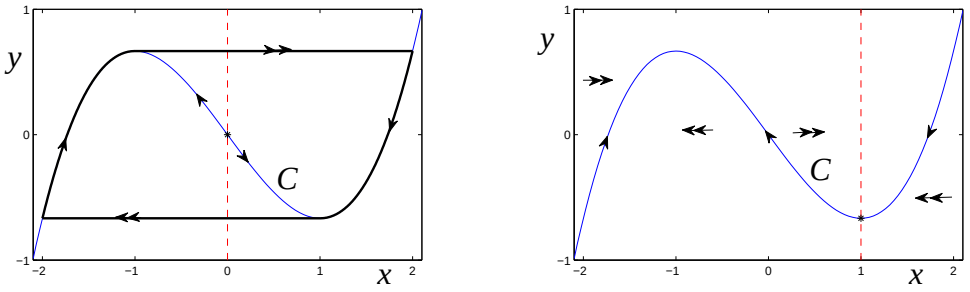

(a) $\lambda = 0$: Singular solution in black.

(b) $\lambda = 1$: Equilibrium point at p_+.

Figure 1.1: The critical manifold (blue) $C = C^{\mathrm{VdP}}$ for Van der Pol's equation (1.3) together with the y-nullcline (dashed red) is shown. Double arrows indicate the fast flow and single arrows the slow flow.

Away from fold points the implicit function theorem applied to $f(x, y, \lambda, 0) = 0$ locally provides a function $h(y) = x$ so that C can be expressed as a graph. Hence the slow subsystem (1.5) can be more succinctly expressed as:

$$\dot{y} = g(h(y), y, \lambda, 0) \tag{1.7}$$

We shall also refer to the flow induced by (1.5),(1.7) as the slow flow. In Van der Pol's equation we could solve the cubic equation $y = c(x)$ for x on $S^{a,-}$, S^r and $S^{a,+}$ to obtain (1.7). It is more convenient in this case to use an alternative procedure to derive the slow flow. We implicitly differentiate $f(x, y, \lambda, 0) = y - c(x) = 0$ with respect to τ, then

$$\dot{y} = \dot{x}x^2 - \dot{x} = \dot{x}(x^2 - 1)$$

Combining this result with the equation for $\dot{y}$ we get:

$$(x^2 - 1)\dot{x} = \lambda - x \qquad \text{or} \qquad \dot{x} = \frac{\lambda - x}{x^2 - 1} \tag{1.8}$$

Note that the slow flow is not well-defined for $x = \pm 1$ as long as $\lambda \neq \pm 1$. In particular, existence and uniqueness theory for ODEs does not apply in this scenario. The same idea for deriving the slow flow also works for a general

fast-slow system and yields:

$$\dot{x} = (D_x f)^{-1}(D_y f)g$$

where all mappings are evaluated for $(x, c(x), \lambda, 0)$ and $c : \mathbb{R}^m \to \mathbb{R}^n$ parametrizes C. To relate the dynamics of the slow flow to the dynamics of the full system for $\epsilon > 0$ the next theorem is of fundamental importance.

Theorem 1.1.1 (Fenichel's Theorem, Part 1)**.** *Assume that f, g are sufficiently smooth. Suppose $S = S_0$ is a compact normally hyperbolic submanifold of the critical manifold C. Then for $\epsilon > 0$ sufficiently small the following holds:*

(F1) There exists a locally invariant manifold S_ϵ diffeomorphic to S_0. Local invariance means that S_ϵ can have boundaries through which trajectories enter or leave.

(F2) S_ϵ has a distance $O(\epsilon)$ from S_0.

(F3) The flow on S_ϵ converges to the slow flow as $\epsilon \to 0$.

(F4) Given $r \in \mathbb{N} \cup \{0\}$ there exists $\epsilon_0 > 0$ such that that S_ϵ is C^r-smooth for all $\epsilon \in (0, \epsilon_0]$.

(F5) S_ϵ is normally hyperbolic and has the same stability properties with respect to the fast variables as S_0 (attracting, repelling or saddle-type).

(F6) For fixed $\epsilon > 0$, S_ϵ is usually not unique but all manifolds satisfying (F1)-(F5) lie at a Hausdorff distance $O(e^{-K/\epsilon})$ from each other for some $K > 0$, $K = O(1)$.

We call a manifold S_ϵ a slow manifold. Note that all asymptotic notation refers to $\epsilon \to 0$.

Remark: We will often apply the convention that objects in the singular limit have sub- or superscript 0 whereas the associated perturbed objects have sub-

or superscript ϵ.

Note that slow manifolds are defined by asymptotic conditions like (F2). Furthermore, their non-uniqueness (F6) and finite smoothness (F4) are not surprising as the proof constructs them as center-type manifolds intersecting the attracting and repelling manifolds of the fast subsystem; cf. [16, 42, 103]. In addition to critical and slow manifolds we can also consider their associated attracting and repelling manifolds. If S_0 is normally hyperbolic we view points on it as hyperbolic equilibria of the fast subsystem and define

$$W^s(S_0) = \bigcup_{p \in S_0} W^s(p), \qquad W^u(S_0) = \bigcup_{p \in S_0} W^u(p)$$

Sometimes we refer to $W^s(S_0)$ and $W^u(S_0)$ as stable and unstable manifolds to the critical manifold.

Theorem 1.1.2 (Fenichel's Theorem, Part 2)**.** *For $\epsilon > 0$ sufficiently small there exist manifolds $W^s(S_\epsilon)$ and $W^u(S_\epsilon)$. The conclusions (F1)-(F6) hold for $W^s(S_\epsilon)$ and $W^u(S_\epsilon)$ if we replace S_ϵ and S_0 by $W^s(S_\epsilon)$ and $W^s(S_0)$ (or similarly by $W^u(S_\epsilon)$ and $W^u(S_0)$).*

In addition to Fenichel's Theorem we can also find coordinate changes that simplify a fast-slow system considerably near a critical manifold.

Theorem 1.1.3. *(Fenichel Normal Form, [42, 72]) Suppose the origin $0 \in C$ is a normally hyperbolic point with m_s stable and m_u unstable fast directions. Then there exists a smooth invertible coordinate change $(x, y) \mapsto (a, b, v) \in \mathbb{R}^{m_s+m_u+n}$ so that a fast-slow system* (6.2) *can be written as:*

$$\begin{aligned} a' &= \Lambda(a, b, v, \epsilon)a \\ b' &= \Gamma(a, b, v, \epsilon)b \\ v' &= \epsilon(m(v, \epsilon) + H(a, b, v, \epsilon)ab) \end{aligned} \tag{1.9}$$

where Λ, Γ *are matrix-valued functions and* H *is bilinear and given in coordinates by*

$$H_i(a, b, v, \epsilon)ab = \sum_{r=1}^{m_s} \sum_{s=1}^{m_u} H_{irs} a_r b_s \tag{1.10}$$

1.1.3 Canards

We shall now consider different types of trajectories in Van der Pol's equation. Consider first the case $\lambda = 0$ ("unforced Van der Pol equation"). For $\epsilon = 0$ the fast and slow flows are indicated in Figure 1.1. A singular orbit can be constructed by concatenating fast and slow flow segments as shown in Figure 1.1(a); note that singular orbits are also called candidates. The singular orbit follows the slow flow on C^{VdP}, then reaches a fold point, "jumps" and follows the fast subsystem until it reaches another branch of the critical manifold. The same mechanism returns the orbit to the initial branch of the critical manifold. It can be shown [93, 86] that the singular orbit perturbs for $\epsilon > 0$ and we have the classical scenario of relaxation oscillations. Note that $(x, y) = (0, 0)$ is an unstable focus for $\lambda = 0$. A direct linear stability analysis shows that for $\lambda > 1$ the unique equilibrium point $(x, y) = (\lambda, \lambda^3/3 - \lambda) =: q$ is a stable focus and undergoes supercritical Hopf bifurcation at $\lambda_H = 1$. The precise analysis of the orbit structure of Van der Pol's equation between the stable focus region and relaxation oscillations was one of the first major steps in the theory of fast-slow systems.

Figure 1.2(a) shows numerical continuation results for $\epsilon = 0.05$. The key feature is that the amplitude of the periodic orbits generated in the Hopf bifurcation grows rapidly in an exponentially small interval in parameter space. This process is called canard explosion and we refer to the Hopf bifurcation as

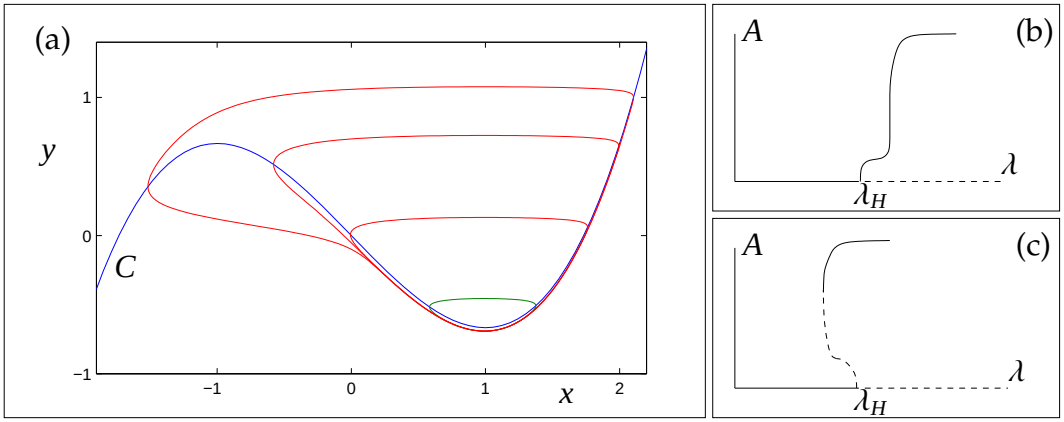

Figure 1.2: (a) Some periodic orbits obtained from numerical continuation of (1.3) for $\epsilon = 0.05$. The green orbit is a typical small limit cycle near the Hopf bifurcation whereas all the red orbits occur in a very small parameter space interval at $\lambda \approx 0.993491$. General sketch of bifurcation diagrams for supercritical (b) and subcritical (c) singular Hopf bifurcation at $\lambda = \lambda_H$. Here A denotes the amplitude if the limit cycle. In Van der Pol's equation (b) applies.

singular Hopf bifurcation. In particular, the red periodic trajectories shown in Figure 1.2(a) follow the repelling slow manifold S^r_ϵ for a long time.

A trajectory of a general fast-slow system is called a canard if it follows a repelling slow manifold for a time that is $O(1)$ on the slow time scale. A trajectory is called a maximal canard if it lies in the intersection of an attracting and a repelling slow manifold; note that this definition requires that we extend slow manifolds obtained by Fenichel's Theorem under the flow of the differential equation. One often calls a fold point $p_* \in C$ a folded singularity if it is an equilibrium point of the desingularized slow flow; see Figure 1.1(b). At a folded singularity the slow flow is well defined and trajectories can continue from an attracting part of the critical manifold to a repelling part or vice versa. The problem with the previous definition is that folded singularities do not persist

for $\epsilon > 0$. Therefore they have no immediate meaning in the full system. Hence one has to be very careful not to confuse folded singularities with equilibrium points of the full system.

The canard explosion in Van der Pol's equation occurs $O(e^{-K/\epsilon})$-close in parameter space to the point where the manifolds $S_\epsilon^{a,+}$ and S_ϵ^r intersect in a maximal canard. A folded singularity occurs for $\lambda = 1$ at $p_+ = (1, -2)$ when the unique equilibrium coincides with the fold point; see Figure 1.1(b). Note that $\lambda = 1 = \lambda_H$ is also the singular Hopf bifurcation point of the system but that this situation is not generic. In fact, in a generic situation the singular Hopf bifurcation point is displaced by $O(\epsilon)$ in parameter space from the folded singularity which can be seen by modifying the slow equation to

$$y' = \epsilon(\lambda - x + ay)$$

for $a \neq 0$. The ideas of folded singularities and singular Hopf bifurcation can be extended to general fast-slow systems and we now summarize some of the key components of each concept starting with singular Hopf bifurcation:

- A singular Hopf bifurcation occurs at $\lambda = \lambda_H(\epsilon)$ which is $O(\epsilon)$-close in parameter space to a folded singularity at $\lambda = \lambda_*$.
- The periodic orbits generated in the bifurcation undergo a canard explosion. A maximal canard orbit exists for $\lambda = \lambda_c(\epsilon)$ which is $O(\epsilon)$-close in parameter space to the folded singularity.
- In the singular limit we have $\lambda_H(0) = \lambda_* = \lambda_c(0)$.
- The system has a pair of singular eigenvalues [13] for the linearized system on the 2-dimensional center manifold [88, 54] at the Hopf bifurcation

point:

$$\mu(\lambda;\epsilon) = \sigma(\lambda;\epsilon) + i\Gamma(\lambda;\epsilon)$$

so that $\sigma(\lambda_H;\epsilon) = 0$, $\sigma_\lambda(\lambda_H;\epsilon) \neq 0$ for any $\epsilon > 0$ sufficiently small and

$$\lim_{\epsilon\to 0}\Gamma(\lambda_H;\epsilon) = \infty \quad \text{on the slow time scale } \tau$$
$$\text{or} \qquad \lim_{\epsilon\to 0}\Gamma(\lambda_H;\epsilon) = 0 \quad \text{on the fast time scale } t$$

A detailed dynamical analysis of canard explosion and the associated singular Hopf bifurcation using geometric or asymptotic methods exists for planar fast-slow system [83, 86, 4, 5, 37, 36]. For this case the bifurcation diagrams for super- and subcritical Hopf bifurcation are shown in Figure 1.2(b)-(c). A summary of some of the results is given in the next theorem.

Theorem 1.1.4 (Canard Explosion in $\mathbb{R}^2$)**.** *Suppose a planar fast-slow system has a generic fold point $p_* = (x_p, y_p) \in C$:*

$$f(p_*,\lambda,0) = 0, \quad f_x(p_*,\lambda,0) = 0, \quad f_{xx}(p_*,\lambda,0) \neq 0, \quad f_y(p_*,\lambda,0) \neq 0 \tag{1.11}$$

and that the fold point is non-degenerate with $g(p_*,\lambda,0) \neq 0$ for $\lambda \neq 0$. Assume the critical manifold is locally attracting for $x < x_p$ and repelling for $x > x_p$ and there exists a folded singularity for $\lambda = 0$ at p_*:

$$g(p_*,0,0) = 0, \quad g_x(p_*,0,0) \neq 0, \quad g_\lambda(p_*,0,0) \neq 0 \tag{1.12}$$

Assuming without loss of generality that $g_x(p_*,0,0) > 0$ (reversing time if necessary) we conclude that singular Hopf bifurcation and canard explosion occurs. The Hopf bifurcation occurs at:

$$\lambda_H = H_1\epsilon + O(\epsilon^{3/2}) \tag{1.13}$$

The system has a maximal canard at λ_c for

$$\lambda_c = (H_1 + K_1)\epsilon + O(\epsilon^{3/2}) \tag{1.14}$$

The Hopf bifurcation is supercritical for $K_1 > 0$ and subcritical for $K_1 < 0$. The coefficients H_1 and K_1 can be calculated explicitly from normal form transformations [86] or by considering the first Lyapunov coefficient of the Hopf bifurcation [87].

Remark: The expansions in (1.13)-(1.14) are in terms of the asymptotic sequence $\{\epsilon^{j/2}\}_{j=0}^{\infty}$.

1.2 Overview

1.2.1 Structure

Chapters 1-2 are introductory and provide the necessary background from the theory of fast-slow systems with a particular focus on the Exchange Lemma. The research contribution of this thesis consists of Chapters 3-6. Each of these chapters consists of a journal publication. The chronological ordering of these chapters has been maintained i.e. Chapter 3 was completed and submitted first and Chapter 6 was finished and submitted last. We hope that this also shows how the research process evolved for this PhD thesis. The papers in Chapters 3-6 have been kept in their original form with a few omissions in Chapter 4. For each paper we have added a section titled "Additions". These sections consist of ideas that did not appear in the journal publications such as additional computations or new analytical calculations. We have included these details to present a more complete picture of each part of the PhD project. This structure of the thesis shows clearly how the results were obtained. Also Chapters 3-6 can be read independently if only a particular result should be of interest to the reader.

However this thesis will never read "smoothly" from the first to the last line as some repetitions occur and no global reorganization of the material has been carried out. Nonetheless the results which are repeated within Chapters 3-6 are very important! Hence we hope that the added bit of reinforcement learning might be actually beneficial to the reader.

1.2.2 Main Results

Here we give an overview of the main results of this thesis and provide the references to the journal publications of Chapters 3-6.

1. Chapter 3, [56]: A detailed description of the FitzHugh-Nagumo equation and known results about its bifurcations is given. The fast-slow decomposition of the system is analyzed for $\epsilon = 0$. A transformation into a three-time scale system is introduced and is used to investigate canards and periodic orbits in the system. Hamiltonian dynamics is used to describe homoclinic orbits representing slow waves and Lin's method is used to calculate the singular limit location of fast waves. The concept of singular bifurcation diagram is introduced and the diagram for the FitzHugh-Nagumo equation is computed. It is shown that the CU-bifurcation structure for $\epsilon > 0$ converges as $\epsilon \to 0$ to the singular limit diagram. For this purpose a specialized numerical splitting method is developed.
2. Chapter 4, [55]: An algorithm to calculate slow manifolds of saddle-type (SMST) is developed. It is based on cubic Hermite interpolation. The error for a linear test problem is calculated and the algorithm is applied to several examples. The main example is the FitzHugh-Nagumo equation

where the algorithm can be used to calculate fast and slow waves for $\epsilon > 0$. This is particularly useful to find an initial starting orbit for a homoclinic orbit continuation algorithm.

3. Chapter 5, [57]: The CU bifurcation structure for $\epsilon > 0$ is investigated in more detail. It is shown that the apparent termination of the homoclinic C-curve is caused by a tangency between the unstable manifold of a slow manifold $W^u(C_{l,\epsilon})$ and the stable manifold of an equilibrium point $W^s(q)$. All the involved manifolds have been calculated. $W^u(C_{l,\epsilon})$ was obtained using the SMST algorithm for the slow manifold and forward integration. $W^s(q)$ was calculated via backward integration and also via a boundary value approach. A two-dimensional map model of the Poincaré return map is introduced to describe the dynamics near the Shil'nikov homoclinic orbit. Further observations include the calculation of the location of a canard explosion for $\epsilon > 0$ and the existence of MMOs that are not generated in a tubular neighborhood of the fast or slow waves.

4. Chapter 6, [87]: The unfolding of a planar singular Hopf bifurcation is known. It was shown by Krupa and Szmolyan [86] that the location of the maximal canard can be calculated up to order $O(\epsilon^{3/2})$ using a special normal form transformation and the blow-up method. We notice that the special normal form transformation is not necessary and calculate a formula in non-blow-up coordinates for the maximal canard location. Then we relate this formula to the first Lyapunov coefficient at the singular Hopf bifurcation and show that standard bifurcation software, such as MatCont [46], can be used to locate the maximal canard. The results are demonstrated for the Van der Pol equation and the FitzHugh-Nagumo equation.

CHAPTER 2

TRACKING INVARIANT MANIFOLDS

In the following chapter we shall restrict to a fast-slow system

$$\begin{aligned} \epsilon \dot{x} &= f(x, y, \epsilon) \\ \dot{y} &= g(x, y, \epsilon) \end{aligned} \tag{2.1}$$

where $(x, y) \in \mathbb{R}^{m+n}$. We make the standing assumption that the critical manifold $C_0 = C$ is normally hyperbolic, i.e. for all $(x, y) \in C$ it follows that $D_x f(x, y, 0)$ has rank m. By Fenichel's Theorem this implies that the associated slow manifold C_ϵ is also normally hyperbolic for ϵ sufficiently small. This assumption shall sometimes be repeated in important theorems but will assumed to hold in any scenario we describe in this chapter if we do not explicitly state any assumptions on C. The main goal of this chapter is to show how the geometric theory of fast-slow systems can be used to prove the existence of homoclinic and heteroclinic orbits.

2.1 Simple Jumps and Transversality

Since the critical manifold $C_0 = C$ is normally hyperbolic we can locally write it as a graph $C = \{(h(y), y) \in \mathbb{R}^{m+n}\}$ and consider the slow flow

$$\dot{y} = g(h(y), y, 0) \tag{2.2}$$

If the slow flow (2.2) has two hyperbolic equilibrium points $p = p_0$ and $q = q_0$ there might be a heteroclinic connection between p and q. The situation is shown in Figure 2.1. In Figure 2.1 we assume a transversal intersection of the stable manifold $W^s(p)$ and the unstable manifold $W^u(q)$ for the equilibria of the

slow flow. In particular the manifolds are stable and unstable manifolds with respect to equation (2.2).

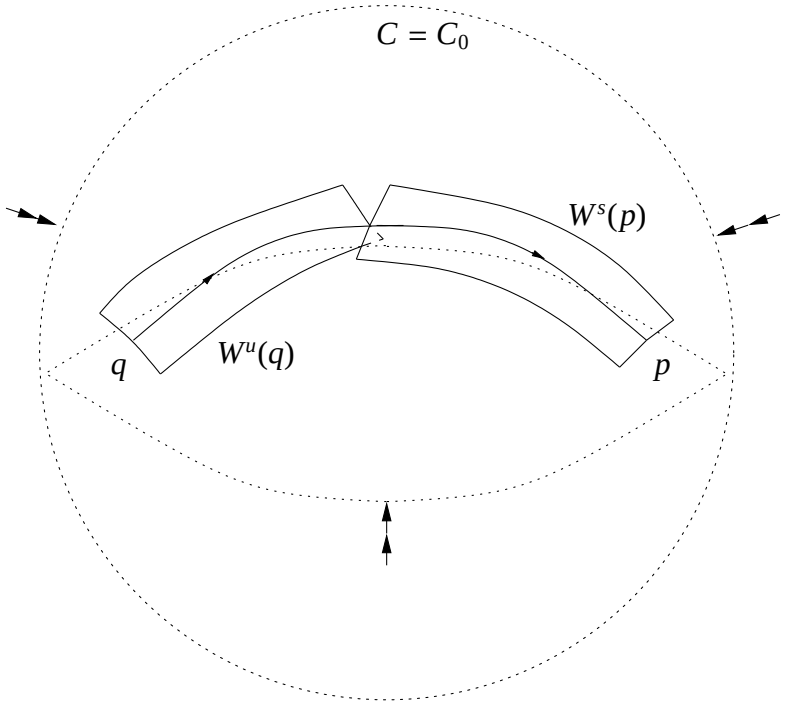

Figure 2.1: The phase space is $\mathbb{R}^4$ with three slow variables and one fast variable. The critical manifold C is a solid ball $D^3 \subset \mathbb{R}^4$. The equilibria $p, q \in D^3$ are shown together with the transversal intersection of their stable and unstable manifolds $W^s(p)$ and $W^u(q)$ for the slow flow (2.2). The transversal intersection gives a heteroclinic connection. The fast slow is indicated by double arrows and is directed toward C.

Perturbing the system for $0 < \epsilon \ll 1$ should also yield a heteroclinic connection between two equilibria of the full system (2.1). This can be justified by Fenichel's Theorem as $C_0 = C$ is normally hyperbolic: C perturbs to a slow manifold C_ϵ, the flow on C_ϵ is close to the slow flow on C and the stability of transversal intersection implies that the flow on the slow manifold still has a heteroclinic connection between two slightly perturbed equilibrium points p_ϵ and q_ϵ. The next step is to ask for the best possible generalizations of the pre-

vious situation. Clearly we also want to include the case when a heteroclinic or homoclinic orbit involves fast *and* slow dynamics. The simplest case for this situation is to assume the existence of two n-dimensional normally hyperbolic invariant manifolds C^1 and C^2 that are contained in the critical manifold C of (2.1). Suppose C^1 and C^2 contain hyperbolic invariant sets P^1 resp. P^2 for the slow flow (2.2); to simplify the abstract setting one can simply think of P^1 and P^2 as equilibrium points. The fast subsystem will be used to find a heteroclinic orbit between P^1 and P^2.

Remark: All the results that follow are going to be applicable in the case $C^1 = C^2$ (and $P^1 = P^2$) which yields homoclinic orbits. Therefore we restrict the discussion, for now, to the case of heteroclinic orbits.

The stable and unstable manifolds of P^1 and P^2 with respect to the slow flow have to be defined. Without loss of generality let us assume we are interested in the unstable manifold of P^1 and the stable manifold of P^2 defined by:

$$\begin{aligned} W^u(P^1) &= \{p \in C^1 : \phi_\tau^{slow}(y) \to P^1 \text{ as } \tau \to -\infty\} \\ W^s(P^2) &= \{p \in C^2 : \phi_\tau^{slow}(y) \to P^1 \text{ as } \tau \to \infty\} \end{aligned}$$

where ϕ_τ^{slow} is the slow flow for equation (2.2). Furthermore certain submanifolds of the stable and unstable manifolds of the critical manifold C have to be defined

$$\begin{aligned} N^1 &= \bigcup_{p \in W^u(P^1)} \{q \in \mathbb{R}^{n+m} : \phi_t^{fast}(q) \to p \text{ as } t \to -\infty\} \\ N^2 &= \bigcup_{p \in W^s(P^2)} \{q \in \mathbb{R}^{n+m} : \phi_t^{fast}(q) \to p \text{ as } t \to \infty\} \end{aligned} \tag{2.3}$$

where ϕ_t^{fast} is the flow of the fast subsystem given by

$$\begin{aligned} x' &= f(x, y, 0) \\ y' &= 0 \end{aligned}$$

and the y-coordinates to be used for a particular flow in (2.3) is determined by the y-coordinates of p. Instead of requiring a transversal intersection of manifolds defined entirely by the slow flow we require a transversal intersection of N^1 and N^2. The situation is shown in Figure 2.2.

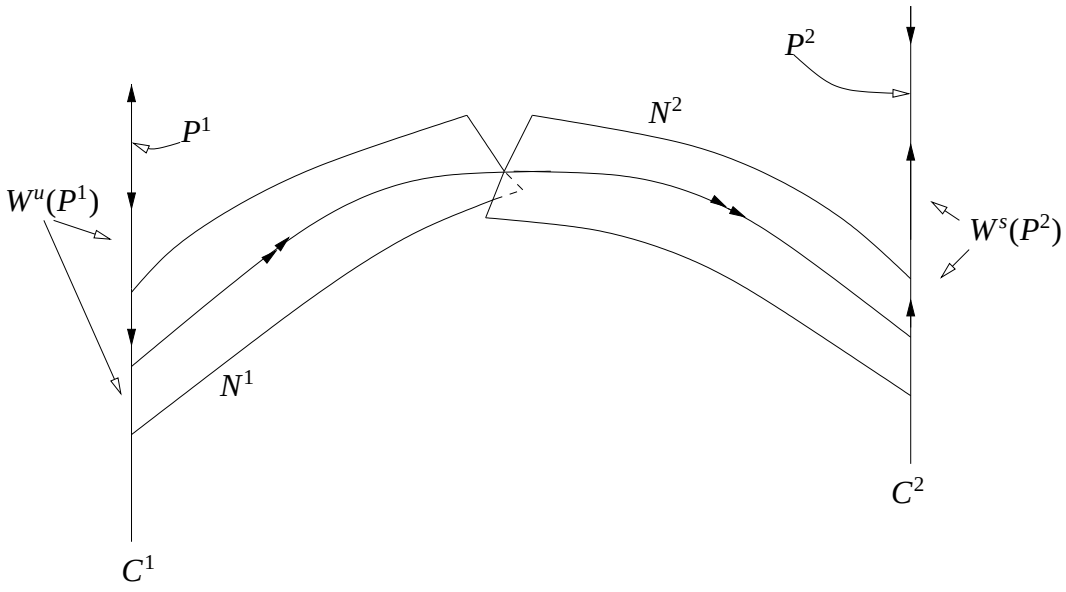

Figure 2.2: Transversal intersection of N^1 and N^2 yields a heteroclinic connection between P^1 and P^2 consisting of two slow segments and one fast segment.

The heteroclinic orbit consists of a trajectory segment of the slow flow on C^1 starting at P^1. This segment connects to a trajectory of a fast subsystem which lies in the transversal intersection of N^1 and N^2. Then the last segment lies on C^2 connecting to P^2. The orbit we obtain in this way is also called a singular orbit as it consists of trajectory segments obtained in the singular limit $\epsilon = 0$.

Theorem 2.1.1. *Suppose P^1 and P^2 are hyperbolic invariant sets for the slow flow and that two normally hyperbolic invariant manifolds N^1 and N^2, as defined by* (2.3)*, intersect transversally. Then there exists ϵ_0 such that for all $\epsilon \in (0, \epsilon_0]$ the fast-slow system* (2.1) *has a transversal heteroclinic connection/orbit between P^1 and P^2. If $N^1 = N^2$ and $P^1 = P^2$ there exists a homoclinic orbit to $P^1 = P^2$.*

Proof. By Fenichel's Theorem the manifolds N^1 and N^2 perturb to slow unstable and slow stable manifolds N^1_ϵ resp. N^2_ϵ. The stability of transversal intersection implies that N^1_ϵ and N^2_ϵ still intersect transversally for ϵ sufficiently small. The result follows. □

From the proof of Fenichel's Theorem, it is clear that we can weaken the hypotheses on N^1 and N^2 slightly and replace the invariance assumptions on N^1 and N^2 by the following:

- N^1 is a compact overflowing invariant manifold with boundary for the fast flow.
- N^2 is a compact inflowing invariant manifold with boundary for the fast flow.

Although this is only a slight modification, it is absolutely necessary since sometimes one is confronted with systems of the form:

$$\begin{aligned} \epsilon \dot{x} &= f(x, y, \mu, \epsilon) \\ \dot{y} &= g(x, y, \mu, \epsilon) \\ \dot{\mu} &= 0 \end{aligned} \tag{2.4}$$

where $\mu \in \mathbb{R}^p$ are parameters. Usually it is assumed that μ is in some compact region in $\mathbb{R}^p$. The extended system with the trivial equation $\dot{\mu} = 0$ does not satisfy the invariance assumptions but it is quite easy to modify the equation $\dot{\mu} = 0$ near the boundary of the manifolds

$$\tilde{N}^i := \{(N^i(\mu), \mu)\} \qquad \text{for } i = 1, 2$$

to make the manifold $\tilde{N}^1$ overflowing invariant and $\tilde{N}^2$ inflowing invariant. The reason why the extended system (2.4) is important is the problem that for some fixed μ_0 the manifolds N^1 and N^2 might be tangential. Varying μ can potentially break this tangential intersection to make it transverse for $\tilde{N}^1$ and $\tilde{N}^2$. This naturally leads to the main problem in applying Theorem 2.1.1 for a concrete example: the verification of the transversality hypothesis might be very difficult. This will be our next step. Suppose we are in the situation described in Theorem 2.1.1. Since N^1 and N^2 intersect there exists a value $y = y_0$ such that in the fast subsystem

$$x' = f(x, y_0, 0)$$

there is a heteroclinic orbit between two equilibrium points, say $p_1 = (x_1(y_0), y_0) \in W^u(P^1)$ and $p_2 = (x_2(y_0), y_0) \in W^s(P^2)$. Denote the heteroclinic orbit by $(x_0(t), y_0) \in \mathbb{R}^{m+n}$. The intersection between N^1 and N^2 at a point $p = (x_0(t), y_0)$ for some t is transverse if and only if

$$T_pN^1 \oplus T_pN^2 = \mathbb{R}^{m+n}$$

Direct dimension counting always gives:

$$\dim(T_pN^1 \oplus T_pN^2) = \dim(T_pN^1) + \dim(T_pN^2) - \dim(T_pN^1 \cap T_pN^2)$$

If we define

$$d = \dim(T_pN^1) + \dim(T_pN^2) - m - n \tag{2.5}$$

we see that N^1 and N^2 intersect transversally if and only if

$$d = \dim(T_p N^1 \cap T_p N^2)$$

Recall that we have assumed that the heteroclinic connection $(x_0(t), y_0)$ occurring in the fast subsystem is one-dimensional. This is equivalent to the assumption that x_0' is the only (up to a scalar multiple) bounded solution to the variational equation:

$$x' = D_x f(x_0(t), y_0, 0)x$$

i.e. there is only one solution that does not diverge from the heteroclinic orbit in forward or backward time: the heteroclinic orbit itself. So we should not be surprised if the adjoint equation to the variational equation is relevant as well. Let ψ denote the unique solution to the adjoint equation:

$$\psi' = -(D_y f(x_0(t), y_0, 0))^T \psi \tag{2.6}$$

Again uniqueness is assumed up to a scalar multiple. Next we can state a very important theorem.

Theorem 2.1.2. *Let N^1 and N^2 be normally hyperbolic manifolds consisting of the unstable fibers of $W^1(P^1)$ and the stable fibers of $W^2(P^2)$ respectively. Let π denote the projection onto the y-coordinates. Then N^1 and N^2 intersect transversally if and only if there are exactly $d-1$ linearly independent solutions $\xi \in T_{y_0}\pi(W^u(P^1)) \cap T_{y_0}\pi(W^s(P^2))$ for the equation*

$$M \cdot \xi = 0 \tag{2.7}$$

where $M \in \mathbb{R}^n$ is defined by

$$M = \int_{-\infty}^{\infty} \psi(t) \cdot D_y f(x_0(t), y_0, 0) d\tau \tag{2.8}$$

We shall not prove this result but refer to [103]. Note that Szmolyan in [103] uses a technical result contained in [95]. To illustrate how the result works we will discuss an example. We shall need that the solution of the adjoint variational equation (2.6) in the case of two fast variables $n = 2$ is given by:

$$\psi(t) = e^{-\int_0^t \mathrm{tr}(D_x f(x_0(s),y_0,0))ds}(-x_2'(t), x_1'(t))^T \tag{2.9}$$

The example to be discussed is a toy model to illustrate the necessary computations in a simple setting.

Example 2.1.3. *Consider the (2,1)-fast-slow system*

$$\begin{aligned} \epsilon\dot{x}_1 &= 1 - (x_1)^2 \\ \epsilon\dot{x}_2 &= y + x_1 x_2 \\ \dot{y} &= y^2 - (x_1)^2 \end{aligned} \tag{2.10}$$

The critical manifold C_0 is easily found and consists of two lines $L_\pm$:

$$\begin{aligned} C_0 &= \{(x_1, x_2, y) \in \mathbb{R}^3 : x_1 = -1 \text{ and } y = x_2 \quad \text{or} \quad x_1 = 1 \text{ and } y = -x_2\} \\ &= L_{x_1=-1} \cup L_{x_1=+1} =: L_- \cup L_+ \end{aligned}$$

A projection into the (x_1, y)-plane of the situation with the singular flows of the fast and slow subsystems is shown in Figure 2.3.

In Figure 2.3 we have shown a singular heteroclinic orbit which connects the two saddle equilibria $p_1 = (-1, 1, 1)$ and $p_2 = (1, 1, -1)$. The unstable manifold of the point p_1 is L_- and the stable manifold of p_2 is L_+. Then define the manifolds N^1 and N^2 as two planes

$$N_1 = \{(x_1, x_2, x_2) \in \mathbb{R}^3 : x_1 \in [-1, 1]\}$$

$$N_2 = \{(x_1, x_2, -x_2) \in \mathbb{R}^3 : x_1 \in [-1, 1]\}$$

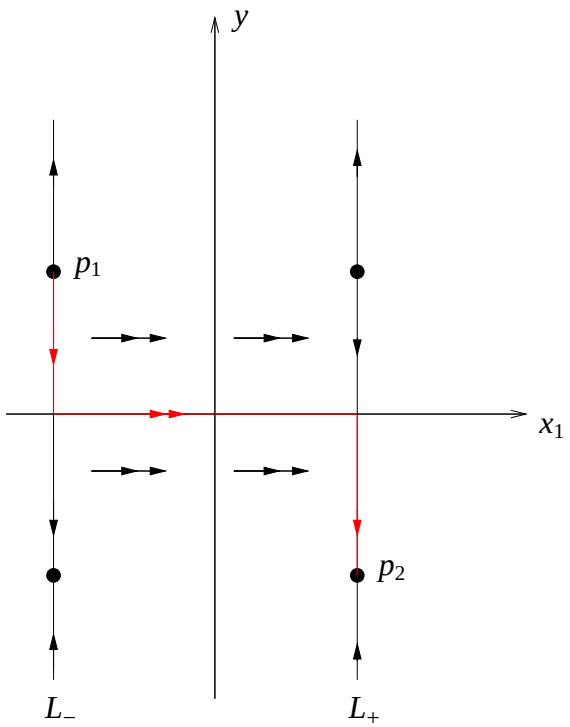

Figure 2.3: Projection of the fast-slow structure of (2.10) into the (x_1, y)-plane. The singular heteroclinic connection between the two equilibrium points is shown in red.

These are precisely the manifolds checked for transversal intersection in Theorem 2.1.2; N^1 *is the part of the unstable manifold of* L_- *and* N^2 *is part of the unstable manifold of* L_+*. Geometrically it is clear that they intersect transversally in the segment*

$$H_{fast} = \{x_1 \in [-1, 1], \quad x_2 = 0, \quad y = 0\}$$

The segment H_{fast} *is a heteroclinic connection for the fast subsystem with* $y = y_0 = 0$*; see Figure 2.3. Hence Theorem 2.1.1 implies that the singular heteroclinic orbit* H *consisting of*

$$\{x_1 = -1, \quad x_2 \in [0, 1], \quad y = x_2\} \cup H_{fast} \cup \{x_1 = 1, \quad x_2 \in [0, 1], \quad y = -x_2\}$$

persists for $\epsilon > 0$ *sufficiently small and* (2.10) *has a heteroclinic orbit. The geometric observation can be verified using the tools of 2.1.2. First one has to calculate the dimension*

d as given in equation (2.5)*. Let p be a point on the heteroclinic orbit H then*

$$d = \dim(T_p N^1) + \dim(T_p N^2) - m - n = 2 + 2 - 2 - 1 = 1$$

The equation $M \cdot \xi = 0$ *is a scalar equation and we aim to show that it has* $d-1 = 1-1 = 0$ *non-trivial solutions i.e. that* $M \neq 0$*. Let* H_{fast} *be denoted in parametrized form by* $(x_1(t), x_2(t), y_0) = (x_0(t), 0)$*; note that we formally should denote e.g.* $x_1(t)$ *by* $(x_1)_0(t)$ *as it is a coordinate along the heteroclinic orbit but we drop the* 0 *subscript for notational convenience. The solution of the adjoint equation is obtained from* (2.9)*:*

$$\psi(t) = e^{\int_0^t x_1(s)ds}(-y_0 - x_1(t)x_2(t), 1 - (x_1(t))^2)^T \tag{2.11}$$

Furthermore a direct calculation yields:

$$D_y f(x_0(t), y_0, 0) = (0, 1)^T$$

Putting the previous results into (2.8) *gives M:*

$$\begin{aligned} M &= \int_{-\infty}^{\infty} \psi(t) \cdot D_y f(x_0(t), y_0, 0) dt \\ &= \int_{-\infty}^{\infty} e^{\int_0^t x_1(s)ds}(-x_1(t)x_2(t), 1 - x_1(t)^2)^T \cdot (0, 1)^T dt \\ &= \int_{-\infty}^{\infty} e^{\int_0^t x_1(s)ds}(1 - x_1(t)^2) dt \end{aligned}$$

Note that $x_1(t)$ *describes the fast segment of the heteroclinic orbit lying between* $x_1 = -1$ *and* $x_1 = 1$*. Hence* $1 - x_1(t)^2 > 0$ *for all* $t \in \mathbb{R}$*. The exponential function is positive as well and we conclude that* $M > 0$*. This implies the existence of the heteroclinic orbit.*

Unfortunately Theorem 2.1.2 does not cover all cases occurring in practice. In the next section we shall give a more detailed introduction to the FitzHugh-Nagumo equation and why certain homoclinic orbits are much more difficult to obtain.

2.2 The FitzHugh-Nagumo Equation

The FitzHugh-Nagumo equation is a simplification of the Hodgkin-Huxley model for an electric potential of a nerve axon [65]. The first version was developed by FitzHugh in [43] and is a two-dimensional system of ODEs:

$$\begin{aligned} \epsilon \dot{u} &= v - \frac{u^3}{3} + u + p \\ \dot{v} &= -\frac{1}{s}(v + \gamma u - a) \end{aligned} \tag{2.12}$$

where u is the electric potential and v an auxiliary variable. Note that for parameter values $a = \gamma = p = 0$ and $s = 1$ we obtain the unforced van der Pol equation. A detailed summary of the bifurcations of (2.12) can be found in [97]. By taking diffusion terms into account in the conduction process one obtains another version of the FitzHugh-Model model due to Nagumo and his co-workers [94]:

$$\begin{cases} u_\tau = \delta u_{xx} + f_a(u) - w \\ w_\tau = \epsilon(u - \gamma w) \end{cases} \tag{2.13}$$

where $f_a(u) = u(u-a)(1-u)$ and γ, δ and $0 < a < 1/2$ are parameters. A good introduction to the derivation and problems associated with (2.13) can be found in [62]. Suppose we assume a traveling wave solution to (2.13) and set $u(x,\tau) = u(x+s\tau) =: u(t)$ and $w(x,\tau) = w(x+s\tau) =: w(t)$, where s represents the wave speed. By the chain rule we get $u_\tau = su'$, $u_{xx} = u''$ and $w_\tau = sw'$. Now set $v = u'$ and substitute into (2.13):

$$\begin{aligned} u' &= v \\ v' &= \frac{1}{\delta}(sv - f_a(u) + w) \\ w' &= \frac{\epsilon}{s}(u - \gamma w) \end{aligned} \tag{2.14}$$

Observe that a homoclinic orbit of (2.14) corresponds to a traveling pulse solution of (2.13). Changing from the fast time t to the slow time τ and re-labeling

variables $x_1 = u$, $x_2 = v$ and $y = w$ we get a fast-slow system in standard form:

$$\begin{aligned} \epsilon \dot{x}_1 &= x_2 \\ \epsilon \dot{x}_2 &= \frac{1}{\delta}(s x_2 - x_1(1 - x_1)(x_1 - a) + y) \\ \dot{y} &= \frac{1}{s}(x_1 - \gamma y) \end{aligned} \tag{2.15}$$

For now we shall refer to (2.15) as "the" FitzHugh-Nagumo equation. The equilibrium points of (2.15) are given by the intersection of the y-nullcline $y = x_1/\gamma$ and the critical manifold

$$C_0 = \{(x_1, 0, f_a(x_1)) \in \mathbb{R}^3 : \text{where } f_a(x_1) = x_1(1 - x_1)(x_1 - a)\}$$

Furthermore we can find the fold points by solving the equation $f_a'(x_1) = 0$. This yields:

$$x_{1,\pm} = \frac{1}{3}(1 + a \pm \sqrt{1 - a + a^2})$$

Obviously the x_2-coordinates of the folds are zero and the y-coordinates are $f_a(x_{1,\pm})$. We shall denote the folds by $x_\pm = (x_{1,\pm}, 0, f_a(x_{1,\pm}))$. They naturally split the critical manifold into three branches:

$$\begin{aligned} C_l &= \{x_1 < x_{1,-}\} \cap C_0 \\ C_m &= \{x_{1,-} < x_1 < x_{1,+}\} \cap C_0 \\ C_r &= \{x_{1,+} < x_1\} \cap C_0 \end{aligned}$$

Theorems 2.1.1 and 2.1.2 can be used to prove the existence of a heteroclinic orbit if there is more than one equilibrium point for (2.15) using the following strategy:

1. Assume that γ is selected so that three hyperbolic equilibrium points exist. Denote the equilibrium point on C_l by $p_1 = (0, 0, 0)$ and the equilibrium

point on C_r by p_2. Both points are saddles and the goal is to prove that a singular heteroclinic orbit between p_1 and p_2 persists.

2. Observe that we can adjust the parameters to obtain a situation with three equilibrium points
3. Extend the system by the equation $s' = 0$. We are in the case where the parameter is used to build a transversal intersection of manifolds as described in the remarks after Theorem 2.1.1.
4. Define N^1 for p_1 and N^2 for p_2, one should have $\dim(N^1) = 2$ and $\dim(N^2) = 3$.
5. We can use the following fact [91]: There exists $s = (1 - 2a)/\sqrt{2}$ such that the fast subsystem at $y = y_0 = 0$ has a heteroclinic connection between the two saddles on C_l and C_r.
6. Observe that it suffices to prove that the second component of M in (2.8) is nonzero.

Now we move on to introduce the scenario in which Theorems 2.1.1 and 2.1.2 no longer work to find particular global orbits in the FitzHugh-Nagumo equation. If we choose γ large enough it is clear that the FitzHugh-Nagumo equation has only one equilibrium point, namely $(0, 0, 0)$. It can be checked that this is the case for $\gamma = 1$. Let us also assume from now on for simplicity that $\delta = 1$ and $a = 1/10$; hence we simply write $f_{1/10}(x_1) = f(x_1)$. It is easy to see from the linearization of (2.15) at $(0, 0, 0)$ that the equilibrium is of saddle-type with 1 unstable and 2 stable directions. The fold points can be described more explicitly:

$$x_{1,\pm} = \frac{1}{30}\left(11 \pm \sqrt{91}\right) \qquad \text{or numerically:} \quad x_{1,+} \approx 0.6846, \quad x_{1,-} \approx 0.0487$$

The geometry of the system for one equilibrium point is illustrated in Figure 2.4.

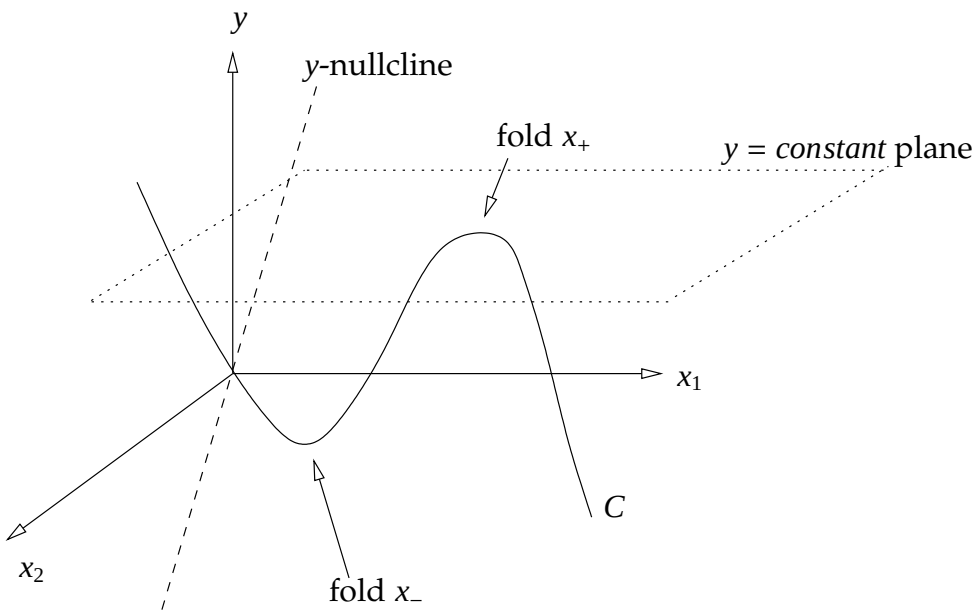

Figure 2.4: Critical manifold C of the FitzHugh-Nagumo equation. The planes $y = constant$ are the domains of the fast subsystems. The equilibrium is located at the origin.

The sign of the y-derivative is given by $(x_1 - y)$. Since it is positive below $y = x_1$ and negative above it we observe that the slow flow on C is directed toward the unique equilibrium point on C_l. The slow flow is pointing in the positive y-direction on the branches C_m and C_r. The fast subsystem is:

$$\begin{aligned} x_1' &= x_2 \\ x_2' &= sx_2 - x_1(1 - x_1)(x_1 - a) + y \end{aligned} \tag{2.16}$$

The phase spaces of the fast subsystems, parametrized by the slow variable y, should be viewed as planes $y = constant$. We will see that it no longer suffices to consider only one particular fast subsystem. There are three different regions for the fast subsystem depending on the number of equilibrium points. We have one equilibrium for (2.16) when the plane intersects C once (i.e. for $y > f(x_{1,+})$ or

$y < f(x_{1,-})$), two equilibrium points if the plane is tangent to C at a fold point (i.e. $y = f(x_{1,\pm})$) and three equilibria if we choose y so that the plane intersects C three times; see Figure 2.4. Let us focus on the last case and stay away from the fold points. In this case the fast subsystem has two saddle equilibria located on C_l and C_r and an unstable spiral on C_m. It was shown analytically in [2] that there exists a wave speed s^* such that (2.16) has a heteroclinic connection between the two saddles at $y = 0$ and for a value of y^* with $0 < y^* < f(x_{1,-})$. The heteroclinic connection at $y = 0$ involves the unstable manifold of the equilibrium point $(0, 0)$ on C_l which is also the unique equilibrium of the full system. Knowing the directions of the slow flow on each of the pieces of the critical manifold we can now draw a trajectory for full system consisting of alternating pieces of fast and slow motion as shown in Figure 2.7. Looking at Figure 2.7 we are tempted to conclude that the FitzHugh-Nagumo equation has a homoclinic orbit as we have just exhibited one in the singular limit. Unfortunately it does not suffice to check just transversality conditions between the unstable manifold $W^u(C_l)$ of the left branch and the stable manifold $W^s(C_r)$ of the right branch of C. In principal we want to conclude the result for the slow manifolds $C_{l,\epsilon}$ and $C_{r,\epsilon}$ and their unstable and stable manifolds for $0 < \epsilon \ll 1$ and ϵ sufficiently small as in Section 2.1.

The problem is that our singular orbit now contains two jumps. In this case we have to follow the unstable manifold M of the equilibrium point until it reaches a neighborhood close to the slow manifold $C_{r,\epsilon}$. Then we must follow M as it evolves near (but not on!) $C_{r,\epsilon}$. The next step is to consider the exit of M in a neighborhood of the second jump point at height $y = y^*$ and then we hope that we can follow it back near $C_{l,\epsilon}$ to conclude that it reaches the stable manifold of

$(0, 0, 0)$.

2.3 The Exchange Lemma I

The Exchange Lemma was initially proved by Jones and Kopell [68]. We shall mainly follow their original paper and an expository presentation in [74]. Recall from the problem of finding homoclinic orbits in the FitzHugh-Nagumo with more than one jump discussed in the previous section that we have to track an invariant manifold in phase phase. For the general situation we start with a fast-slow system

$$\begin{aligned} \epsilon \dot{x} &= f(x, y, \epsilon) \\ \dot{y} &= g(x, y, \epsilon) \end{aligned} \tag{2.17}$$

with $x \in \mathbb{R}^m$ and $y \in \mathbb{R}^n$. We include in (2.17) possible parameters in the system in the vector y as slow variables. In the FitzHugh-Nagumo equation that would mean including the equation for the wave speed $\dot{s} = 0$ and re-labeling s to a suitable indexed y-coordinate. Let S_0 denote some compact normally hyperbolic submanifold of the critical manifold and let S_ϵ be the corresponding slow manifold. Note that we shall assume that S_0 is in fact uniformly normally hyperbolic meaning that $D_x f(p)$ has eigenvalues uniformly bounded away from zero for each $p \in S_0$.

Recall from Theorem 1.1.3 that we can transform a fast-slow system near a

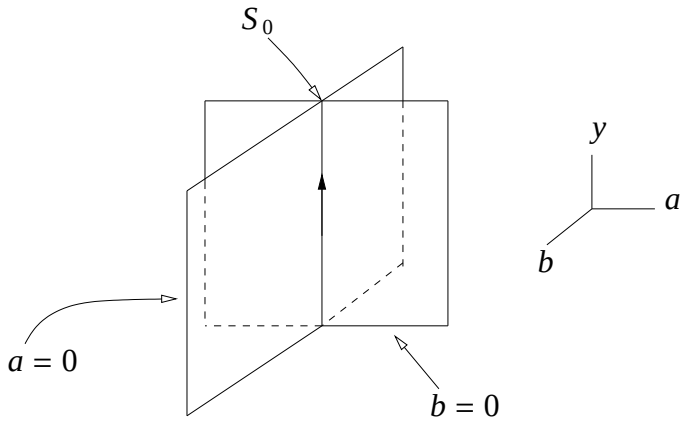

Figure 2.5: A fast-slow system near a normally hyperbolic critical manifold S_0 in Fenichel Normal Form. In this picture we have suppressed all coordinates y_i with $i > 1$.

normally hyperbolic critical manifold S_0 into Fenichel normal form:

$$\begin{aligned} a' &= \Lambda(a,b,y,\epsilon)a \\ b' &= \Gamma(a,b,y,\epsilon)b \\ y' &= \epsilon(h(y,\epsilon) + H(a,b,y,\epsilon)(a,b)) \end{aligned} \tag{2.18}$$

with $a \in \mathbb{R}^k$, $b \in \mathbb{R}^l$, $y \in \mathbb{R}^n$ and $k + l = m$; Λ and Γ are matrix-valued functions and H is a bilinear-form valued function which can be written explicitly as

$$y_i' = \epsilon\left(h_i(y,\epsilon) + \sum_{u=1}^{k}\sum_{s=1}^{l} H_{ius}a_u b_s\right)$$

Sometimes also the tensor notation $H(a,b,y,\epsilon) \otimes a \otimes b = H(a,b,y,\epsilon)(a,b)$ is employed. The matrix-valued functions Λ and Γ are defined by separating the fast unstable and fast stable directions. More precisely, in (2.18) the critical manifold S_0 is $\{a = 0, b = 0\}$ and normal hyperbolicity implies there are λ_0, γ_0 such that any eigenvalue λ_i of $\Lambda(0,0,y,0)$ or any eigenvalue γ_i of $\Gamma(0,0,y,0)$ satisfies

$$\text{Re}\,\lambda_i > \lambda_0 > 0, \qquad \text{Re}\,\gamma_i < \gamma_0 < 0$$

in a region

$$B = \{(a,b,y) : |a| < \delta, |b| < \delta, y \text{ in a given compact region}\}$$

with $\delta > 0$ sufficiently small. The same holds for $\epsilon > 0$ sufficiently small so that (2.18) is still valid and we can find $\lambda_\epsilon > 0$ and $\gamma_\epsilon < 0$ which are the weak unstable and weak stable eigenvalues near S_ϵ. In equations (2.18) we can rectify the slow flow. Without loss of generality we assume that the slow flow is pointing in the direction y_1 so that we can reduce the problem of analyzing the flow near a normally hyperbolic slow manifold S_ϵ to:

$$\begin{aligned} a' &= \Lambda(a, b, y, \epsilon)a \\ b' &= \Gamma(a, b, y, \epsilon)b \\ y' &= \epsilon(U + H(a, b, y, \epsilon)(a, b)) \end{aligned} \tag{2.19}$$

where $U = (1, 0, \ldots, 0)^T$. Observe that the stable and unstable manifolds W^s and W^u of S_ϵ are given by $\{a = 0\}$ and $\{b = 0\}$ respectively. Let M be a $(k + 1)$-dimensional invariant manifold. M is the manifold we want to follow in phase space. We remark that the dimensional requirement on M can be generalized but for simplicity we shall only consider the case of $(k+1)$ dimensions. Suppose M intersects the boundary of the region/box B in $\{b = \delta\}$ at some point q. If q is close enough to the stable manifold $W^s(S_\epsilon) = \{a = 0\}$ then a trajectory starting at q stays near S_ϵ for a long time (e.g. a time that is $O(1/\epsilon)$ on the fast time scale t). We want to find estimates on the fast coordinates (a, b) to quantify the situation more precisely.

Lemma 2.3.1. *There exists constants $c_a, c_b, K > 0$ such that for $s \leq t$ the following three results hold*

(R1) $|b(t)| \leq c_b|b(s)|e^{\gamma_0(t-s)}$

(R2) $|a(t)| \geq c_a|a(s)|e^{\lambda_0(t-s)}$

(R3) $|\int_t^s a(\sigma)d\sigma| \leq K$ *(independent of ϵ, t, s)*

as long as a trajectory remains in B.

Proof. We start by proving (R1). Since the eigenvalues of $\Lambda(a, b, y, \epsilon)$ are close to the ones of $\Lambda(0, 0, y, \epsilon)$ we see that near each point $z = (a, b, y) \in B$ there is a neighborhood N of z such that an estimate of the form

$$|b(t)| \leq C_N |b(s)| e^{\gamma_0 (t-s)}$$

holds if $b(\sigma) \in N$ with $\sigma \in (s, t)$ and ϵ sufficiently small. By compactness of B we can cover B by a finite number of such neighborhoods. In fact, if we consider all trajectories segments lying in B we can cover each segment by an open cover. Taking the union of those open covers will cover B and then we extract a finite subcover by compactness. Therefore we get an estimate for an arbitrary trajectory given by

$$|b(t)| \leq C_{N_1} C_{N_2} \cdots C_{N_m} |b(s)| e^{\gamma_0 (t-s)}$$

for some finite fixed $m \in \mathbb{N}$. Now (R1) follows and (R2) is immediate by using the same method of proof as for (R1). This leaves the estimate (R3). Using (R2) we find

$$|a(\sigma)| \leq \frac{1}{c_a} |a(t)| e^{\gamma_0 (\sigma - t)} \qquad \text{for } \sigma \leq t$$

Integrating both sides of the last equation yields:

$$\int_s^t |a(\sigma)| d\sigma \leq \frac{1}{c_a} |a(t)| \int_s^t e^{\lambda_0 (\sigma - t)} d\sigma \leq \frac{|a(t)|}{c_a \lambda_0} (1 - e^{\lambda_0 (s-t)})$$

Since $|a(t)| \leq \delta$ and $\lambda_0 > 0$ we can conclude (R3) holds. □

Now we can track trajectories inside B. Since the manifold M is invariant a trajectory starting at $q \in M \cap \{|b| = \delta\}$ has to stay inside M for all time. Hence we can follow a neighborhood of q in M under the flow as shown by the next result.

Theorem 2.3.2. *Let $\bar{q} \in M \cap \{|a| = \delta\}$ be the exit point of a trajectory starting at $q \in M \cap \{|b| = \delta\}$ that spends a time t that is $O(1/\epsilon)$ in B. Let V be a neighborhood of q in M. If V is sufficiently small then the image of V under the time t map is close to*

$$\{|a| = \delta, y_i - y_i(0) = 0, i > 1\}$$

in the C^0-norm where $y_i(0)$ denotes the y-coordinates of q.

The situation is illustrated in Figure 2.6.

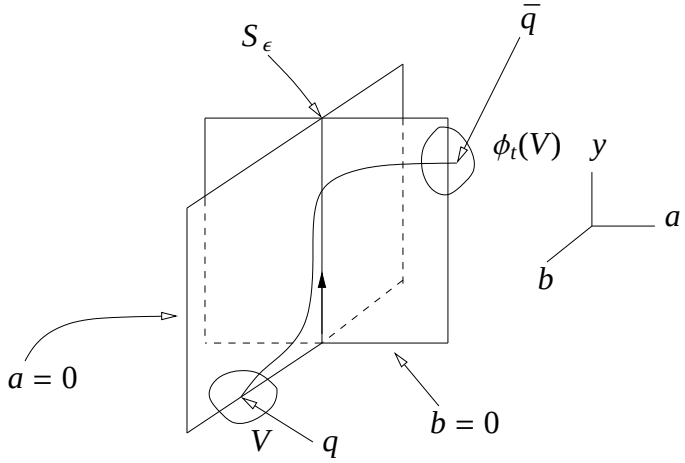

Figure 2.6: In this picture we have suppressed all coordinates y_i with $i > 1$. The image of the neighborhood V near the exit point $\bar{q}$ is denoted by $\phi_t(V)$; it is very close to the unstable manifold $W^u(S_\epsilon) = \{|b| = 0\}$ near the exit point.

Proof. From Lemma 2.3.1, (R1) we find that $b(t)$ is small. Hence we are left with the y_i coordinates with $i > 1$. Since $b(t)$ is small we clearly have for $i > 1$:

$$y_i' \leq \epsilon \left(\sum_{u=1}^{k} H_{iu} a_u \right) := \epsilon \bar{H}_i \cdot a$$

where $\bar{H}_i$ is a k-vector of functions. As $\bar{H}_i$ is smooth and B is compact we can let d_i be a bound for $|\bar{H}_i|$. Therefore

$$\int_0^t y_i d\sigma \leq \epsilon \int_0^t \bar{H}_i \cdot a d\sigma$$

implies using the Fundamental Theorem of Calculus that

$$|y_i(t) - y_i(0)| \leq \epsilon \int_0^t d_i |a(\sigma)| d\sigma \tag{2.20}$$

Using Lemma 2.3.1, (R3) we can conclude that the right-hand side of (2.20) is $O(\epsilon)$. □

Often Theorem 2.3.2 is called a C^0-Exchange Lemma and we might ask why there is any need to consider a refined version of it as we just tracked the manifold M near the slow manifold S_ϵ. The problem is that every trajectory exits near $\bar{q}$ almost tangent to the unstable manifold $W^u(S_\epsilon)$. Hence we have no information about the part of the tangent spaces of M in the center directions. In this case we cannot rely on any results about transversality obtained in the singular limit $\epsilon = 0$ for an intersection of $W^u(S_0)$ with some other manifold, say N, to conclude that M is transversal to N for $\epsilon > 0$. We have information about the location of the manifold M itself ("C^0-information") but not sufficient knowledge about its tangent spaces ("C^1-information"). As the tangent spaces determine whether an intersection is transversal the C^0-Exchange Lemma is insufficient. Note carefully that the situation just described occurs for the FitzHugh-Nagumo equation (2.15) if we try to follow the unstable manifold of the unique equilibrium point during its second jump; see Figure 2.7.

2.4 The Exchange Lemma II

The C^1-closeness result we want is the following (cf. Figure 2.6):

Theorem 2.4.1 (**Exchange Lemma**). *Let M be a $(k+1)$-dimensional invariant manifold. Assume $M \cap \{|b| = \delta\}$ intersects $\{a = 0\}$ transversely. Let $\bar{q} \in M \cap \{|a| = \delta\}$ be the*

exit point of a trajectory starting at $q \in M \cap \{|b| = \delta\}$ *that spends a time* $t = O(1/\epsilon)$ *in B. Let V be a neighborhood of q in M. The image of V under the time t map is close in the* C^1*-norm to*

$$\{|a| = \delta, y_i - y_i(0) = 0, i > 1\}$$

where $y_i(0)$ *denotes the y-coordinates of q. In particular M is* C^1*-close to* $\{|a| = \delta, y_i - y_i(0) = 0, i > 1\}$ *near* $\bar{q}$*.*

Remark: The key feature of both Exchange Lemmas (Theorems 2.3.2 and 2.4.1) is that we have traded information about transversality and variation of certain center directions (here: y_i with $y_i > 1$) near q with new information near the exit point $\bar{q}$ given by a C^1-closeness result to a certain submanifold of the unstable manifold $W^u(S_\epsilon)$. The idea used by Jones and Kopell [68] to achieve a tracking of the tangent spaces to M is to consider $(k+1)$-differential forms that are dual to $(k+1)$ planes in $k+l+n$ space and describe their evolution by a differential equation. As usual we shall simply write $(k+1)$-forms with the implicit assumption that all forms are sufficiently differentiable. A basic $(k+1)$-form is given by

$$P_{\sigma_1 \cdots \sigma_{k+1}} := d\sigma_1 \wedge \ldots \wedge d\sigma_{k+1}$$

where $\sigma_j \in \{a_i, b_i, y_i\}$. Furthermore we know that a basis of all forms is given by restricting to increasing indices. Here we agree on the ordering

$$a_1 < a_2 < \cdots < a_k < b_1 < \cdots < b_l < y_1 < \cdots < y_n$$

It will be convenient to use a projectivized versions of the $P_{\sigma_1 \ldots \sigma_{k+1}}$:

$$\hat{P}_{\sigma_1 \cdots \sigma_{k+1}} = \frac{P_{\sigma_1 \cdots \sigma_{k+1}}}{P_{a_1 \cdots a_k y_1}}$$

A priori we cannot say that $\hat{P}$ will always be well defined everywhere as $P_{a_1 \cdots a_k y_1}$ might be zero. But we shall see that near S_ϵ we always have $P_{a_1 \cdots a_k y_1} \neq 0$, i.e.

the components of tangent planes of M at points of trajectories in B will always have non-vanishing components in the a_i and the y_1 directions. In fact, the hyperplane H spanned by the a_i and the y_1 coordinates can be defined by requiring that

$$P_{\sigma_1 \cdots \sigma_{k+1}}(v) = 0 \qquad \text{for all } v \in H \text{ and } (\sigma_1, \ldots, \sigma_{k+1}) \neq (a_1, \ldots, a_k, y_1)$$

Therefore we can easily restate the Exchange Lemma in an equivalent form using differential forms.

Theorem 2.4.2 (Exchange Lemma - differential form conclusion)**.** *Under the same assumptions as in Theorem 2.4.1 we conclude that at* $\overline{q}$*:*

$$\hat{P}_{\sigma_1 \cdots \sigma_{k+1}} = O(\epsilon)$$

for all $(\sigma_1, \ldots, \sigma_{k+1}) \neq (a_1, \ldots, a_k, y_1)$*.*

In the next section we give a proof of the Exchange Lemma for the simplest non-trivial case in phase space dimension four for a system with two fast and two slow variables.

2.5 A Proof in $\mathbb{R}^4$

Here we prove Theorem 2.4.2 for a $(2,2)$-fast-slow system in Fenichel Normal Form near the slow manifold S_ϵ with $z := (a, b, y_1, y_2)$ and $a, b, y_1, y_2 \in \mathbb{R}$

$$\begin{aligned} a' &= \Lambda(z, \epsilon)a \\ b' &= \Gamma(z, \epsilon)b \\ y_1' &= \epsilon g_1(z, \epsilon) = \epsilon(1 + H_1(a, b, y, \epsilon)ab) \\ y_2' &= \epsilon g_2(z, \epsilon) = \epsilon(H_2(a, b, y, \epsilon)ab) \end{aligned} \tag{2.21}$$

Hence we have $k = 1 = l$ and $n = 2$ in view of the notation in the previous two sections. Also we still work in a suitable neighbourhood/box

$$\mathfrak{B} = \{(a, b, y) : |a| < \delta, |b| < \delta, y \text{ in a given compact region}\} \tag{2.22}$$

We divide the proof into several steps:

- *Step 1:* We want to track tangent planes to a two-dimensional invariant manifold. To measure how these planes evolve under the flow we are going to develop evolution equations for differential 2-forms that are dual to planes in $\mathbb{R}^4$.
- *Step 2:* We are going to show that the evolution equations derived in Step 1 are of a special form due to the structure of Fenichel Normal Form. In this process we are going to split the coordinates of 2-forms into two groups. One is formed by P_{ay_1}, P_{ay_2} and the other by the four other basic 2-forms spanning $\bigwedge^2 \mathbb{R}^4$. Both groups are going to satisfy fundamental estimates under the flow.
- *Step 3:* The assumptions of the Exchange Lemma on transversality at the entry point to $\mathfrak{B}$ and spending a time of order $O(1/\epsilon)$ in $\mathfrak{B}$ will be used. They provide estimates on the initial conditions at the entry point q.
- *Step 4:* In $\mathfrak{B}$ we are going to follow the reference solution that starts at the entry point q, tracks the slow manifold and then exits near $\bar{q}$. The first key component is to show that the form P_{ay_1} never vanishes inside $\mathfrak{B}$. This allows us to consider forms projectivized/divided by P_{ay_1}. The general strategy is to follow the reference solution through a compact neighbourhood inside $\mathfrak{B}$, show that inside this neighbourhood all estimates we want

from the evolution equations hold and then extend this procedure by compactness of $\mathfrak{B}$.

- *Step 5:* This step provides the basic estimates to control the evolution of all 2-forms inside $\mathfrak{B}$. The estimates appear to be rather involved but the essential tool is just Gronwall's Lemma.
- *Step 6:* This step collects all the previous results and derives from estimates at q the final estimates at $\overline{q}$. This final part of the proof is subdivided into three parts. The first tracks M from q to S_ϵ, the second follows M near S_ϵ and the third deals with the exit from S_ϵ towards $\overline{q}$. The overall patching strategy is the same as in Step 4.

Step 1: We start with a remark on 2-forms in $\mathbb{R}^4$. Let σ_i for $i = 1, 2, 3, 4$ be coordinates in $\mathbb{R}^4$. Observe that if P is a 2-plane then the natural first attempt to define how to evaluate a 2-form on P is to take two independent vectors that span P and then evaluate the 2-form on those vectors; this process is only defined up to a multiple as we can scale basis vectors inside P. To avoid this ambiguity consider a unit rectangle R of P and evaluate the form on the vectors spanning it. We can interpret this process geometrically in the usual way; for example, consider $(d\sigma_1 \wedge d\sigma_2)(P)$ which can be evaluated projecting R onto the (σ_1, σ_2)-plane along the coordinate axes σ_3 and σ_4 and then taking the area of this projection. Hence we have defined the evaluation of 2-forms on planes up to orientation; the orientation will not matter for us in the following as we will only consider absolute values when evaluating 2-forms on planes. Furthermore observe that e.g. the (σ_1, σ_2)-plane is characterized by vanishing of all basic 2-forms execept $d\sigma_1 \wedge d\sigma_2$ and $d\sigma_2 \wedge d\sigma_1$.

The variational equations describing a flow of the differential forms da, db, dy_1 and dy_2 associated to (2.21) are:

$$\begin{aligned} da' &= \Lambda(z,\epsilon)da + a(\nabla\Lambda \cdot dz) \\ db' &= \Gamma(z,\epsilon)db + b(\nabla\Gamma \cdot dz) \\ dy_1' &= \epsilon\nabla g_1(z,\epsilon) \cdot dz \\ dy_2' &= \epsilon\nabla g_2(z,\epsilon) \cdot dz \end{aligned}$$

where $dz = (da, db, dy_1, dy_2)^T$ and ∇ denotes the usual gradient operator so e.g.

$$\nabla\Lambda = \left(\frac{\partial\Lambda}{\partial a}, \frac{\partial\Lambda}{\partial b}, \frac{\partial\Lambda}{\partial y_1}, \frac{\partial\Lambda}{\partial y_2}\right)^T$$

To calculate the evolution equations for the two-forms $P_{\sigma_1\sigma_2}$ we use the product rule, e.g.

$$\begin{aligned} P'_{ay_1} &= (da \wedge dy_1)' = da' \wedge dy_1 + da \wedge dy_1' \\ &= (\Lambda(z,\epsilon)da + a\nabla\Lambda \cdot dz) \wedge dy_1 + \epsilon da \wedge (\nabla g_1 \cdot dz) \\ &=: \Lambda(z,\epsilon)P_{ay_1} + aR_1 + \epsilon R_2 \end{aligned}$$

where $\cdot$ denotes the usual dot product between vectors in $\mathbb{R}^4$. We shall drop the argument (z,ϵ) for simplicity from now on. The calculations for the other 2-forms are similar and we get the desired evolution equations:

$$\begin{aligned} P'_{ay_1} &= \Lambda P_{ay_1} + aR_1 + \epsilon R_2 \\ P'_{ay_2} &= \Lambda P_{ay_2} + aR_3 + \epsilon R_4 \\ P'_{ab} &= (\Lambda + \Gamma)P_{ab} + aR_5 + bR_6 \\ P'_{by_1} &= \Gamma P_{by_1} + bR_7 + \epsilon R_8 \\ P'_{by_2} &= \Gamma P_{by_2} + bR_9 + \epsilon R_{10} \\ P'_{y_1y_2} &= \epsilon(R_{11} + R_{12}) \end{aligned} \tag{2.23}$$

where

$$
\begin{aligned}
R_1 &= (\nabla\Lambda \cdot dz) \wedge dy_1 & R_7 &= (\nabla\Gamma \cdot dz) \wedge dy_1 \\
R_2 &= da \wedge (\nabla g_1 \cdot dz) & R_8 &= db \wedge (\nabla g_1 \cdot dz) \\
R_3 &= (\nabla\Lambda \cdot dz) \wedge dy_2 & R_9 &= (\nabla\Gamma \cdot dz) \wedge dy_2 \\
R_4 &= da \wedge (\nabla g_2 \cdot dz) & R_{10} &= db \wedge (\nabla g_2 \cdot dz) \\
R_5 &= (\nabla\Lambda \cdot dz) \wedge db & R_{11} &= dy_1 \wedge (\nabla g_1 \cdot dz) \\
R_6 &= da \wedge (\nabla\Gamma \cdot dz) & R_{12} &= (\nabla g_2 \cdot dz) \wedge dy_2
\end{aligned}
$$

Note that we only considered the six 2-forms $P_{ay_1}, P_{ay_2}, P_{ab}, P_{by_1}, P_{by_2}, P_{y_1y_2}$ as they span the space of two-forms $\bigwedge^2 \mathbb{R}^4$. To simplify notation we let

$$
\begin{aligned}
Z &:= (P_{ay_1}, P_{ay_2})^T = (Z_1, Z_2) \\
X &:= (P_{ab}, P_{by_1}, P_{by_2}, P_{y_1y_2})^T = (X_1, X_2, X_3, X_4)^T.
\end{aligned}
$$

Step 2: The next lemma provides fundamental estimates which we shall use throughout this section.

Lemma 2.5.1. *The equations for (Z, X) can be written in the form:*

$$
\begin{aligned}
Z' &= \Lambda Z + \eta_1(Z, X, t) \\
X' &= BX + \eta_2(Z, X, t)
\end{aligned} \tag{2.24}
$$

where $B = B(z, \epsilon)$ is a 4×4 matrix-valued function. The following conditions hold:

(i) For $a = 0$, $b = 0$, $\epsilon = 0$ we have $\eta_1 = 0$, $\eta_2 = 0$.

(ii) The matrix B satisfies:

$$
\left\| \exp\left(\int_s^t (B - \Lambda(Id)) d\xi \right) \right\| \leq \bar{M} \exp(-\mu(t - s)) \tag{2.25}
$$

for some $\bar{M} \geq 1$, $\mu > 0$ and $t > s$.

(iii) Denote by η_{1i} the i-th row of η_1. Then

$$\eta_{1i} = F_i(Z_i, X, t) + G_i(Z, X, t)$$

where the following estimates are satisfied

$$\begin{aligned} |F_i(Z_i, X, t)| &\leq \tilde{C}|a|(|Z_i| + ||X||) \\ |G_i(Z, X, t)| &\leq \epsilon\tilde{K}|a|(||Z|| + ||X||) \end{aligned}$$

for some fixed constants $\tilde{C}, \tilde{K} < \infty$.

(iv) Furthermore we find

$$\eta_2 = E(X, t) + H(Z, X, t)$$

where the following estimates are satisfied

$$\begin{aligned} ||E(X, t)|| &\leq \hat{C}|a|||X|| \\ ||H(Z, X, t)|| &\leq \hat{K}(\epsilon + |b|)(||Z|| + ||X||) \end{aligned}$$

for some fixed constants $\hat{C}, \hat{K} < \infty$.

Proof. From the evolution equations (2.23) we find that

$$\begin{aligned} Z' &= \Lambda Z + \begin{pmatrix} aR_1 + \epsilon R_2 \\ aR_3 + \epsilon R_4 \end{pmatrix} \\ &= \Lambda Z + \begin{pmatrix} a(\Lambda_a Z_1 + \Lambda_b X_2 - \Lambda_{y_2} X_4) + \epsilon(g_{1b} X_1 + g_{1y_1} Z_1 + g_{1y_2} Z_2) \\ a(\Lambda_a Z_2 + \Lambda_b X_3 + \Lambda_{y_1} X_4) + \epsilon(g_{2b} X_1 + g_{2y_1} Z_1 + g_{2y_2} Z_2) \end{pmatrix} \end{aligned} \tag{2.26}$$

where letter subscripts denote the partial derivative with respect to the indicated variable; note that the antisymmetry property of differential forms has been used extensively in the calculation (2.26). From (2.26) we see that $Z' = \Lambda Z$

when $a = 0$ and $\epsilon = 0$. We also have

$$\begin{aligned} X' &= \begin{pmatrix} \Lambda + \Gamma & 0 & 0 & 0 \\ 0 & \Gamma & 0 & 0 \\ 0 & 0 & \Gamma & 0 \\ 0 & 0 & 0 & 0 \end{pmatrix} \begin{pmatrix} X_1 \\ X_2 \\ X_3 \\ X_4 \end{pmatrix} + \begin{pmatrix} aR_5 + bR_6 \\ bR_7 + \epsilon R_8 \\ bR_9 + \epsilon R_{10} \\ \epsilon R_{11} + \epsilon R_{12} \end{pmatrix} \\ &= BX + \begin{pmatrix} a(\Lambda_a X_1 - \Lambda_{y_1} X_2 - \Lambda_{y_2} X_3) + b(\Gamma_b X_1 + \Gamma_{y_1} Z_1 + \Gamma_{y_2} Z_2) \\ b(\Gamma_a Z_1 + \Gamma_b X_2 - \Gamma_{y_2} X_4) + \epsilon(-g_{1a} X_1 + g_{1y_1} X_2 + g_{1y_2} X_3) \\ b(\Lambda_a Z_2 + \Lambda_b X_3 + \Lambda_{y_1} X_4) + \epsilon(-g_{2a} X_1 + g_{2y_1} X_2 + g_{2y_2} X_3) \\ \epsilon(-g_{1a} Z_1 - g_{1b} X_2 + g_{1y_2} X_4 + g_{1a} Z_2 + g_{2b} X_3 + g_{2y_1} X_4) \end{pmatrix} \end{aligned} \tag{2.27}$$

Hence for $a = 0$, $b = 0$ and $\epsilon = 0$ we must have $\eta_2 = 0$ which completes the proof of (i). For (ii) note that

$$B - \Lambda(Id) = \begin{pmatrix} \Gamma & 0 & 0 & 0 \\ 0 & \Gamma - \Lambda & 0 & 0 \\ 0 & 0 & \Gamma - \Lambda & 0 \\ 0 & 0 & 0 & -\Lambda \end{pmatrix} \tag{2.28}$$

Recall that $\Lambda \geq \Lambda_0 > 0$ and $\Gamma \leq \Gamma_0 < 0$ for (z, ϵ) in a suitable compact subset, which we called $\mathfrak{B}$, near the critical manifold by Fenichel Normal Form Theory. Therefore the matrix in (2.28) has eigenvalues bounded above by some negative fixed number, say $-\mu$ with $\mu > 0$; using this observation (ii) follows. We can group the terms on the right-hand side in (2.26) as follows:

$$\begin{aligned} F_1(Z_1, X, t) &:= a(\Lambda_a Z_1 + \Lambda_b X_2 - \Lambda_{y_2} X_4) \\ G_1(Z, X, t) &:= \epsilon(g_{1b} X_1 + g_{1y_1} Z_1 + g_{1y_2} Z_2) \\ F_2(Z_2, X, t) &:= a(\Lambda_a Z_2 + \Lambda_b X_3 + \Lambda_{y_1} X_4) \\ G_2(Z, X, t) &:= \epsilon(g_{2b} X_1 + g_{2y_1} Z_1 + g_{2y_2} Z_2) \end{aligned}$$

Using the triangle inequality we arrive at the estimates required in (iii). Now set $E(X, t)$ equal to all the terms of $X' - BX$ that do not vanish at $b = 0$ and $\epsilon = 0$.

Then let $H(Z, X, t) := X' - BX - E(X, t)$ and use the triangle inequality again. This shows (iv) and completes the proof. □

Step 3: We want to incorporate the assumptions of the Exchange Lemma into estimates on the initial conditions of Z_i and X_i at q. We assumed that the trajectory spends at least $O(1/\epsilon)$ in a box $\mathfrak{B}$ and we also have a transversality condition at the entry point q. This will constrain the values of (Z, X) on T_qM. Let $\hat{X}_i := X_i/Z_1$ and $\hat{Z}_2 = Z_2/Z_1$ as suggested in the differential form version of the Exchange Lemma in Theorem 2.4.2.

Lemma 2.5.2. *There exists $\bar{K} > 0$ such that at T_qM we have $|Z_1| > \bar{K}\epsilon$, $|\hat{X}_i| < 1/(\bar{K}\epsilon)$ and $|\hat{Z}_2|$ is exponentially small.*

Proof. Recall that we defined evaluating forms on T_qM as evaluating them on a projected unit hypercube. Therefore we must have $|X_i(T_qM)| \leq 1$. Since T_qM is transverse with respect to $\{|a| = 0\}$ we find that there is a $\bar{K}$ such that $|Z_1(T_qM)| > \bar{K}\epsilon$. Therefore

$$|\hat{X}_i(T_qM)| = \frac{|X_i(T_qM)|}{|Z_1(T_qM)|} < 1/(\bar{K}\epsilon).$$

It remains to show that $|\hat{Z}_2|$ is exponentially small and so we must try to estimate $|Z_2|$. Here we view T_qM as spanned by two vectors, one defined by the vector field (2.21), denoted by v, and a vector orthogonal to it in T_qM, say $v^\perp$. Up to a scalar multiple we find that

$$|Z_2(T_qM)| = \text{const} \cdot \left| \det \begin{pmatrix} v_1 & v_4 \\ v_1^\perp & v_4^\perp \end{pmatrix} \right| = \text{const} \cdot |v_1 v_4^\perp - v_4 v_1^\perp| \tag{2.29}$$

since evaluating the differential form $da \wedge dy_2 = Z_2$ on two vectors amounts to picking out the a and y_2 components and then applying the determinant. By the definition of v we look at equation (2.21) and see that $|v_1|$ is $O(|a|)$. Since $|v_4^\perp|$

is bounded by a constant we have an $O(|a|)$ estimate on the first term of (2.29). Next, we recall that the equation for y_2' in the Fenichel Normal form is

$$y_2' = \epsilon g_2(z, \epsilon) = \epsilon(H_2(a, b, y, \epsilon)ab)$$

This means that v_4 also contains a multiplicative factor of $O(|a|)$ when we estimate it. If we could show that $|a|$ is exponentially small at q then the result will follow easily. Indeed, Lemma 2.3.1 says that the a-coordinate will expand at least by a positive rate $\Lambda_0 > 0$ inside $\mathfrak{B}$. Now we use the hypothesis that the trajectory through q stays an $O(1/\epsilon)$ time in $\mathfrak{B}$ and therefore $|a|$ must have been exponentially small at q

$$|a| < k_1 e^{-k_2/\epsilon} \qquad \text{for some constants } k_i > 0.$$

Hence $|Z_2|$ is exponentially small which immediately yields that $|\hat{Z}_2|$ is exponentially small. □

Step 4: Our next goal is to estimate the size of $\hat{Z}_i$ and $\hat{X}_i$ evaluated on the tangent space to M which evolves under the flow. Our reference solution is the trajectory starting at q and ending up at $\bar{q}$. We know from Lemma 2.5.2 that $|Z_1| > \bar{K}\epsilon$ which means that in a neighbourhood of q the projectivized forms are well-defined (i.e. the denominator is nonzero). The next lemma provides this well-definedness inside $\mathfrak{B}$.

Lemma 2.5.3. *There is a constant $C > 0$ such that*

$$|Z_1|' \geq (\Lambda - C|a|(1 + ||\hat{X}|| + \epsilon||\hat{Z}||))|Z_1| \tag{2.30}$$

Proof. First, we work near q, then $|Z_1| \neq 0$ and so we calculate:

$$\begin{aligned} |Z_1|' &= \frac{d}{dt}\sqrt{Z_1^2} = \frac{2Z_1'Z_1}{2\sqrt{Z_1^2}} \\ &= \frac{\Lambda Z_1^2}{|Z_1|} + \frac{\eta_{11}Z_1}{|Z_1|} = \Lambda|Z_1| + \frac{\eta_{11}Z_1}{|Z_1|} \end{aligned}$$

Using Lemma 2.5.1 we then find that

$$\begin{aligned} |Z_1|' &\geq \Lambda|Z_1| - (|F_1| + |G_1|) \\ &\geq (\Lambda - \tilde{C}|a|)|Z_1| - \tilde{C}|a|\|X\| - \epsilon\tilde{K}|a|(\|Z\| + \|X\|) \end{aligned}$$

Now choose C such that $C > \tilde{C} + \epsilon\tilde{K}$ and $C > \tilde{K}$ and we obtain (2.30) near q. By making the box $\mathfrak{B}$ sufficiently small we can make $|a|$ small enough so that, since $\Lambda \geq \Lambda_0 > 0$, we always have

$$(\Lambda - C|a|(1 + \|\hat{X}\| + \epsilon\|\hat{Z}\|)) > 0$$

Hence we find near q that $|Z_1|' > 0$ and so $|Z_1|$ is increasing; if we now leave a neighbourhood of q then we still have $|Z_1| > \bar{K}\epsilon$. Repeating the argument above in a compact set away from q and covering $\mathfrak{B}$ by finitely many compact sets yields $|Z_1| \neq 0$ inside $\mathfrak{B}$ and the estimate (2.30). □

Step 5: The next lemma is fundamental to control $\hat{Z}_i$ inside $\mathfrak{B}$.

Lemma 2.5.4. *There are constants $C, K > 0$, where C is as in Lemma 2.5.3, so that the following inequalities hold*

$$|\hat{Z}_i|' \leq (\alpha(t) + 2C|a|)|\hat{Z}_i| + \alpha(t) \tag{2.31}$$

$$\|\hat{X}_i\| \leq \bar{M}\left[\|\hat{X}_0\|e^{\int_0^t \beta_1(s)ds} + \int_0^t e^{\int_s^t \beta_1(r)dr}\beta_2(s)ds\right] \tag{2.32}$$

where α, β_1 and β_2 are:

$$\begin{aligned}
\alpha(t) &= C|a|(\|\hat{X}\| + \epsilon(1 + \|\hat{Z}\|)) \\
\beta_1(t) &= -\mu + C(\delta + |a|\|\hat{X}\|) \\
\beta_2(t) &= K[(\epsilon + |b| + \epsilon|a|\|\hat{X}\|)\|\hat{Z}\| + \epsilon + |b|]
\end{aligned}$$

The constant $\mu > 0$ carries over from Lemma 2.5.1 and $\delta > 0$ defines the neighbourhood size of $\mathfrak{B}$ as given in (2.22).

Proof. We start by proving (2.31). A direct calculation as in the previous lemma gives

$$|\hat{Z}_i|' = -\frac{\eta_{11}\hat{Z}_i^2}{Z_1|\hat{Z}_i|} + \frac{\eta_{1i}\hat{Z}_i}{Z_1|\hat{Z}_i|} \tag{2.33}$$

The chain and quotient rules used for calculating (2.33) are only valid for $|Z_i| \neq 0$, when $Z_i = 0$ we only obtain left and right limits for the derivative of opposite sign. If we estimate the right-hand side of (2.33) then

$$|\hat{Z}_i|' \leq \left|\frac{\eta_{11}}{Z_1}\right| |\hat{Z}_i| + \left|\frac{\eta_{1i}}{Z_1}\right|$$

which is independent of such left and right limits. Using Lemma 2.5.1 again we find

$$\begin{aligned}
\left|\frac{\eta_{11}}{Z_1}\right| &\leq \tilde{C}|a|(1 + \|\hat{X}\|) + \epsilon\tilde{K}|a|(1 + \|\hat{Z}\| + \|\hat{X}\|) \\
\left|\frac{\eta_{1i}}{Z_1}\right| &\leq \tilde{C}|a|(|\hat{Z}_i| + \|\hat{X}\|) + \epsilon\tilde{K}|a|(1 + \|\hat{Z}\| + \|\hat{X}\|)
\end{aligned}$$

The desired estimate (2.31) now follows if we choose C again such that $C > \tilde{C} + \epsilon\tilde{K}$ and $C > \tilde{K}$. This completes the first part of the proof. For the second part we again use calculus first:

$$\begin{aligned}
\hat{X}_i' &= \frac{d}{dt}\left(\frac{X_i}{Z_1}\right) = \frac{Z_1X_i' - X_iZ_1'}{Z_1^2} \\
&= \frac{Z_1(B_{ii}X_i + \eta_{2i}) - X_i(\Lambda Z_1 + \eta_{11})}{Z_1^2} \\
&= (B_{ii} - \Lambda)\hat{X}_i + \left[\frac{\eta_{2i}}{Z_1} - \frac{\eta_{11}}{Z_1}\hat{X}_i\right]
\end{aligned}$$

This result can be written more compactly in vector form as:

$$\hat{X}' = (B - \Lambda)\hat{X} + \left[\frac{\eta_2}{Z_1} - \frac{\eta_{11}}{Z_1}\hat{X}\right]$$

From Lemma 2.5.1 we get that

$$\left\|\frac{\eta_2}{Z_1}\right\| \leq \hat{C}|a|\|\hat{X}\| + \hat{K}(\epsilon + |b|)(1 + \|\hat{Z}\| + \|\hat{X}\|)$$

Since we have already found an estimate on $|\eta_{11}/Z_1|$ above it now follows that

$$\left|\frac{\eta_2}{Z_1} - \frac{\eta_{11}}{Z_1}\hat{X}\right| \leq \beta_3(t)\|\hat{X}\| + \beta_2(t) \tag{2.34}$$

where

$$\beta_3(t) = C^*|a|(1 + \|\hat{X}\|) + K(\epsilon + |b|)$$

and the constants are chosen so that $C^* > \tilde{C} + \epsilon\tilde{K} + \tilde{C}$ and $K > \max(\tilde{K}, \hat{K})$. Basically the estimate (2.34) controls the nonlinear term for the equations of $\hat{X}$. We proceed by considering an integrating factor:

$$J(t) := \exp\left(-\int_0^t (B - \Lambda\mathrm{Id})ds\right)$$

The standard integrating factor calculation then reads

$$\begin{aligned}
& \hat{X}'J - (B - \Lambda)\hat{X}J = J\left[\frac{\eta_2}{Z_1} - \frac{\eta_{11}}{Z_1}\hat{X}\right] \\
\Rightarrow \quad & (\hat{X}J)' = J\left[\frac{\eta_2}{Z_1} - \frac{\eta_{11}}{Z_1}\hat{X}\right] \\
\Rightarrow \quad & \int_0^t (\hat{X}J)'ds = \int_0^t J\left[\frac{\eta_2}{Z_1} - \frac{\eta_{11}}{Z_1}\hat{X}\right]ds \\
\Rightarrow \quad & \hat{X} = J(t)^{-1}\hat{X}_0 + J(t)^{-1}\int_0^t J\left[\frac{\eta_2}{Z_1} - \frac{\eta_{11}}{Z_1}\hat{X}\right]ds
\end{aligned}$$

The inverse of the matrix $J(t)$ is

$$J(t)^{-1} = \exp\left(\int_0^t (B - \Lambda\mathrm{Id})ds\right)$$

Recall from Lemma 2.5.1 that we have the estimate

$$\exp\left(\int_s^t (B - \Lambda \mathrm{Id})dr\right) \leq \bar{M}e^{-\mu(t-s)}$$

Therefore we can now estimate $\|\hat{X}\|$ as follows:

$$\begin{aligned} \|\hat{X}\| &\leq \|J(t)^{-1}\hat{X}_0\| + \int_0^t \|J(t)^{-1}J(s)\| \left\| \frac{\eta_2}{Z_1} - \frac{\eta_{11}}{Z_1}\hat{X} \right\| ds \\ &\leq \bar{M}\left[e^{-\mu t}\|\hat{X}_0\| + \int_0^t e^{-\mu(t-s)}(\beta_3(s)\|\hat{X}\| + \beta_2(s))ds \right] \end{aligned} \tag{2.35}$$

The last equation is in a form to apply a generalized Gronwall inequality which states that if $u, v, c \geq 0$, c is differentiable and $v(t) \leq c(t) + \int_0^t u(s)v(s)ds$ then

$$v(t) \leq c(0)\exp\int_0^t u(s)ds + \int_0^t c'(s)\left[\exp\int_s^t u(r)dr\right]ds$$

For a proof see [20]. If we multiply (2.35) by $e^{\mu t}$ and apply the generalized Gronwall inequality we obtain:

$$e^{\mu t}\|\hat{X}\| \leq \bar{M}\left[\|\hat{X}_0\| e^{\int_0^t \beta_3(s)ds} + \int_0^t e^{\mu s}\beta_2(s)e^{\int_s^t \beta_3(r)dr}ds \right]$$

We know from the size of the neighbourhood/box $\mathfrak{B}$ that $|a| < \delta$ and $|b| < \delta$ and so

$$-\mu + \beta_3 \leq -\mu + C(\delta + |a|\|\hat{X}\|) = \beta_1$$

where C is chosen so that $C > C^* + 2K\delta$ and ϵ is sufficiently small, in particular less than δ. Since we have that

$$e^{-\mu(t-s)} = \exp\int_s^t (-\mu)dr$$

the final result (2.32) follows. □

Step 6: Having all the estimates in place we can proceed to the proof of the Exchange Lemma.

Proof. (of Theorem 2.4.2) The argument consists of three parts which are quite typical for many multiple time scale proofs:

1. Follow the trajectory from q for an $O(1/\epsilon)$ time until $|b|$ is exponentially small; this describes the approach towards the slow manifold

$$S_\epsilon = \{a = 0, b = 0\}.$$

2. Follow the trajectory while $|a|$ and $|b|$ stay exponentially small near S_ϵ.
3. Consider the region where $|a|$ grows to $\delta > 0$; this captures the departure from S_ϵ.

Let $T = O(1/\epsilon)$ denote the time the trajectory from q to $\bar{q}$ takes to pass through $\mathfrak{B}$. We can assume without loss of generality that q corresponds to $t = 0$.

Part 1: Let $T_1 \in (0, T)$ be a time of order $O(1/\epsilon)$ such that $|a|$ is exponentially small for $t < T_1$. Then at $t = T_1$ we have that $\|\hat{Z}\|$ is exponentially small and $\|\hat{X}\| = O(\epsilon + \delta)$.

Proof of Part 1: Clearly there is such a time T_1 by Lemma 2.3.1 since if T_1 would not exist then the trajectory would already leave $\mathfrak{B}$ before T. We will assume that $\|\hat{Z}\| \leq 1$ and $\|\hat{X}\| \leq 1/(\bar{K}\epsilon)$ for $t \in (0, T_1)$; this will be justified at the end of the proof for Step 1. Recall from Lemma 2.5.2 that $\|\hat{X}(0)\| \leq 1/(\bar{K}\epsilon)$. Note that we have

$$\beta_1(t) \leq -\mu/2 \tag{2.36}$$

$$\beta_2(t) \leq 2K(\epsilon + \delta) \tag{2.37}$$

since $|a|$ is exponentially small, $|b| \leq \delta$ and $\|\hat{Z}\| \leq 1$ (see Lemma 2.5.4). Then we can use (2.32) and get

$$\begin{aligned} \|\hat{X}_i\| &\leq \bar{M}\left[\|\hat{X}_0\| e^{\int_0^t \beta_1(s)ds} + \int_0^t e^{\int_s^t \beta_1(r)dr}\beta_2(s)ds\right] \\ &\leq \bar{M}\left[\frac{1}{\bar{K}\epsilon}e^{-\frac{\mu}{2}t} + \int_0^t e^{-\frac{\mu}{2}(t-s)}2K(\epsilon+\delta)ds\right] \\ &\leq \bar{M}\left[\frac{1}{\bar{K}\epsilon}e^{-\frac{\mu}{2}t} + \frac{4K}{\mu}(\epsilon+\delta)\right] \end{aligned} \tag{2.38}$$

Looking at (2.38) we see that the first term is exponentially small for $T_1 = O(1/\epsilon)$ and so we have $\|\hat{X}\| \leq O(\epsilon+\delta)$. Since $|a|$ is exponentially small we also have

$$\alpha(t) + 2C|a| \leq K_2 e^{-c_2/\epsilon} =: \kappa \tag{2.39}$$

for some $K_2, c_2 > 0$. Using (2.31) and the usual Gronwall Lemma we compute

$$\begin{aligned} |\hat{Z}_i(t)| &\leq |\hat{Z}_i|e^{\kappa t} + \int_0^t e^{\kappa(t-s)}\kappa ds \\ &= |\hat{Z}_i(0)|e^{\kappa t} + e^{\kappa t} - 1 \end{aligned} \tag{2.40}$$

But since κ is exponentially small and $t \leq O(1/\epsilon)$ we see that κt must be exponentially small. But $e^{\kappa t} - 1 \approx \kappa t$ which means that the second term of (2.40) is exponentially small. In Lemma 2.5.2 we showed that $|\hat{Z}_i(0)|$ is exponenentially small and this implies that $|\hat{Z}_i|$ is exponentially small. This establishes the two estimates we want for Step 1 as long as we can show that $\|\hat{Z}\| \leq 1$ and $\|\hat{X}\| \leq 1/(\bar{K}\epsilon)$. Indeed, we know that $|\hat{Z}_i(0)|$ is exponenentially small and so there is a time $0 < t^* \leq T_1$ such that $\|\hat{Z}\| \leq 1$ for $t \in [0, t^*]$. Up to this time the estimates derived so far hold which means that at $t = t^*$ we have $\|\hat{Z}\|$ exponentially small; now we can just cover $[0, T_1]$ by a finite number of time intervals. Applying a similar argument to the assumed estimate for $\|\hat{X}\|$ we get the result.

Part 2: Let $T_2 < T_2 < T$ be any time $T_2 = O(1/\epsilon)$ such that $T - T_2 = O(1/\epsilon)$ and for $t \in [T_1, T_2]$ we have $|a|$ and $|b|$ exponentially. Then at $t = T_2$, $\|\hat{X}\| = O(\epsilon)$ and

$\|\hat{Z}\|$ is still exponentially small.

Proof of Part 2: We can repeat the argument of Step 1 and notice that we can improve on the estimate of β_2 since $|b|$ is now exponentially small to get

$$\beta_2 \leq 2K\epsilon$$

Then looking at (2.38) we find that

$$\|\hat{X}\| \leq 4\bar{M}K\epsilon/\mu + \text{exp. small terms} \tag{2.41}$$

With respect to $\|\hat{Z}\|$ the estimate (2.40) is still valid which completes the proof of Step 2.

Note that our strategy so far was to assume some crude priori bounds on $\|\hat{Z}\|$ and $\|\hat{X}\|$. Then in Steps 1 and 2 it was shown that the a priori bounds can be refined on a compact time interval. Hence we were able to cover the desired time intervals $[0, T_1]$ and $[T_1, T_2]$ by a finite number of subintervals; at the left endpoints of the subintervals the a priori ones held. The third step is proven by precisely the same strategy.

Part 3: In $[T_2, T]$, we have that $|b|$ is exponentially small and $|a| = O(\delta)$. Then it follows that at $t = T$, $\|\hat{X}\| = O(\epsilon)$ and $\|\hat{Z}\| = O(\epsilon)$.

Proof of Part 3: We consider the a priori bounds $\|\hat{Z}\| \leq 1$ and $\|\hat{X}\| \leq K_3\epsilon$ for some $K_3 > 0$ which are satisfied at T_2. Observe that for $\|\hat{X}\| = O(\epsilon)$ we find that $|a|\|\hat{X}\| = O(\epsilon)$ since $|a| \leq \delta$. This implies that for ϵ and δ sufficiently small we still

have the estimates (2.36) and (2.41). Using (2.32) as in Step 1 we get:

$$\|\hat{X}\| \leq \bar{M}\left[e^{-(\frac{\mu}{2})(t-T_2)}\|\hat{X}(T_2)\| + \frac{4K\epsilon}{\mu} + \text{exp. small terms}\right] \tag{2.42}$$

Therefore it follows that $\|\hat{X}\| = O(\epsilon)$. For $\|\hat{Z}\|$ we observe that the left-hand side of (2.39) non longer satisfies an exponential estimate since $\alpha(t) + 2C|a| = O(\delta)$. We have to look at $\alpha(t)$ again which is given by:

$$\begin{aligned} \alpha(t) &= C|a|(\|\hat{X}\| + \epsilon(1 + \|\hat{Z}\|)) \\ &\leq C|a|(K_3\epsilon + \epsilon(1+1)) = 3C|a|\epsilon(K_3 + 2) \end{aligned}$$

Applying Gronwall's Lemma again to (2.31) we find

$$|\hat{Z}_i(t)| \leq |\hat{Z}_i(T_2)|e^{3C\int_{T_2}^{t}|a|ds} + \epsilon\int_{T_2}^{t} e^{3C\int_{s}^{t}|a|dr}C(K_3+2)|a|ds \tag{2.43}$$

From Lemma (2.3.1) we know that $\int_{T_2}^{t}|a|ds$ and $\int_{s}^{t}|a|ds$ stay finite. Therefore the first term on the right-hand side of (2.43) is exponentially small and the second term is $O(\epsilon)$. This is precisely what is required for the differential form conclusion of the Exchange Lemma i.e. $\|\hat{X}\| = O(\epsilon)$ and $\|\hat{Z}\| = O(\epsilon)$ near the exit point $\bar{q}$. □

Remark: The proof presented here only applies to $\mathbb{R}^4$ but contains all necessary steps for more general cases. In particular, observe that the low-dimensionality significantly simplifies Lemma 2.5.1 which calculates the equations of motion for the differential forms. Once this Lemma is proved in higher-dimensional cases the rest of the proof carries over almost verbatim.

2.6 Fast Waves in FitzHugh-Nagumo Equation

Having the Exchange Lemma available we can proceed with the idea developed in Section 2.2. Recall that the goal is to prove the existence of a homoclinic orbit

in the FitzHugh-Nagumo equation

$$\begin{aligned} \epsilon \dot{x}_1 &= x_2 \\ \epsilon \dot{x}_2 &= \frac{1}{\delta}(s x_2 - x_1(1-x_1)(x_1 - a) + y) \\ \dot{y} &= \frac{1}{s}(x_1 - \gamma y) \end{aligned} \tag{2.44}$$

In contrast to the ideas developed in Section 2.1 we want to construct the homoclinic orbit as a perturbation of a singular solution consisting of two fast and two slow segments. The situation is shown in Figure 2.7.

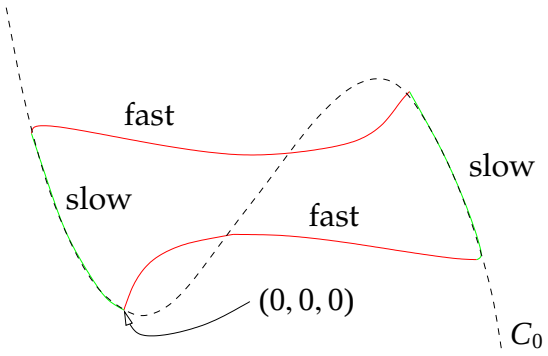

Figure 2.7: Sketch of the singular homoclinic orbit in the FitzHugh-Nagumo equation (2.44). It consists of two fast segments (red) and two slow segments (green).

Consider the FitzHugh-Nagumo equation in the singular limit $\epsilon = 0$. As discussed previously we know that there exists a wave speed s^* such that the fast subsystem defined by $y = 0$ at the height of the equilibrium has a heteroclinic connection between its two saddle equilibria $(x_1, x_2) = (0, 0)$ and $(x_1, x_2) = (1, 0)$. Then we follow the slow flow on the critical manifold C_r until we reach another fast subsystem with $y = y^* > 0$ that has another heteroclinic connection. We denote the two equilibria of this system by $(x^*_{1,r}, 0)$ and $(x^*_{1,l}, 0)$. After traversing the second heteroclinic connection we follow the slow flow on C_l down to the equilibrium $(0, 0, 0)$. The result we want to prove is:

Theorem 2.6.1. *If $\epsilon > 0$ is sufficiently small the FitzHugh-Nagumo equation* (2.44) *has a homoclinic orbit for a wave speed s that is $O(\epsilon)$ close to s^*. The homoclinic orbit lies within $O(\epsilon)$ Hausdorff-distance of the singular orbit and is locally unique.*

Before we describe the detailed proof we outline the strategy. Regarding $s \in [s^* - \delta, s^* + \delta]$ as a parameter the origin $0 = (0,0,0) = (x_1, x_2, y)$ in (2.15) has a one-dimensional unstable manifold $W^u(0,s)$; here $\delta > 0$ is assumed to be sufficiently small. If we take he union over all these parameter values we obtain a center-unstable manifold

$$W^{cu} = \bigcup_{s\in[s^*-\delta,s^*+\delta]} W^u(0,s)$$

We can view this manifold as the center-unstable manifold of the equilibrium the FitzHugh-Nagumo equation extended by $s' = 0$:

$$\begin{aligned} x_1' &= x_2 \\ x_2' &= \frac{1}{5}(sx_2 - f(x_1) + y) \\ y' &= \frac{\epsilon}{s}(x_1 - y) \\ s' &= 0 \end{aligned} \tag{2.45}$$

Similarly we consider the three-dimensional center-stable manifold W^{cs}. The goal is to show that W^{cu} intersects W^{cs} transversely in (x_1, x_2, y, s) space. Counting dimensions we get that if the intersection is transverse then the manifolds must intersect in a curve for some s_0 near s^*. Note that this value s_0 is fixed since there is no flow in the s-direction in (2.45). Hence we have a homoclinic orbit for $s = s_0$ which is locally unique. This "simplifies" the problem to demonstrating the transversality of W^{cu} and W^{cs}. Obviously we have to use information about the singular limit versions of these manifolds. If we set $\epsilon = 0$ in (2.45) and set $y = 0$ then we obtain a three-dimensional system which has a two-dimensional

center-unstable manifold $W^{cu}(0,0,s)$ to $(x_1,x_2)=(0,0)$. Similarly we get a two-dimensional center-stable manifold $W^{cs}(1,0,s)$ to the second saddle-equilibrium of the fast subsystem $(x_1,x_2)=(1,0)$. We want that the two manifolds intersect along the heteroclinic connection for $s=s^*$. The situation is abstractly shown in Figure 2.8.

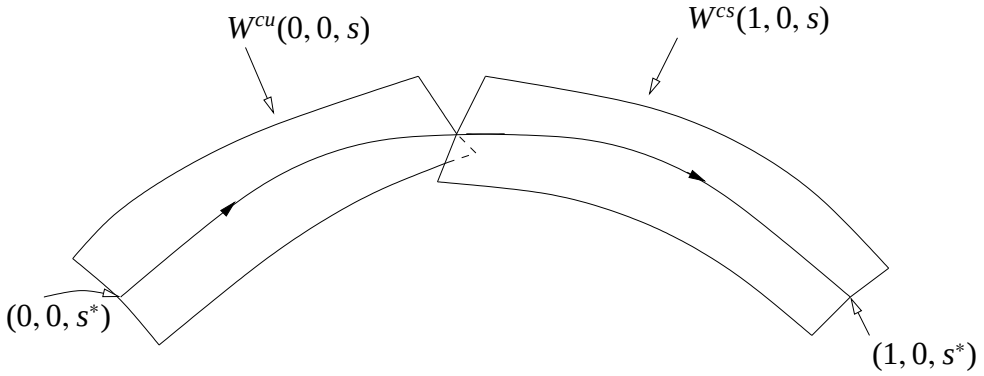

Figure 2.8: Sketch of transversal intersection of the manifolds $W^{cu}(0,0,s)$ and $W^{cs}(1,0,s)$.

The geometric reason for the transversal intersection is that the heteroclinic connection breaks for $s \neq s^*$. There are many ways to prove this claim but for now we shall just state it.

Lemma 2.6.2. *$W^{cu}(0,0,s)$ intersects $W^{cs}(1,0,s)$ transversely in (x_1,x_2,s) space along the curve defined by $s=s^*$.*

A similar result should hold for the second heteroclinic connection from C_r to C_l. Now fix $s=s^*$ and let y vary in a neighborhood of y^*.

Lemma 2.6.3. *$W^{cu}(x^*_{1,r},0,y)$ intersects $W^{cs}(x^*_{1,l},0,y)$ transversely in (x_1,x_2,y) space along the curve defined by $y=y^*$.*

The next step is to define $\bar{C_r}$ as the compact part of C_r given by $y\in[-\delta,y^*+\delta]$

and set $I_\delta := [s^* - \delta, s^* + \delta]$. We want to follow W^{cu} close to the slow manifold $S_{r,\epsilon}$ associated to $\overline{C_r} \times I_\delta$ using the Exchange Lemma. Having all definitions and preliminaries in place we can outline the proof of Theorem 2.6.1.

Proof. (of Theorem 2.6.1, Sketch, see [69]) We now work in the four-dimensional space (x_1, x_2, y, s) and with equation (2.45). For $\epsilon > 0$ sufficiently small we can assume that the center-unstable manifold W^{cu} is close to the singular object $W^{cu}(0, 0, s)$. The stability of transverse intersection under perturbation and Lemma 2.6.2 imply that W^{cu} intersects the stable manifold $W^s(S_{r,\epsilon})$ of the slow manifold $S_{r,\epsilon}$ transversely. Now we can apply the Exchange Lemma to follow W^{cu} close to $S_{r,\epsilon}$ and conclude that it can be followed for ϵ sufficiently small up to $y \approx y^*$ and that it leaves the vicinity of $S_{r,\epsilon}$ C^1-close to $W^u(S_{r,\epsilon})$. Note that the C^1 conclusion is crucial here for the following step.

Since W^{cu} is now C^1-close to $W^u(S_{r,\epsilon})$ it is also C^1-close to the singular object $W^{cu}(x^*_{1,r}, 0, y)$. Hence we can use Lemma 2.6.3 and the stability of transversal intersection (transversality is defined by a C^1 condition!) to conclude that W^{cu} intersects the stable manifold $W^s(S_{l,\epsilon})$ of the compact part of the slow manifold $S_{l,\epsilon}$ associated to $C_l \times I_\delta$ transversely. Now we can follow W^{cu} close to $S_{l,\epsilon}$. Since $S_{l,\epsilon}$ is very close to $C_l \times I_\delta$ for $\epsilon > 0$ sufficiently small by Fenichel Theory we have that W^{cu} - after we have followed it around - is close to the center-stable manifold of the origin W^{cs}. Hence can conclude the transversal intersection of two-dimensional manifold W^{cu} and the three-dimensional manifold W^{cs}. □

Remark: Note that this procedure not only defined a one-dimensional intersection curve fixing s_0 close to s^* but also fixed a value y_0 close to y^* determining

where the second "fast jump" occurred in the homoclinic orbit.

It remains to show Lemma 2.6.2 and Lemma 2.6.3. Since their proofs are very similar we only prove Lemma 2.6.2.

Proof. (of Lemma 2.6.2) We use differential forms as we did in the proof of the Exchange Lemma. Hence we look at the variational equations for the fast subsystem with $s' = 0$ appended are:

$$\begin{aligned} (dx_1)' &= dx_2 \\ (dx_2)' &= s dx_2 + x_2 ds - f'(x_1) dx_1 \\ (ds)' &= 0 \end{aligned}$$

We define 2-forms by a simplified notation, e.g. $P_{x_1x_2} = dx_1 \wedge dx_2$. The equation on 2-forms to use for the transversality argument is:

$$P'_{x_1x_2} = sP_{x_1x_2} + x_2 P_{x_1s} \tag{2.46}$$

This equation can be derived, as usual, by differentiating the form $dx_1 \wedge dx_2$ using the chain rule and the form of the variational equation. We want to look at $P_{x_1x_2}$ and P_{x_1s} evaluated on tangent planes to the manifolds $W^{cu}(0,0,s) =: M_u$ and $W^{cs}(1,0,s) =: M_s$. Note that we assume that the tangent vectors have been normalized before we evaluate the forms. We shall denote values of the forms on these planes by $P^{\pm}_{x_1x_2}$ and $P^{\pm}_{x_1s}$ where "+" indicates unstable and "-" indicates stable. Suppose we can show that $P^{+}_{x_1x_2}$ and $P^{+}_{x_1s}$ have the same sign and $P^{-}_{x_1x_2}$ and $P^{-}_{x_1s}$ have opposite signs. Now look at the vector of forms $(P_{x_1x_2}, P_{x_1s}, P_{x_2s})$. In this scenario they are linearly independent tangent vectors to M_u and M_s. This means that M_u and M_s intersect transversely.

Hence we reduced the problem to checking signs. Obviously M_u and M_s have the vector field $(x_2, sx_2 - f(x_1), 0)$ as tangent vector. Consider another tangent vector given by $(a^{\pm}, b^{\pm}, c = 1)$. We want to take the third coordinate to be 1 to assure that the vector is linearly independent from the vector field and this is justified since $(ds)' = 0$ (Check!). We can make the two vectors orthonormal using the Gram-Schmidt algorithm. We conclude that the forms $P^{\pm}_{\dots}$ are equal - up to a positive normalization factor $N > 0$ - to the corresponding 2×2 subdeterminant of the 2×3 matrix

$$\begin{pmatrix} x_2 & sx_2 - f(x_1) & 0 \\ a^{\pm} & b^{\pm} & 1 \end{pmatrix}$$

In particular for $P^{\pm}_{x_1 s}$ this means:

$$P^{\pm}_{x_1 s} = N \begin{vmatrix} x_2 & 0 \\ a^{\pm} & 1 \end{vmatrix} = N x_2$$

From the fast subsystem it follows that $x_2 > 0$ on M_u and M_s. Therefore $P^{\pm}_{x_1 s} = N x_2 > 0$ and equation (2.46) can be simplified to:

$$P^{\pm'}_{x_1 x_2} = s P_{x_1 x_2} + N (x_2)^2 \tag{2.47}$$

The next step is to look at the signs of $P^{\pm}_{x_1 x_2}$. Observe that M_u and M_s both have a line of equilibrium points with a tangent vector in the s-direction; this follows directly from the construction as we have appended the equation $s' = 0$. For any plane containing such a line the form $P_{x_1 x_2}$ must vanish. Suppose the time variable in the differential equations we have written down so far is t. Then if $t \to \infty$ we must have $P^{-}_{x_1 x_2} \to 0$ due to the location of the line of equilibrium points. This implies that $P_{x_1 x_2} < 0$ since equation (2.47) has a positive right-hand side for t sufficiently large. Similarly it follows that if $t \to -\infty$ then $P^{+}_{x_1 x_2} \to 0$ and so $P^{+}_{x_1 x_2} > 0$. This shows the sign condition we want. □

CHAPTER 3

PAPER I: "HOMOCLINIC ORBITS OF THE FITZHUGH-NAGUMO EQUATION: THE SINGULAR LIMIT"

3.1 Abstract

The FitzHugh-Nagumo equation has been investigated with a wide array of different methods in the last three decades. Recently a version of the equations with an applied current was analyzed by Champneys, Kirk, Knobloch, Oldeman and Sneyd [18] using numerical continuation methods. They obtained a complicated bifurcation diagram in parameter space featuring a C-shaped curve of homoclinic bifurcations and a U-shaped curve of Hopf bifurcations. We use techniques from multiple time-scale dynamics to understand the structures of this bifurcation diagram based on geometric singular perturbation analysis of the FitzHugh-Nagumo equation. Numerical and analytical techniques show that if the ratio of the time-scales in the FitzHugh-Nagumo equation tends to zero, then our singular limit analysis correctly represents the observed CU-structure. Geometric insight from the analysis can even be used to compute bifurcation curves which are inaccessible via continuation methods. The results of our analysis are summarized in a singular bifurcation diagram.

3.2 Introduction

3.2.1 Fast-Slow Systems

Fast-slow systems of ordinary differential equations (ODEs) have the general form:

$$\begin{aligned} \epsilon \dot{x} &= \epsilon \frac{dx}{d\tau} = f(x, y, \epsilon) \\ \dot{y} &= \frac{dy}{d\tau} = g(x, y, \epsilon) \end{aligned} \tag{3.1}$$

where $x \in \mathbb{R}^m$, $y \in \mathbb{R}^n$ and $0 \leq \epsilon \ll 1$ represents the ratio of time scales. The functions f and g are assumed to be sufficiently smooth. In the singular limit $\epsilon \to 0$ the vector field (3.1) becomes a differential-algebraic equation. The algebraic constraint $f = 0$ defines the critical manifold $C_0 = \{(x, y) \in \mathbb{R}^m \times \mathbb{R}^n : f(x, y, 0) = 0\}$. Where $D_x f(p)$ is nonsingular, the implicit function theorem implies that there exists a map $h(x) = y$ parameterizing C_0 as a graph. This yields the implicitly defined vector field $\dot{y} = g(h(y), y, 0)$ on C_0 called the slow flow.

We can change (3.1) to the fast time scale $t = \tau/\epsilon$ and let $\epsilon \to 0$ to obtain the second possible singular limit system

$$\begin{aligned} x' &= \frac{dx}{dt} = f(x, y, 0) \\ y' &= \frac{dy}{dt} = 0 \end{aligned} \tag{3.2}$$

We call the vector field (3.2) parametrized by the slow variables y the fast subsystem or the layer equations. The central idea of singular perturbation analysis is to use information about the fast subsystem and the slow flow to understand the full system (3.1). One of the main tools is Fenichel's Theorem (see

[39, 40, 41, 42]). It states that for every ϵ sufficiently small and C_0 normally hyperbolic there exists a family of invariant manifolds C_ϵ for the flow (3.1). The manifolds are at a distance $O(\epsilon)$ from C_0 and the flows on them converge to the slow flow on C_0 as $\epsilon \to 0$. Points $p \in C_0$ where $D_x f(p)$ is singular are referred to as fold points[1].

Beyond Fenichel's Theorem many other techniques have been developed. More detailed introductions and results can be found in [1, 71, 49] from a geometric viewpoint. Asymptotic methods are developed in [93, 47] whereas ideas from nonstandard analysis are introduced in [28]. While the theory is well developed for two-dimensional fast-slow systems, higher-dimensional fast-slow systems are an active area of current research. In the following we shall focus on the FitzHugh-Nagumo equation viewed as a three-dimensional fast-slow system.

3.2.2 The FitzHugh-Nagumo Equation

The FitzHugh-Nagumo equation is a simplification of the Hodgin-Huxley model for an electric potential of a nerve axon [65]. The first version was developed by FitzHugh [43] and is a two-dimensional system of ODEs:

$$\begin{aligned} \epsilon \dot{u} &= v - \frac{u^3}{3} + u + p \\ \dot{v} &= -\frac{1}{s}(v + \gamma u - a) \end{aligned} \tag{3.3}$$

[1]The projection of C_0 onto the x coordinates may have more degenerate singularities than fold singularities at some of these points.

A detailed summary of the bifurcations of (3.3) can be found in [97]. Nagumo et al. [94] studied a related equation that adds a diffusion term for the conduction process of action potentials along nerves:

$$\begin{cases} u_\tau = \delta u_{xx} + f_a(u) - w + p \\ w_\tau = \epsilon(u - \gamma w) \end{cases} \tag{3.4}$$

where $f_a(u) = u(u-a)(1-u)$ and p, γ, δ and a are parameters. A good introduction to the derivation and problems associated with (3.4) can be found in [62]. Suppose we assume a traveling wave solution to (3.4) and set $u(x,\tau) = u(x+s\tau) = u(t)$ and $w(x,\tau) = w(x+s\tau) = w(t)$, where s represents the wave speed. By the chain rule we get $u_\tau = su'$, $u_{xx} = u''$ and $w_\tau = sw'$. Set $v = u'$ and substitute into (3.4) to obtain the system:

$$\begin{aligned} u' &= v \\ v' &= \frac{1}{\delta}(sv - f_a(u) + w - p) \\ w' &= \frac{\epsilon}{s}(u - \gamma w) \end{aligned} \tag{3.5}$$

System (3.5) is the FitzHugh-Nagumo equation studied in this paper. Observe that a homoclinic orbit of (3.5) corresponds to a traveling pulse solution of (3.4). These solutions are of special importance in neuroscience [62] and have been analyzed using several different methods. For example, it has been proved that (3.5) admits homoclinic orbits [63, 15] for small wave speeds ("slow waves") and large wave speeds ("fast waves"). Fast waves are stable [70] and slow waves are unstable [44]. It has been shown that double-pulse homoclinic orbits [38] are possible. If (3.5) has two equilibrium points and heteroclinic connections exist, bifurcation from a twisted double heteroclinic connection implies the existence of multi-pulse traveling front and back waves [22]. These results are based on the assumption of certain parameter ranges for which we refer to the original

papers. Geometric singular perturbation theory has been used successfully to analyze (3.5). In [69] the fast pulse is constructed using the exchange lemma [72, 68, 14]. The exchange lemma has also been used to prove the existence of a codimension two connection between fast and slow waves in (s, ϵ, a)-parameter space [82]. An extension of Fenichel's theorem and Melnikov's method can be employed to prove the existence of heteroclinic connections for parameter regimes of (3.5) with two fixed points [103]. The general theory of relaxation oscillations in fast-slow systems applies to (3.5) (see e.g. [93, 51]) as does - at least partially - the theory of canards (see e.g. [104, 35, 37, 86]).

The equations (3.5) have been analyzed numerically by Champneys, Kirk, Knobloch, Oldeman and Sneyd [18] using the numerical bifurcation software AUTO [32, 33]. They considered the following parameter values:

$$\gamma = 1, \qquad a = \frac{1}{10}, \qquad \delta = 5$$

We shall fix those values to allow comparison of our results with theirs. Hence we also write $f_{1/10}(u) = f(u)$. Changing from the fast time t to the slow time τ and relabeling variables $x_1 = u$, $x_2 = v$ and $y = w$ we get:

$$\begin{aligned} \epsilon \dot{x}_1 &= x_2 \\ \epsilon \dot{x}_2 &= \frac{1}{5}(s x_2 - x_1(x_1 - 1)(\frac{1}{10} - x_1) + y - p) = \frac{1}{5}(s x_2 - f(x_1) + y - p) \\ \dot{y} &= \frac{1}{s}(x_1 - y) \end{aligned} \tag{3.6}$$

From now on we refer to (3.6) as "the" FitzHugh-Nagumo equation. Investigating bifurcations in the (p, s) parameter space one finds C-shaped curves of homoclinic orbits and a U-shaped curve of Hopf bifurcations; see Figure 3.1. Only part of the bifurcation diagram is shown in Figure 3.1. There is another

curve of homoclinic bifurcations on the right side of the U-shaped Hopf curve. Since (3.6) has the symmetry

$$x_1 \to \frac{11}{15} - x_1, \quad x_2 \to \frac{11}{15} - x_2, \quad y \to -y, \quad p \to \frac{11}{15}\left(1 - \frac{33}{225}\right) - p \tag{3.7}$$

we shall examine only the left side of the U-curve. The homoclinic C-curve is difficult to compute numerically by continuation methods using AUTO [32, 33] or MatCont [46]. The computations seem infeasible for small values of $\epsilon \leq 10^{-3}$. Furthermore multi-pulse homoclinic orbits can exist very close to single pulse ones and distinguishing between them must necessarily encounter problems with numerical precision [18]. The Hopf curve and the bifurcations of limit cycles shown in Figure 3.1 have been computed using MatCont. The curve of homoclinic bifurcations has been computed by a new method to be described in Section 3.4.2.

Since the bifurcation structure shown in Figure 3.1 was also observed for other excitable systems, Champneys et al. [18] introduced the term CU-system. Bifurcation analysis from the viewpoint of geometric singular perturbation theory has been carried out for examples with one fast and two slow variables [60, 11, 50, 92]. Since the FitzHugh-Nagumo equation has one slow and two fast variables, the situation is quite different and new techniques have to be developed. Our main goal is to show that many features of the complicated 2-parameter bifurcation diagram shown in Figure 3.1 can be derived with a combination of techniques from singular perturbation theory, bifurcation theory and robust numerical methods. We accurately locate where the system has canards and determine the orbit structure of the homoclinic and periodic orbits associated to the C-shaped and U-shaped bifurcation curves, without computing the canards themselves. We demonstrate that the basic CU-structure of the system

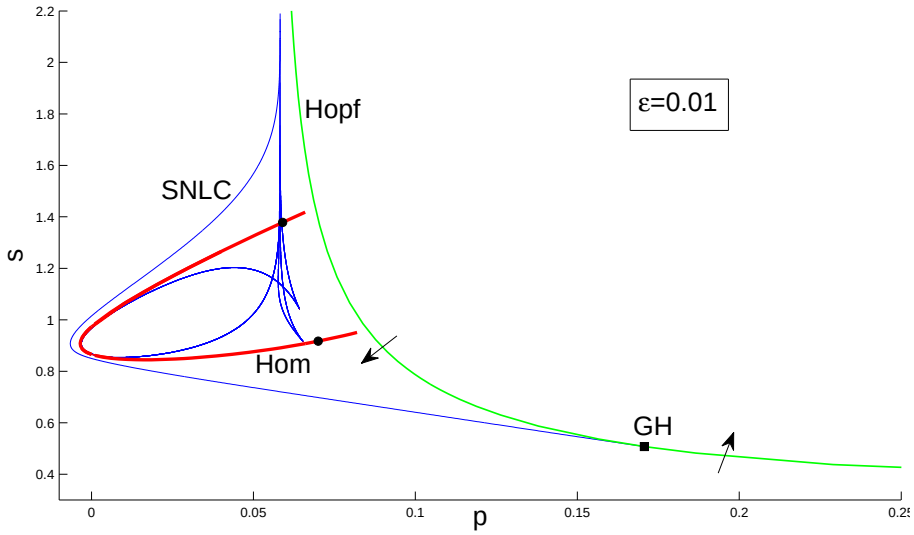

Figure 3.1: Bifurcation diagram of (3.6). Hopf bifurcations are shown in green, saddle-node of limit cycles (SNLC) are shown in blue and GH indicates a generalized Hopf (or Bautin) bifurcation. The arrows indicate the side on which periodic orbits are generated at the Hopf bifurcation. The red curve shows (possible) homoclinic orbits; in fact, homoclinic orbits only exist to the left of the two black dots (see Section 3.4.2). Only part of the parameter space is shown because of the symmetry (3.7). The homoclinic curve has been thickened to indicate that multipulse homoclinic orbits exist very close to single pulse ones (see [38]).

can be computed with elementary methods that do not use continuation methods based on collocation. The analysis of the slow and fast subsystems yields a "singular bifurcation diagram" to which the basic CU structure in Figure 3.1 converges as $\epsilon \to 0$.

Remark: We have also investigated the termination mechanism of the C-shaped homoclinic curve described in [18]. Champneys et al. observed that the homoclinic curve does not reach the U-shaped Hopf curve but turns around and folds back close to itself. We compute accurate approximations of the ho-

moclinic orbits for smaller values ϵ than seems possible with AUTO in this region. One aspect of our analysis is a new algorithm for computing invariant slow manifolds of saddle type in the full system. This work will be described elsewhere.

3.3 The Singular Limit

The first step in our analysis is to investigate the slow and fast subsystems separately. Let $\epsilon \to 0$ in (3.6); this yields two algebraic constraints that define the critical manifold:

$$C_0 = \left\{ (x_1, x_2, y) \in \mathbb{R}^3 : x_2 = 0 \quad y = x_1(x_1 - 1)(\frac{1}{10} - x_1) + p = c(x_1) \right\}$$

Therefore C_0 is a cubic curve in the coordinate plane $x_2 = 0$. The parameter p moves the cubic up and down inside this plane. The critical points of the cubic are solutions of $c'(x_1) = 0$ and are given by:

$$x_{1,\pm} = \frac{1}{30}\left(11 \pm \sqrt{91}\right) \qquad \text{or numerically:} \quad x_{1,+} \approx 0.6846, \quad x_{1,-} \approx 0.0487$$

The points $x_{1,\pm}$ are fold points with $|c''(x_{1,\pm})| \neq 0$ since C_0 is a cubic polynomial with distinct critical points. The fold points divide C_0 into three segments

$$C_l = \{x_1 < x_{1,-}\} \cap C_0, \quad C_m = \{x_{1,-} \leq x_1 \leq x_{1,+}\} \cap C_0, \quad C_r = \{x_{1,+} < x_1\} \cap C_0$$

We denote the associated slow manifolds by $C_{l,\epsilon}$, $C_{m,\epsilon}$ and $C_{r,\epsilon}$. There are two possibilities to obtain the slow flow. One way is to solve $c(x_1) = y$ for x_1 and substitute the result into the equation $\dot{y} = \frac{1}{s}(x_1 - y)$. Alternatively differentiating $y = c(x_1)$ implicitly with respect to τ yields $\dot{y} = \dot{x}_1 c'(x_1)$ and therefore

$$\frac{1}{s}(x_1 - y) = \dot{x}_1 c'(x_1) \qquad \Rightarrow \qquad \dot{x}_1 = \frac{1}{sc'(x_1)}(x_1 - c(x_1)) \tag{3.8}$$

One can view this as a projection of the slow flow, which is constrained to the critical manifold in $\mathbb{R}^3$, onto the x_1-axis. Observe that the slow flow is singular at the fold points. Direct computation shows that the fixed point problem $x_1 = c(x_1)$ has only a single real solution. This implies that the critical manifold intersects the diagonal $y = x_1$ only in a single point x_1^* which is the unique equilibrium of the slow flow (3.8). Observe that $q = (x_1^*, 0, x_1^*)$ is also the unique equilibrium of the full system (3.6) and depends on p. Increasing p moves the equilibrium from left to right on the critical manifold. The easiest practical way to determine the direction of the slow flow on C_0 is to look at the sign of $(x_1 - y)$. The situation is illustrated in Figure 3.2.

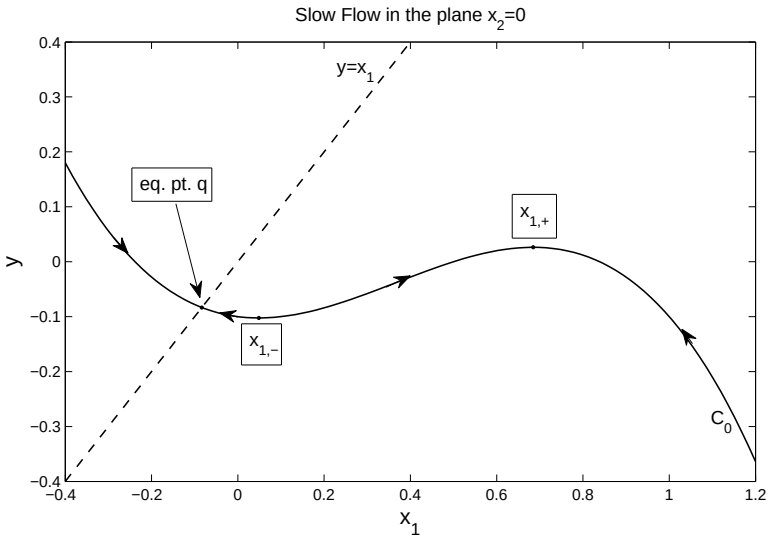

Figure 3.2: Sketch of the slow flow on the critical manifold C_0

3.3.1 The Slow Flow

We are interested in the bifurcations of the slow flow depending on the parameter p. The bifurcations occur when x_1^* passes through the fold points. The values

of p can simply be found by solving the equations $c'(x_1) = 0$ and $c(x_1) - x_1 = 0$ simultaneously. The result is:

$$p_- \approx 0.0511 \qquad \text{and} \qquad p_+ \approx 0.5584$$

where the subscripts indicate the fold point at which each equilibrium is located.

The singular time-rescaling $\bar{\tau} = sc'(x_1)/\tau$ of the slow flow yields the desingularized slow flow

$$\frac{dx_1}{d\bar{\tau}} = x_1 - c(x_1) = x_1 + \frac{x_1}{10}(x_1 - 1)(10x_1 - 1) - p \tag{3.9}$$

Time is reversed by this rescaling on C_l and C_r since $s > 0$ and $c'(x_1)$ is negative on these branches. The desingularized slow flow (3.9) is smooth and has no bifurcations as p is varied.

3.3.2 The Fast Subsystem

The key component of the fast-slow analysis for the FitzHugh-Nagumo equation is the two-dimensional fast subsystem

$$\begin{aligned} x_1' &= x_2 \\ x_2' &= \frac{1}{5}(sx_2 - x_1(x_1 - 1)(\frac{1}{10} - x_1) + y - p) \end{aligned} \tag{3.10}$$

where $p \geq 0$, $s \geq 0$ are parameters and y is fixed. Since y and p have the same effect as bifurcation parameters we set $p - y = \bar{p}$. We consider several fixed y-values and the effect of varying p (cf. Section 3.4.2) in each case. There are either one, two or three equilibrium points for (3.10). Equilibrium points satisfy $x_2 = 0$ and lie on the critical manifold, i.e. we have to solve

$$0 = x_1(x_1 - 1)(\frac{1}{10} - x_1) + \bar{p} \tag{3.11}$$

for x_1. We find that there are three equilibria for approximately $\bar{p}_l = -0.1262 < \bar{p} < 0.0024 = \bar{p}_r$, two equilibria on the boundary of this p interval and one equilibrium otherwise. The Jacobian of (3.10) at an equilibrium is

$$A(x_1) = \begin{pmatrix} 0 & 1 \\ \frac{1}{50}\left(1 - 22x_1 + 30x_1^2\right) & \frac{s}{5} \end{pmatrix}$$

Direct calculation yields that for $p \notin [\bar{p}_l, \bar{p}_r]$ the single equilibrium is a saddle. In the case of three equilibria, we have a source that lies between two saddles. Note that this also describes the stability of the three branches of the critical manifold C_l, C_m and C_r. For $s > 0$ the matrix A is singular of rank 1 if and only if $30x_1^2 - 22x_1 + 1 = 0$ which occurs for the fold points $x_{1,\pm}$. Hence the equilibria of the fast subsystem undergo a fold (or saddle-node) bifurcation once they approach the fold points of the critical manifold. This happens for parameter values $\bar{p}_l$ and $\bar{p}_r$. Note that by symmetry we can reduce to studying a single fold point. In the limit $s = 0$ (corresponding to the case of a "standing wave") the saddle-node bifurcation point becomes more degenerate with $A(x_1)$ nilpotent.

Our next goal is to investigate global bifurcations of (3.10); we start with homoclinic orbits. For $s = 0$ it is easy to see that (3.10) is a Hamiltonian system:

$$\begin{aligned} x_1' &= \frac{\partial H}{\partial x_2} = x_2 \\ x_2' &= -\frac{\partial H}{\partial x_1} = \frac{1}{5}(-x_1(x_1 - 1)(\frac{1}{10} - x_1) - \bar{p}) \end{aligned} \tag{3.12}$$

with Hamiltonian function

$$H(x_1, x_2) = \frac{1}{2}x_2^2 - \frac{(x_1)^2}{100} + \frac{11(x_1)^3}{150} - \frac{(x_1)^4}{20} + \frac{x_1\bar{p}}{5} \tag{3.13}$$

We will use this Hamiltonian formulation later on to describe the geometry of homoclinic orbits for slow wave speeds. Assume that $\bar{p}$ is chosen so that (3.12)

has a homoclinic orbit $x_0(t)$. We are interested in perturbations with $s > 0$ and note that in this case the divergence of (3.10) is s. Hence the vector field is area expanding everywhere. The homoclinic orbit breaks for $s > 0$ and no periodic orbits are created. Note that this scenario does not apply to the full three-dimensional system as the equilibrium q has a pair of complex conjugate eigenvalues so that a Shil'nikov scenario can occur. This illustrates that the singular limit can be used to help locate homoclinic orbits of the full system, but that some characteristics of these orbits change in the singular limit.

We are interested next in finding curves in $(\bar{p}, s)$-parameter space that represent heteroclinic connections of the fast subsystem. The main motivation is the decomposition of trajectories in the full system into slow and fast segments. Concatenating fast heteroclinic segments and slow flow segments can yield homoclinic orbits of the full system [62, 15, 69, 82]. We describe a numerical strategy to detect heteroclinic connections in the fast subsystem and continue them in parameter space. Suppose that $\bar{p} \in (\bar{p}_l, \bar{p}_r)$ so that (3.10) has three hyperbolic equilibrium points x_l, x_m and x_r. We denote by $W^u(x_l)$ the unstable and by $W^s(x_l)$ the stable manifold of x_l. The same notation is also used for x_r and tangent spaces to $W^s(.)$ and $W^u(.)$ are denoted by $T^s(.)$ and $T^u(.)$. Recall that x_m is a source and shall not be of interest to us for now. Define the cross section Σ by

$$\Sigma = \{(x_1, x_2) \in \mathbb{R}^2 : x_1 = \frac{x_l + x_r}{2}\}.$$

We use forward integration of initial conditions in $T^u(x_l)$ and backward integration of initial conditions in $T^s(x_r)$ to obtain trajectories γ^+ and γ^- respectively. We calculate their intersection with Σ and define

$$\gamma_l(\bar{p}, s) := \gamma^+ \cap \Sigma, \qquad \gamma_r(\bar{p}, s) := \gamma^- \cap \Sigma$$

We compute the functions γ_l and γ_r for different parameter values of $(\bar{p}, s)$ numerically. Heteroclinic connections occur at zeros of the function

$$h(\bar{p}, s) := \gamma_l(\bar{p}, s) - \gamma_r(\bar{p}, s)$$

Once we find a parameter pair $(\bar{p}_0, s_0)$ such that $h(\bar{p}_0, s_0) = 0$, these parameters can be continued along a curve of heteroclinic connections in $(\bar{p}, s)$ parameter space by solving the root-finding problem $h(\bar{p}_0 + \delta_1, s_0 + \delta_2) = 0$ for either δ_1 or δ_2 fixed and small. We use this method later for different fixed values of y to compute heteroclinic connections in the fast subsystem in (p, s) parameter space. The results of these computations are illustrated in Figure 3.3. There are two distinct branches in Figure 3.3. The branches are asymptotic to $\bar{p}_l$ and $\bar{p}_r$ and approximately form a "V". From Figure 3.3 we conjecture that there exists a double heteroclinic orbit for $\bar{p} \approx -0.0622$.

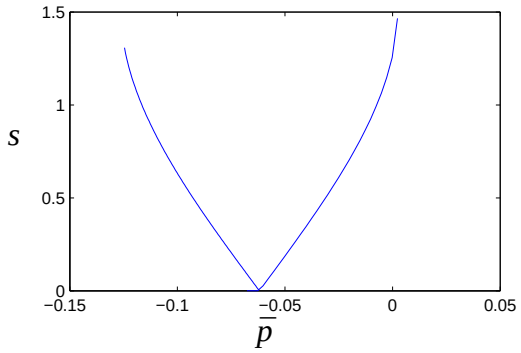

Figure 3.3: Heteroclinic connections for equation (3.10) in parameter space.

Remarks: If we fix $p = 0$ our initial change of variable becomes $-y = \bar{p}$ and our results for heteroclinic connections are for the FitzHugh-Nagumo equation without an applied current. In this situation it has been shown that the heteroclinic connections of the fast subsystem can be used to prove the existence of

homoclinic orbits to the unique saddle equilibrium $(0, 0, 0)$ (cf. [69]). Note that the existence of the heteroclinics in the fast subsystem was proved in a special case analytically [2] but Figure 3.3 is - to the best of our knowledge - the first explicit computation of where fast subsystem heteroclinics are located. The paper [78] develops a method for finding heteroclinic connections by the same basic approach we used, i.e. defining a codimension one hyperplane H that separates equilibrium points.

Figure 3.3 suggests that there exists a double heteroclinic connection for $s = 0$. Observe that the Hamiltonian in our case is $H(x_1, x_2) = \frac{(x_2)^2}{2} + V(x_1)$ where the function $V(x_1)$ is:

$$V(x_1) = \frac{px_1}{5} - \frac{(x_1)^2}{100} + \frac{11(x_1)^3}{150} - \frac{(x_1)^4}{20}$$

The solution curves of (3.12) are given by $x_2 = \pm\sqrt{2(\text{const.} - V(x_1))}$. The structure of the solution curves entails symmetry under reflection about the x_1-axis. Suppose $\bar{p} \in [\bar{p}_l, \bar{p}_r]$ and recall that we denoted the two saddle points of (3.10) by x_l and x_r and that their location depends on $\bar{p}$. Therefore, we conclude that the two saddles x_l and x_r must have a heteroclinic connection if they lie on the same energy level, i.e. they satisfy $V(x_l) - V(x_r) = 0$. This equation can be solved numerically to very high accuracy.

Proposition 3.3.1. *The fast subsystem of the FitzHugh-Nagumo equation for $s = 0$ has a double heteroclinic connection for $\bar{p} = \bar{p}^* \approx -0.0619259$. Given a particular value $y = y_0$ there exists a double heteroclinic connection for $p = \bar{p}^* + y_0$ in the fast subsystem lying in the plane $y = y_0$.*

3.3.3 Two Slow Variables, One Fast Variable

From continuation of periodic orbits in the full system - to be described in Section 3.4.1 - we observe that near the U-shaped curve of Hopf bifurcations the x_2-coordinate is a faster variable than x_1. In particular, the small periodic orbits generated in the Hopf bifurcation lie almost in the plane $x_2 = 0$. Hence to analyze this region we set $\bar{x_2} = x_2/\epsilon$ to transform the FitzHugh-Nagumo equation (3.6) into a system with 2 slow and 1 fast variable:

$$\begin{aligned} \dot{x}_1 &= \bar{x_2} \\ \epsilon^2 \dot{\bar{x_2}} &= \frac{1}{5}(s\epsilon\bar{x_2} - x_1(x_1-1)(\frac{1}{10} - x_1) + y - p) \\ \dot{y} &= \frac{1}{s}(x_1 - y) \end{aligned} \tag{3.14}$$

Note that (3.14) corresponds to the FitzHugh-Nagumo equation in the form (cf. (3.4)):

$$\begin{cases} u_\tau = 5\epsilon^2 u_{xx} + f(u) - w + p \\ w_\tau = \epsilon(u - w) \end{cases} \tag{3.15}$$

Therefore the transformation $\bar{x_2} = x_2/\epsilon$ can be viewed as a rescaling of the diffusion strength by ϵ^2. We introduce a new independent small parameter $\bar{\delta} = \epsilon^2$ and then let $\bar{\delta} = \epsilon^2 \to 0$. This assumes that $O(\epsilon)$ terms do not vanish in this limit, yielding the diffusion free system. Then the slow manifold S_0 of (3.14) is:

$$S_0 = \left\{ (x_1, \bar{x_2}, y) \in \mathbb{R}^3 : \bar{x_2} = \frac{1}{s\epsilon}\left(f(x_1) - y + p\right) \right\} \tag{3.16}$$

Proposition 3.3.2. *Following time rescaling by s, the slow flow of system* (3.14) *on* S_0 *in the variables* (x_1, y) *is given by*

$$\begin{aligned} \epsilon\dot{x}_1 &= f(x_1) - y + p \\ \dot{y} &= x_1 - y \end{aligned} \tag{3.17}$$

In the variables $(x_1, \bar{x_2})$ *the vector field* (3.17) *becomes*

$$\begin{aligned} \dot{x}_1 &= \bar{x_2} \\ \epsilon\dot{\bar{x_2}} &= -\frac{1}{s^2}\left(x_1 - f(x_1) - p\right) + \frac{\bar{x_2}}{s}\left(f'(x_1) - \epsilon\right) \end{aligned} \tag{3.18}$$

Remark: The reduction to equations (3.17)-(3.18) suggests that (3.14) is a three time-scale system. Note however that (3.14) is not given in the three time-scale form $(\epsilon^2\dot{z}_1, \epsilon\dot{z}_2, \dot{z}_3) = (h_1(z), h_2(z), h_3(z))$ for $z = (z_1, z_2, z_3) \in \mathbb{R}^3$ and $h_i : \mathbb{R}^3 \to \mathbb{R}$ $(i = 1, 2, 3)$. The time-scale separation in (3.17)-(3.18) results from the singular $1/\epsilon$ dependence of the critical manifold S_0; see (3.16).

Proof. (of Proposition 3.3.2) Use the defining equation for the slow manifold (3.16) and substitute it into $\dot{x}_1 = \bar{x_2}$. A rescaling of time by $t \to st$ under the assumption that $s > 0$ yields the result (3.17). To derive (3.18) differentiate the defining equation of S_0 with respect to time:

$$\dot{\bar{x_2}} = \frac{1}{s\epsilon}\left(\dot{x}_1 f'(x_1) - \dot{y}\right) = \frac{1}{s\epsilon}\left(\bar{x_2} f'(x_1) - \dot{y}\right)$$

The equations $\dot{y} = \frac{1}{s}(x_1 - y)$ and $y = -s\epsilon\bar{x_2} + f(x_1) + p$ yield the equations (3.18). □

Before we start with the analysis of (3.17) we note that detailed bifurcation calculations for (3.17) exist. For example, Rocsoreanu et al. [97] give a detailed overview on the FitzHugh equation (3.17) and collect many relevant references. Therefore we shall only state the relevant bifurcation results and focus on the fast-slow structure and canards. Equation (3.17) has a critical manifold given by $y = f(x_1) + p = c(x_1)$ which coincides with the critical manifold of the full FitzHugh-Nagumo system (3.6). Formally it is located in $\mathbb{R}^2$ but we still denote it by C_0. Recall that the fold points are located at

$$x_{1,\pm} = \frac{1}{30}\left(11 \pm \sqrt{91}\right) \qquad \text{or numerically:} \quad x_{1,+} \approx 0.6846, \quad x_{1,-} \approx 0.0487$$

Also recall that the y-nullcline passes through the fold points at:

$$p_- \approx 0.0511 \qquad \text{and} \qquad p_+ \approx 0.5584$$

We easily find that supercritical Hopf bifurcations are located at the values

$$p_{H,\pm}(\epsilon) = \frac{2057}{6750} \pm \sqrt{\frac{11728171}{182250000} - \frac{359\epsilon}{1350} + \frac{509\epsilon^2}{2700} - \frac{\epsilon^3}{27}} \tag{3.19}$$

For the case $\epsilon = 0.01$ we get $p_{H,-}(0.01) \approx 0.05632$ and $p_{H,+}(0.01) \approx 0.55316$. The periodic orbits generated in the Hopf bifurcations exist for $p \in (p_{H,-}, p_{H,+})$. Observe also that $p_{H,\pm}(0) = p_\pm$; so the Hopf bifurcations of (3.17) coincide in the singular limit with the fold bifurcations in the one-dimensional slow flow (3.8). We are also interested in canards in the system and calculate a first order asymptotic expansion for the location of the maximal canard in (3.17) following [83]; recall that trajectories lying in the intersection of attracting and repelling slow manifolds are called maximal canards. We restrict to canards near the fold point $(x_{1,-}, c(x_{1,-}))$.

Proposition 3.3.3. *Near the fold point* $(x_{1,-}, c(x_{1,-}))$ *the maximal canard in* (p, ϵ) *parameter space is given by:*

$$p(\epsilon) = x_{1,-} - c(x_{1,-}) + \frac{5}{8}\epsilon + O(\epsilon^{3/2})$$

Proof. Let $\bar{y} = y - p$ and consider the shifts

$$x_1 \to x_1 + x_{1,-}, \quad \bar{y} \to \bar{y} + c(x_{1,-}), \quad p \to p + x_{1,-} - c(x_{1,-})$$

to translate the equilibrium of (3.17) to the origin when $p = 0$. This gives

$$\begin{aligned} x_1' &= x_1^2\left(\frac{\sqrt{91}}{10} - x_1\right) - \bar{y} = \bar{f}(x_1, \bar{y}) \\ y' &= \epsilon(x_1 - \bar{y} - p) = \epsilon(\bar{g}(x_1, \bar{y}) - p) \end{aligned} \tag{3.20}$$

Now apply Theorem 3.1 in [83] to find that the maximal canard of (3.20) is given by:

$$p(\epsilon) = \frac{5}{8}\epsilon + O(\epsilon^{3/2})$$

Shifting the parameter p back to the original coordinates yields the result. □

If we substitute $\epsilon = 0.01$ in the previous asymptotic result and neglect terms of order $O(\epsilon^{3/2})$ then the maximal canard is predicted to occur for $p \approx 0.05731$ which is right after the first supercritical Hopf bifurcation at $p_{H,-} \approx 0.05632$. Therefore we expect that there exist canard orbits evolving along the middle branch of the critical manifold $C_{m,0.01}$ in the full FitzHugh-Nagumo equation. Maximal canards are part of a process generally referred to as canard explosion [36, 86, 29]. In this situation the small periodic orbits generated in the Hopf bifurcation at $p = p_{H,-}$ undergo a transition to relaxation oscillations within a very small interval in parameter space. A variational integral determines whether the canards are stable [86, 51].

Proposition 3.3.4. *The canard cycles generated near the maximal canard point in parameter space for equation (3.17) are stable.*

Proof. Consider the differential equation (3.17) in its transformed form (3.20). Obviously this will not affect the stability analysis of any limit cycles. Let $x_l(h)$ and $x_m(h)$ denote the two smallest x_1-coordinates of the intersection between

$$\bar{C_0} := \{(x_1, \bar{y}) \in \mathbb{R}^2 : \bar{y} = \frac{\sqrt{91}}{10}x_1^2 - x_1^3 = \phi(x_1)\}$$

and the line $\bar{y} = h$. Geometrically x_l represents a point on the left branch and x_m a point on the middle branch of the critical manifold $\bar{C_0}$. Theorem 3.4 in [86] tells us that the canards are stable cycles if the function

$$R(h) = \int_{x_l(h)}^{x_m(h)} \frac{\partial \bar{f}}{\partial x_1}(x_1, \phi(x_1)) \frac{\phi'(x_1)}{\bar{g}(x_1, \phi(x_1))} dx_1$$

is negative for all values $h \in (0, \phi(\frac{\sqrt{91}}{15})]$ where $x_1 = \frac{\sqrt{91}}{15}$ is the second fold point of $\bar{C_0}$ besides $x_1 = 0$. In our case we have

$$R(h) = \int_{x_l(h)}^{x_m(h)} \frac{(\frac{\sqrt{91}}{5}x_1 - 3x_1^2)^2}{x - \frac{\sqrt{91}}{10}x_1^2 + x_1^3} dx$$

with $x_l(h) \in [-\frac{\sqrt{91}}{30}, 0)$ and $x_m(h) \in (0, \frac{\sqrt{91}}{15}]$. Figure 3.4 shows a numerical plot of the function $R(h)$ for the relevant values of h which confirms the required result.

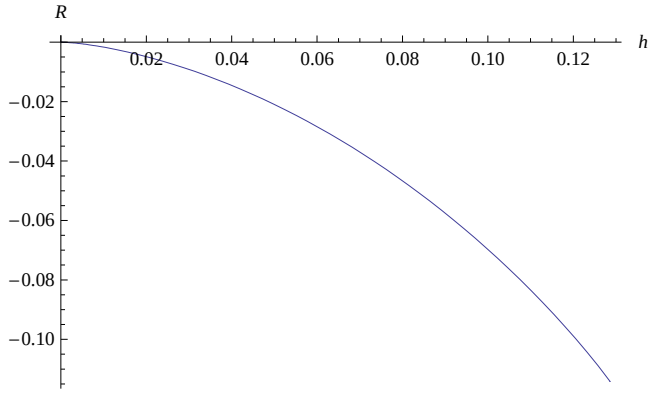

Figure 3.4: Plot of the function $R(h)$ for $h \in (0, \phi(\frac{\sqrt{91}}{15})]$.

Remark: We have computed an explicit algebraic expression for $R'(h)$ with a computer algebra system. This expression yields $R'(h) < 0$ for $h \in (0, \phi(\frac{\sqrt{91}}{15})]$, confirming that $R(h)$ is decreasing.

□

As long as we stay on the critical manifold C_0 of the full system, the analysis of the bifurcations and geometry of (3.17) give good approximations to the dynamics of the FitzHugh-Nagumo equation because the rescaling $x_2 = \epsilon\bar{x_2}$ leaves the plane $x_2 = 0$ invariant. Next we use the dynamics of the $\bar{x_2}$-coordinate in system (3.18) to obtain better insight into the dynamics when $x_2 \neq 0$. The critical

manifold D_0 of (3.18) is:

$$D_0 = \{(x_1, \bar{x_2}) \in \mathbb{R}^2 : s\bar{x_2}c'(x_1) = x_1 - c(x_1)\}$$

We are interested in the geometry of the periodic orbits shown in Figure 3.5 that emerge from the Hopf bifurcation at $p_{H,-}$. Observe that the amplitude of the orbits in the x_1 direction is much larger that than in the x_2-direction. Therefore we predict only a single small excursion in the x_2 direction for p slightly larger than $p_{H,-}$ as shown in Figures 3.5(a) and 3.5(c). The wave speed changes the amplitude of this x_2 excursion with a smaller wave speed implying a larger excursion. Hence equation (3.17) is expected to be a very good approximation for periodic orbits in the FitzHugh-Nagumo equation with fast wave speeds. Furthermore the periodic orbits show two x_2 excursions in the relaxation regime after the canard explosion; see Figure 3.5(b).

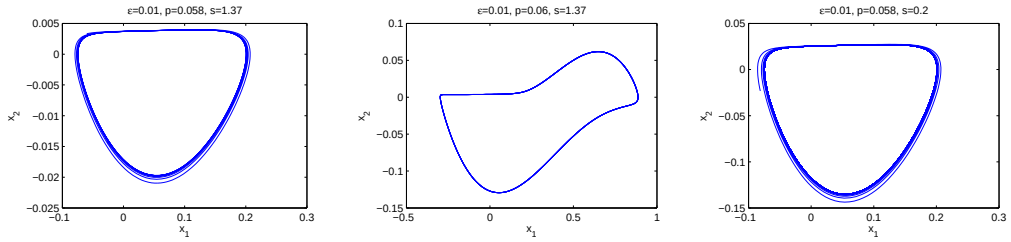

(a) Small orbit near Hopf point ($p = 0.058$, $s = 1.37$)

(b) Orbit after canard explosion ($p = 0.06$, $s = 1.37$)

(c) Different wave speed ($p = 0.058$, $s = 0.2$)

Figure 3.5: Geometry of periodic orbits in the (x_1, x_2)-variables of the 2-variable slow subsystem (3.18). Note that here $x_2 = \epsilon\bar{x_2}$ is shown. Orbits have been obtained by direct forward integration for $\epsilon = 0.01$.

3.4 The Full System

3.4.1 Hopf Bifurcation

The characteristic polynomial of the linearization of the FitzHugh-Nagumo equation (3.6) at its unique equilibrium point is

$$P(\lambda) = \frac{\epsilon}{5s} + \left(-\frac{\epsilon}{s} - \lambda\right)\left(-\frac{1}{50} + \frac{11x_1^*}{25} - \frac{3(x_1^*)^2}{5} - \frac{s\lambda}{5} + \lambda^2\right)$$

Denoting $P(\lambda) = c_0 + c_1\lambda + c_2\lambda^2 + c_3\lambda^3$, a necessary condition for P to have pure imaginary roots is that $c_0 = c_1c_2$. The solutions of this equation can be expressed parametrically as a curve $(p(x_1^*), s(x_1^*))$:

$$\begin{aligned} s(x_1^*)^2 &= \frac{50\epsilon(\epsilon - 1)}{1 + 10\epsilon - 22x_1^* + 30(x_1^*)^2} \\ p(x_1^*) &= (x_1^*)^3 - 1.1(x_1^*)^2 + 1.1 \end{aligned} \tag{3.21}$$

Proposition 3.4.1. *In the singular limit $\epsilon \to 0$ the U-shaped bifurcation curves of the FitzHugh-Nagumo equation have vertical asymptotes given by the points $p_- \approx 0.0510636$ and $p_+ \approx 0.558418$ and a horizontal asymptote given by $\{(p, s) : p \in [p_-, p_+] \quad and \quad s = 0\}$. Note that at $p_\pm$ the equilibrium point passes through the two fold points.*

Proof. The expression for $s(x_1^*)^2$ in (3.21) is positive when $1 + 10\epsilon - 22x_1^* + 30(x_1^*)^2 < 0$. For values of x_1^* between the roots of $1 - 22x_1^* + 30(x_1^*)^2 = 0$, $s(x_1^*)^2 \to 0$ in (3.21) as $\epsilon \to 0$. The values of p_- and p_+ in the proposition are approximations to the value of $p(x_1^*)$ in (3.21) at the roots of $1 - 22x_1^* + 30(x_1^*)^2 = 0$. As $\epsilon \to 0$, solutions of the equation $s(x_1^*)^2 = c > 0$ in (3.21) yield values of x_1^* that tend to one of the two roots of $1 - 22x_1^* + 30(x_1^*)^2 = 0$. The result follows. □

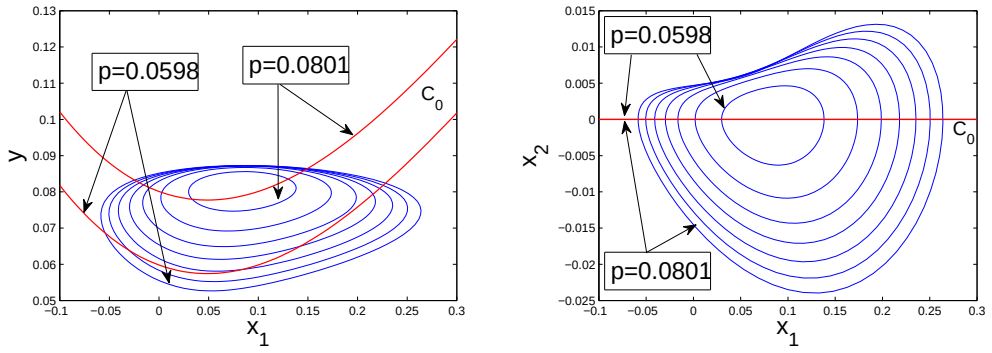

(a) Projection onto (x_1, y) (b) Projection onto (x_1, x_2)

Figure 3.6: Hopf bifurcation at $p \approx 0.083$, $s = 1$ and $\epsilon = 0.01$. The critical manifold C_0 is shown in red and periodic orbits are shown in blue. Only the first and the last critical manifold for the continuation run are shown; not all periodic orbits obtained during the continuation are displayed.

The analysis of the slow subsystems (3.17) and (3.18) gives a conjecture about the shape of the periodic orbits in the FitzHugh-Nagumo equation. Consider the parameter regime close to a Hopf bifurcation point. From (3.17) we expect one part of the small periodic orbits generated in the Hopf bifurcation to lie close to the slow manifolds $C_{l,\epsilon}$ and $C_{m,\epsilon}$. Using the results about equation (3.18) we anticipate the second part to consist of an excursion in the x_2 direction whose length is governed by the wave speed s. Figure 3.6 shows a numerical continuation in MatCont [46] of the periodic orbits generated in a Hopf bifurcation and confirms the singular limit analysis for small amplitude orbits.

Furthermore we observe from comparison of the x_1 and x_2 coordinates of the periodic orbits in Figure 3.6(b) that orbits tend to lie close to the plane defined by $x_2 = 0$. More precisely, the x_2 diameter of the periodic orbits is observed to be $O(\epsilon)$ in this case. This indicates that the rescaling of Section 3.3.3 can help to describe the system close to the U-shaped Hopf curve. Note that it is difficult to

check whether this observation of an $O(\epsilon)$-diameter in the x_2-coordinate persists for values of $\epsilon < 0.01$ since numerical continuation of canard-type periodic orbits is difficult to use for smaller ϵ.

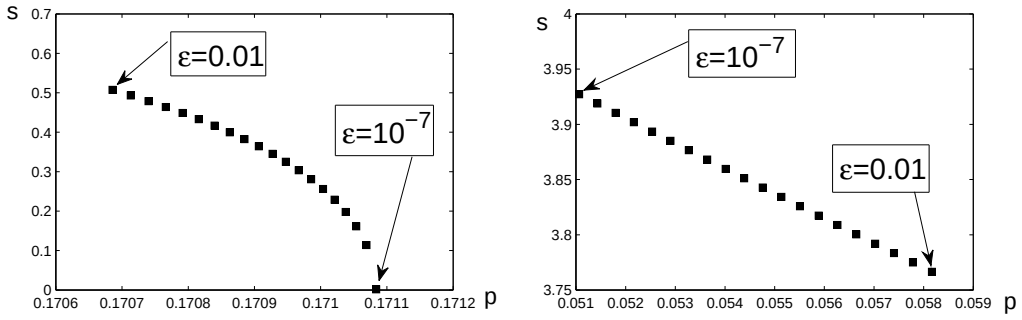

(a) GH_1^ϵ (b) GH_2^ϵ

Figure 3.7: Tracking of two generalized Hopf points (GH) in (p, s, ϵ)-parameter space. Each point in the figure corresponds to a different value of ϵ. The point GH_1^ϵ in 3.7(a) corresponds to the point shown as a square in Figure 3.1 and the point GH_2^ϵ in 3.7(b) is further up on the left branch of the U-curve and is not displayed in Figure 3.1.

In contrast to this, it is easily possible to compute the U-shaped Hopf curve using numerical continuation for very small values of ϵ. We have used this possibility to track two generalized Hopf bifurcation points in three parameters (p, s, ϵ). The U-shaped Hopf curve has been computed by numerical continuation for a mesh of parameter values for ϵ between 10^{-2} and 10^{-7} using MatCont [46]. The two generalized Hopf points $GH_{1,2}^\epsilon$ on the left half of the U-curve were detected as codimension two points during each continuation run. The results of this "three-parameter continuation" are shown in Figure 3.7.

The two generalized Hopf points depend on ϵ and we find that their singular

limits in (p, s)-parameter space are approximately:

$$GH_1^0 \approx (p = 0.171, s = 0) \qquad \text{and} \qquad GH_2^0 \approx (p = 0.051, s = 3.927)$$

We have not found a way to recover these special points from the fast-slow decomposition of the system. This suggests that codimension two bifurcations are generally difficult to recover from the singular limit of fast-slow systems.

Furthermore the Hopf bifurcations for the full system on the left half of the U-curve are subcritical between GH_1^ϵ and GH_2^ϵ and supercritical otherwise. For the transformed system (3.14) with two slow and one fast variable we observed that in the singular limit (3.17) for $\epsilon^2 \to 0$ the Hopf bifurcation is supercritical. In the case of $\epsilon = 0.01$ the periodic orbits for (3.6) and (3.17) exist in overlapping regions for the parameter p between the p-values of $GH_1^{0.01}$ and $GH_2^{0.01}$. This result indicates that (3.14) can be used to describe periodic orbits that will interact with the homoclinic C-curve.

3.4.2 Homoclinic Orbits

In the following discussion we refer to "the" C-shaped curve of homoclinic bifurcations of system (3.5) as the parameters yielding a "single-pulse" homoclinic orbit. The literature as described in Section 3.2.2 shows that close to single-pulse homoclinic orbits we can expect multi-pulse homoclinic orbits that return close to the equilibrium point multiple times. Since the separation of slow manifolds $C_{\cdot,\epsilon}$ is exponentially small, homoclinic orbits of different types will always occur in exponentially thin bundles in parameter space. Values of $\epsilon < 0.005$ are small enough that the parameter region containing all the homoclinic orbits will be

indistinguishable numerically from "the" C-curve that we locate.

The history of proofs of the existence of homoclinic orbits in the FitzHugh-Nagumo equation is quite extensive. The main step in their construction is the existence of a "singular" homoclinic orbit γ_0. We consider the case when the fast subsystem has three equilibrium points which we denote by $x_l \in C_l$, $x_m \in C_m$ and $x_r \in C_r$. Recall that x_l coincides with the unique equilibrium $q = (x_1^*, 0, x_1^*)$ of the full system for $p < p_-$. A singular homoclinic orbit is always constructed by first following the unstable manifold of x_l in the fast subsystem given by $y = x_1^*$.

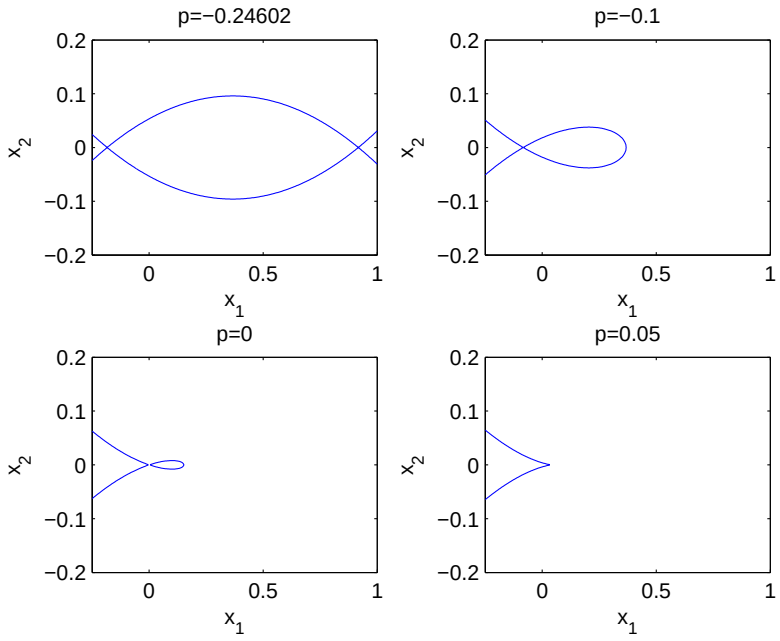

Figure 3.8: Homoclinic orbits as level curves of $H(x_1, x_2)$ for equation (3.12) with $y = x_1^*$.

First assume that $s = 0$. In this case the Hamiltonian structure - see Section 3.3.2 and equation (3.12) - can be used to show the existence of a singular

homoclinic orbit. Figure 3.8 shows level curves $H(x_1, x_2) = H(x_1^*, 0)$ for various values of p. The double heteroclinic connection can be calculated directly using Proposition 3.3.1 and solving $x_1^* + \bar{p}^* = p$ for p.

Proposition 3.4.2. *There exists a singular double heteroclinic connection in the FitzHugh-Nagumo equation for $s = 0$ and $p \approx -0.246016 = p^*$.*

Techniques developed in [103] show that the singular homoclinic orbits existing for $s = 0$ and $p \in (p^*, p_-)$ must persist for perturbations of small positive wave speed and sufficiently small ϵ. These orbits are associated to the lower branch of the C-curve. The expected geometry of the orbits is indicated by their shape in the singular limit shown in Figure 3.8. The double heteroclinic connection is the boundary case between the upper and lower half of the C-curve. It remains to analyze the singular limit for the upper half. In this case, a singular homoclinic orbit is again formed by following the unstable manifold of x_l when it coincides with the equilibrium $q = (x_1^*, 0, x_1^*)$ but now we check whether it forms a heteroclinic orbit with the stable manifold of x_r. Then we follow the slow flow on C_r and return on a heteroclinic connection to C_l for a different y-coordinate with $y > x_1^*$ and $y < c(x_{1,+}) = f(x_1) + p$. From there we connect back via the slow flow. Using the numerical method described in Section 3.3.2 we first set $y = x_1^*$; note that the location of q depends on the value of the parameter p. The task is to check when the system

$$\begin{aligned} x_1' &= x_2 \\ x_2' &= \frac{1}{5}\left(f(x_1) + y - p\right) \end{aligned} \tag{3.22}$$

has heteroclinic orbits from C_l to C_r with $y = x_1^*$. The result of this computation is shown in Figure 3.9 as the red curve. We have truncated the result at $p = -0.01$. In fact, the curve in Figure 3.9 can be extended to $p = p^*$. Obviously

we should view this curve as an approximation to the upper part of the C-curve.

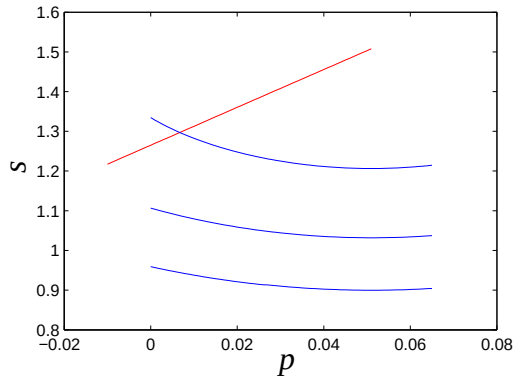

Figure 3.9: Heteroclinic connections for equation (3.22) in parameter space. The red curve indicates left-to-right connections for $y = x_1^*$ and the blue curves indicate right-to-left connections for $y = x_1^* + v$ with $v = 0.125, 0.12, 0.115$ (from top to bottom).

If the connection from C_r back to C_l occurs with vertical coordinate $x_1^* + v$, it is a trajectory of system (3.22) with $y = x_1^* + v$. Figure 3.9 shows values of (p, s) at which these heteroclinic orbits exist for $v = 0.125, 0.12, 0.115$. An intersection between a red and a blue curve indicates a singular homoclinic orbit. Further computations show that increasing the value of v slowly beyond 0.125 yields intersections everywhere along the red curve in Figure 3.9. Thus the values of v on the homoclinic orbits are expected to grow as s increases along the upper branch of the C-curve. Since there cannot be any singular homoclinic orbits for $p \in (p_-, p_+)$ we have to find the intersection of the red curve in Figure 3.9 with the vertical line $p = p_-$. Using the numerical method to detect heteroclinic connections gives:

Proposition 3.4.3. *The singular homoclinic curve for positive wave speed terminates at $p = p_-$ and $s \approx 1.50815 = s^*$ on the right and at $p = p^*$ and $s = 0$ on the left.*

In (p, s)-parameter space define the points:

$$A = (p^*, 0), \qquad B = (p_-, 0), \qquad C = (p_-, s^*) \tag{3.23}$$

In Figure 3.10 we have computed the homoclinic C-curve for values of ϵ between 10^{-2} and $5 \cdot 10^{-5}$. Together with the singular limit analysis above, this yields strong numerical evidence for the following conjecture:

Conjecture 3.4.4. *The C-shaped homoclinic bifurcation curves converge to the union of the segments AB and AC as* $\epsilon \to 0$.

Remark 1: Figure 4 of Krupa, Sandstede and Szmolyan [82] shows a "wedge" that resembles shown in Figure 3.10. The system that they study sets $p = 0$ and varies a with $a \approx 1/2$. For $a = 1/2$ and $p = 0$, the equilibrium point q is located at the origin and the fast subsystem with $y = 0$ has a double heteroclinic connection at q to the saddle equilibrium $(1, 0, 0) \in C_r$. The techniques developed in [82] use this double heteroclinic connection as a starting point. Generalizations of the results in [82] might provide a strategy to prove Conjecture 3.4.4 rigorously, a possibility that we have not yet considered. However, we think that 1-homoclinic orbits in the regime we study come in pairs and that the surface of 1-homoclinic orbits in (p, s, ϵ) space differs qualitatively from that described by Krupa, Sandstede and Szmolyan.

Remark 2: We have investigated the termination or turning mechanism of the C-curve at its upper end. The termination points shown in Figure 3.1 have been obtained by a different geometric method. It relies on the observation that, in addition to the two fast heteroclinic connections, we have to connect near C_l back to the equilibrium point q to form a homoclinic orbit; the two heteroclinic connections might persist as intersections of suitable invariant manifolds

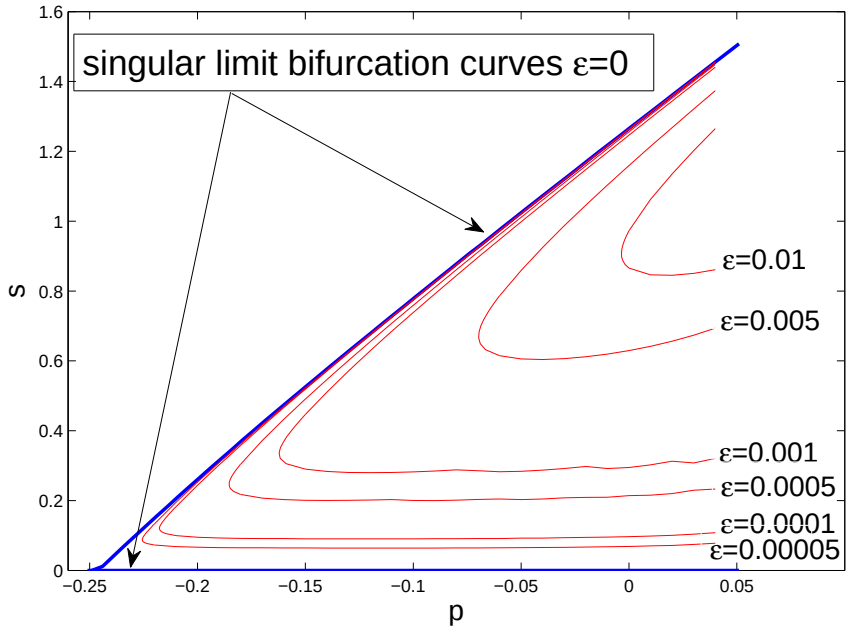

Figure 3.10: Singular limit ($\epsilon = 0$) of the C-curve is shown in blue and parts of several C-curves for $\epsilon > 0$ have been computed (red).

but we also have to investigate how the flow near $C_{l,\epsilon}$ interacts with the stable manifold $W^s(q)$. These results will be reported elsewhere, but we note here that $p_{turn}(\epsilon) \to p_-$.

The numerical calculations of the C-curves for $\epsilon \leq 10^{-3}$ are new. Numerical continuation using the boundary value methods implemented in AUTO [33] or MatCont [46] becomes very difficult for these small values of ϵ [18]. Even computing with values $\epsilon = O(10^{-2})$ using boundary value methods is a numerically challenging problem. The method we have used does not compute the homoclinic orbits themselves while it locates the homoclinic C-curve accurately in parameter space. To motivate our approach consider Figure 3.11 which shows the unstable manifold $W^u(q)$ for different values of s and fixed p. We observe

that homoclinic orbits can only exist near two different wave speeds s_1 and s_2 which define the parameters where $W^u(q) \subset W^s(C_{l,\epsilon})$ or $W^u(q) \subset W^s(C_{r,\epsilon})$. Figure 3.11 displays how $W^u(q)$ changes as s varies for the fixed value $p = 0.05$. If s differs from the points s_1 and s_2 that define the lower and upper branches of the C-curve for the given value of p, then $|x_1|$ increases rapidly on $W^u(q)$ away from q. The changes in sign of x_1 on $W^u(q)$ identify values of s with homoclinic orbits. The two splitting points that mark these sign changes are visible in Figure 3.11. Since trajectories close to the slow manifolds separate exponentially away from them, we are able to assess the sign of x_1 unambiguously on trajectories close to the slow manifold and find small intervals $(p, s_1 \pm 10^{-15})$ and $(p, s_2 \pm 10^{-15})$ that contain the values of s for which there are homoclinic orbits.

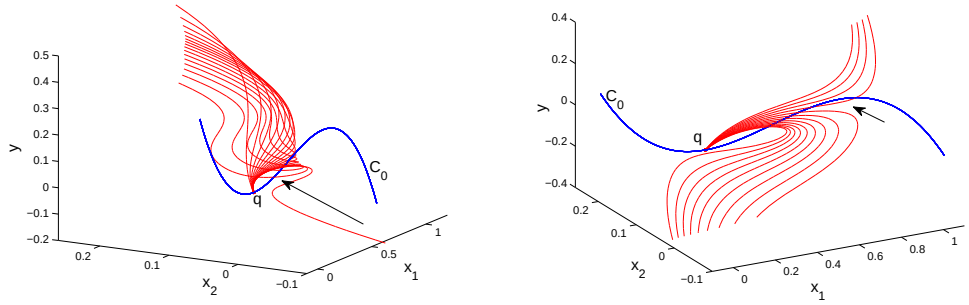

(a) $\epsilon = 0.01$, $p = 0.05$, $s \in [0.1, 0.9]$ (b) $\epsilon = 0.01$, $p = 0.05$, $s \in [0.9, 1.5]$

Figure 3.11: Strong "splitting", marked by an arrow, of the unstable manifold $W^u(q)$ (red) used in the calculation of the homoclinic C-curve for small values of ϵ. The critical manifold C_0 is shown in blue. The spacing in s is 0.05 for both figures.

The geometry of the orbits along the upper branch of the C-curve is obtained by approximating it with two fast singular heteroclinic connections and parts of the slow manifolds $C_{r,\epsilon}$ and $C_{l,\epsilon}$; this process has been described several times in the literature when different methods were used to prove the existence of "fast

waves" (see e.g. [63, 15, 69]).

3.5 Conclusions

Our results are summarized in the singular bifurcation diagram shown in Figure 3.12. This figure shows information obtained by a combination of fast-slow decompositions, classical dynamical systems techniques and robust numerical algorithms that work for very small values of ϵ. It recovers and extends to smaller values of ϵ the CU-structure described in [18] for the FitzHugh-Nagumo equation. The U-shaped Hopf curve was computed with an explicit formula, and the homoclinic C-curve was determined by locating transitions between different dynamical behaviors separated by the homoclinic orbits. All the results shown as solid lines in Figure 3.12 have been obtained by considering a singular limit. The lines *AB* and *AC* as well as the slow flow bifurcation follow from the singular limit $\epsilon \to 0$ yielding the fast and slow subsystems of the FitzHugh-Nagumo equation (3.6). The analysis of canards and periodic orbits have been obtained from equations (3.17) and (3.18) where the singular limit $\epsilon^2 \to 0$ was used (see Section 3.3.3). We have also shown the C- and U-curves in Figure 3.12 as dotted lines to orient the reader how the results from Proposition 3.4.1 and Conjecture 3.4.4 fit in.

We also observed that several dynamical phenomena are difficult to recover from the singular limit fast-slow decomposition. In particular, the codimension two generalized Hopf bifurcation does not seem to be observable from the singular limit analysis. Furthermore the homoclinic orbits can be constructed from

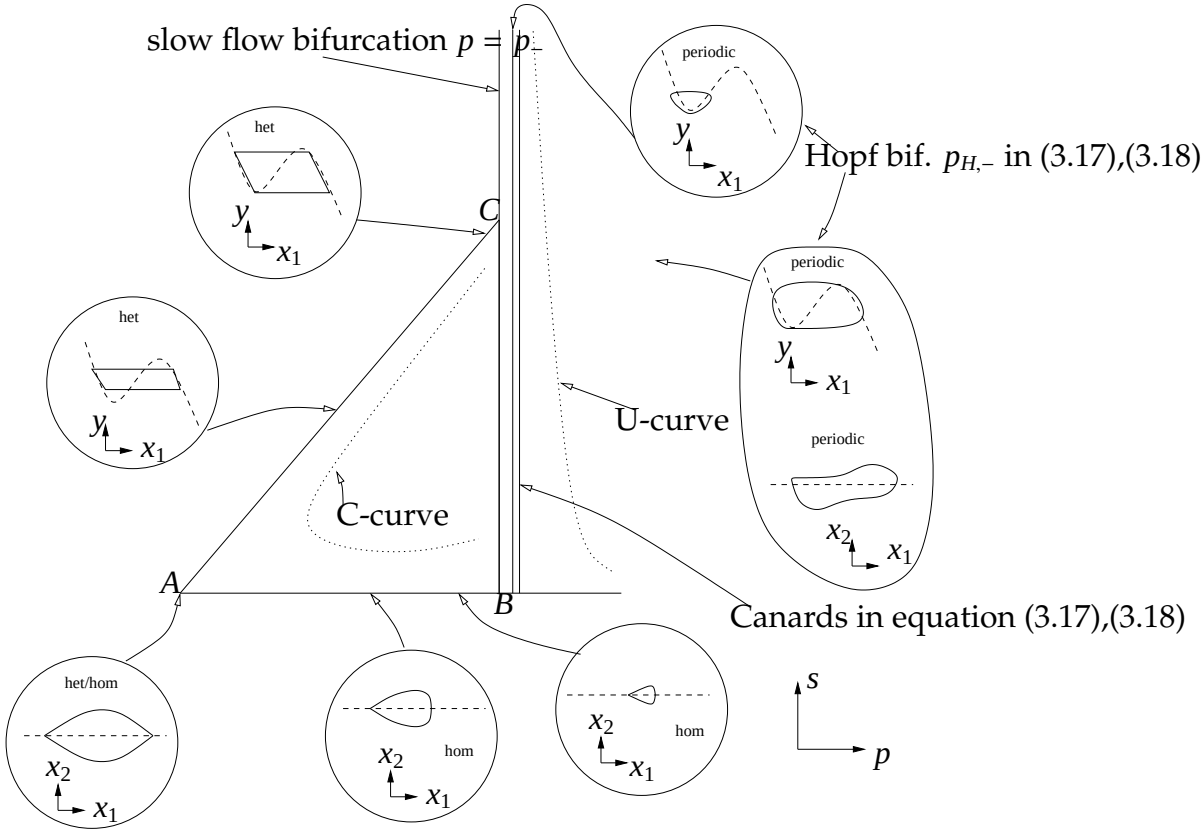

Figure 3.12: Sketch of the singular bifurcation diagram for the FitzHugh-Nagumo equation (3.6). The points A, B and C are defined in (3.23). The part of the diagram obtained from equations (3.17),(3.18) corresponds to the case "$\epsilon^2 = 0$ and $\epsilon \neq 0$ and small". In this scenario the canards to the right of $p = p_-$ are stable (see Proposition 3.3.4). The phase portrait in the upper right for equation (3.17) shows the geometry of a small periodic orbit generated in the Hopf bifurcation of (3.17). The two phase portraits below it show the geometry of these periodic orbits further away from the Hopf bifurcation for (3.17),(3.18).

the singular limits but it cannot be determined directly from the fast and slow subsystems that they are of Shil'nikov-type.

The type of analysis pursued here seems to be very useful for other multiple time-scale problems involving multi-parameter bifurcation problems. In future work, we shall give a geometric analysis of the folding/turning mechanism of the homoclinic C-curve, a feature of this system we have not been able to determine directly from our singular limit analysis. That work relies upon new methods for calculating $C_{l,\epsilon}$ and $C_{r,\epsilon}$ which are invariant slow manifolds of "saddle-type" with both stable and unstable manifolds.

We end with brief historical remarks. The references cited in this paper discuss mathematical challenges posed by the FitzHugh-Nagumo equation, how these challenges have been analyzed and their relationship to general questions about multiple time-scale systems. Along the line AB in Figure 3.12 we encounter a perturbation problem regarding the persistence of homoclinic orbits that can be solved using Fenichel theory [103]. The point A marks the connection between fast and slow waves in (p, s)-parameter space which has been investigated in (ϵ, s)-parameter space in [82]. We view this codimension 2 connectivity as one of the key features of the FitzHugh-Nagumo system. The perturbation problem for homoclinic orbits close to the line AC was solved using several methods and was put into the context of multiple time-scale systems in [68, 69], where the Exchange Lemma overcame difficulties in tracking $W^u(q)$ when it starts jumping away from $C_{r,\epsilon}$. This theory provides rigorous foundations that support our numerical computations and their interpretation.

3.6 Additions

In Section 3.3.3 we considered the re-scaling $\bar{x_2} = x_2/\epsilon$ giving a system which formally has two slow and one fast variable (3.14). Note that the slow flow of (3.14) is another fast-slow system with one fast and one slow variable as shown in Proposition 3.3.2. This suggests that there should exist a direct re-scaling that converts the FHN equation into a three time-scale system [80, 81]. Consider the FitzHugh-Nagumo equation on the fast time scale:

$$\begin{aligned} x_1' &= x_2 \\ x_2' &= \frac{1}{5}(sx_2 - f(x_1) + y - p) \\ y' &= \frac{\epsilon}{s}(x_1 - y) \end{aligned} \tag{3.24}$$

If we make the general re-scaling ansatz for (3.24) given by

$$(x_1, x_2, y, t, s, p) \mapsto (\epsilon^\alpha X_1, \epsilon^\beta X_2, \epsilon^\gamma Y, \epsilon^\delta T, \epsilon^\rho S, \epsilon^\sigma P)$$

it is not difficult to derive algebraic equations for $(\alpha, \beta, \gamma, \delta, \rho, \sigma)$ so that (3.24) has a three-scale structure of the form:

$$\begin{aligned} X_1' &= F_1 \\ \epsilon X_2' &= F_2 \\ Y' &= \epsilon G \end{aligned} \tag{3.25}$$

for functions F_1, F_2 and G. This yields the next proposition.

Proposition 3.6.1. *Consider the re-scaling*

$$(x_1, x_2, y, t, s, p) \mapsto (X_1, \epsilon^{1/2} X_2, \gamma Y, \epsilon^{-1/2} T, \epsilon^{-1/2} S, P) \tag{3.26}$$

Then (3.24) *transforms to a three time scale system of the form* (3.25) *i.e.* X_2 *is the fastest variable,* X_1 *an intermediate variable and* Y *is the slow variable.*

Proof. Plugging in (3.26) into (3.24) gives:

$$\begin{aligned} \epsilon^{-(-1/2)}X_1' &= \epsilon^{1/2}X_2 \\ \epsilon^{1/2-(-1/2)}X_2' &= \frac{1}{5}(\epsilon^{1/2-1/2}S\,X_2 - f(X_1) + Y - P) \\ \epsilon^{-(-1/2)}Y' &= \frac{\epsilon^{1+1/2}}{S}(X_1 - Y) \end{aligned} \tag{3.27}$$

The result now follows by straightforward algebraic simplification. □

CHAPTER 4

PAPER II: "COMPUTING SLOW MANIFOLDS OF SADDLE-TYPE"

4.1 Abstract

Slow manifolds are important geometric structures in the state spaces of dynamical systems with multiple time scales. This paper introduces an algorithm for computing trajectories on slow manifolds that are normally hyperbolic with both stable and unstable fast manifolds. We present two examples of bifurcation problems where these manifolds play a key role and a third example in which saddle type slow manifolds are part of a traveling wave profile of a partial differential equation. Initial value solvers are incapable of computing trajectories on saddle-type slow manifolds, so the slow manifold of saddle-type (SMST) algorithm presented here is formulated as a boundary value method. We take an empirical approach here to assessing the accuracy and effectiveness of the algorithm.

4.2 Introduction

Slow-fast vector fields have the form

$$\begin{aligned} \epsilon \dot{x} &= f(x, y, \epsilon) \\ \dot{y} &= g(x, y, \epsilon) \end{aligned} \tag{4.1}$$

with $x \in R^m$ the vector of fast variables, $y \in R^n$ the vector of slow variables and ϵ a small parameter that represents the ratio of time scales. The pair (x, y) will be denoted by z and the vector field will be written $\dot{z} = F(z)$. Invariant slow manifolds on which the motion of the system has speed that is $O(1)$ are a common feature of slow-fast systems. Nevertheless, simulation of these systems with explicit numerical integration algorithms is limited to time steps that are $O(\epsilon)$ due to numerical instabilities. Indeed, trajectories often spend most of their time following attracting slow manifolds. Implicit "stiff" integration methods [61] compute trajectories along the attracting slow manifolds, taking time steps that are $O(1)$ while avoiding the numerical instabilities of explicit methods. However, no initial value solver will compute forward trajectories that evolve on non-attracting slow manifolds because the geometric instability of these trajectories is such that nearby initial conditions diverge from one another at exponential rates commensurate with the fast time scale. Even an exact initial value solver in the presence of round-off errors of magnitude δ will amplify this round-off error to unit magnitude in a time that is $O(-\epsilon \log(\delta))$. Trajectories on slow manifolds that are repelling in all normal directions can be computed by reversing time, but different strategies are needed to compute trajectories that lie on slow manifolds of saddle type. This paper presents an algorithm that directly computes accurate trajectories of slow manifolds of saddle-type. The most similar work on computing these manifolds have been AUTO computations that continue families of trajectories to obtain portions of a saddle-type slow manifold. Examples include a slow manifold that lies in the unstable manifold of a three dimensional model of a cardiac pacemaker [79] and segments of homoclinic orbits in the model of FitzHugh-Nagumo traveling-waves [18] studied further in Section 3.3 of this paper.

The existence of normally hyperbolic slow manifolds is established by Fenichel theory [42, 71]. The singular limit $\epsilon = 0$ of system (4.1) is a differential algebraic equation with trajectories confined to the critical manifold $S = S_0$ defined by $f = 0$. At points of S where $D_x f$ is a regular $m \times m$ matrix, the implicit function theorem implies that S is locally the graph of a function $x = h(y)$. This equation yields the vector field $\dot{y} = g(h(y), y, 0)$ for the slow flow on S. The geometry is more complicated at fold points of S where $D_x f$ is singular. It is often possible to extend the slow flow to the fold points after a rescaling of the vector field [51]. Fenichel proved the existence of invariant slow manifolds S_ϵ where all eigenvalues of $D_x f$ have nonzero real parts. For $\epsilon > 0$ small, these normally hyperbolic slow manifolds are within an $O(\epsilon)$ distance from the critical manifold S_0 and the flow on S_ϵ converges to the slow flow on S_0 as $\epsilon \to 0$. Fenichel theory is usually developed in the context of overflowing slow manifolds with boundaries. Trajectories may leave these manifolds through their boundaries. In this setting, slow manifolds are not unique, but the distance between a pair of slow manifolds is "exponentially small," i.e. of order $O(\exp(-c/\epsilon))$ for a suitable positive c, independent of ϵ [71].

The next section of this paper presents the SMST (slow manifold of saddle-type) algorithm. This section gives an estimate of the order of accuracy of the algorithm, augmented by analysis of a linear system for which there are explicit solutions of both the solutions of the differential equations and the boundary value solver.

The third section of the paper presents numerical investigations of three examples:

1. A three-dimensional version of the Morris-Lecar model for bursting neu-

rons that was used by David Terman in his analysis of the transition between bursts with different numbers of spikes [105, 90],

2. A three-dimensional system whose homoclinic orbits yield traveling-wave profiles for the FitzHugh-Nagumo model [18],
3. A four-dimensional model of two coupled neurons studied by Guckenheimer, Hoffman and Weckesser [53].

Empirical tests of the precision of the algorithm are given for the Morris-Lecar model.

4.3 The SMST Algorithm

This section describes a collocation method called the SMST algorithm for computing slow manifolds of saddle-type in slow-fast systems. Collocation methods [21, 3, 30, 31] are a well established method for solving boundary value problems. The algorithm described in this paper is not a new collocation method [59, 48]: the subtlety lies in the formulation of a boundary value problem that yields discrete systems of equations with well-conditioned Jacobians. The crucial part of the geometry is to specify boundary conditions for trajectory segments on a slow manifold that yield well-conditioned discretizations. Two issues that must be dealt with in formulating the algorithm are that (1) the boundary conditions must determine a unique slow manifold in circumstances where there is an entire "tube" of such manifolds, and (2) any pair of trajectories that lie close to the slow manifold are "exponentially close" along most of their length.

A trajectory segment $\gamma : [a, b] \to R^{m+n}$ of system (4.1) is determined by its initial point $\gamma(a)$ or by another set of $m + n$ boundary conditions. Our goal is to compute trajectories that follow a slow manifold, but we do not know any points on that manifold. What we do know is that trajectories approach a slow manifold at a fast exponential rate and then diverge from the manifold at a fast exponential rate. We find these trajectories as solutions to a two point boundary value problem with boundary conditions at both $\gamma(a)$ and $\gamma(b)$ that constrain the trajectory to follow the slow manifold except for short time segments near its ends. The singular limit of the trajectories we seek are candidates γ_0 that consist of a fast initial segment approaching the critical manifold S along a strong stable manifold, followed by a slow segment along S, followed by a fast segment that leaves S along a strong unstable manifold. For small $\epsilon > 0$, we seek $m + n$ boundary conditions that determine a unique trajectory near the candidate. Initial conditions that do not lie in the strong stable manifold of a point $p \in S$ will diverge from the slow manifold S at a fast exponential rate. Therefore, trajectories that follow the slow manifold have initial conditions that are exponentially close to the (unknown) stable manifold of S. If the boundary conditions at a allow the initial point of γ to vary along a submanifold B_l that is transverse to the stable manifold of S, then the solver can determine a point that lies close enough to the stable manifold that it tracks S for the desired distance. Similarly, when trajectories remain close to S for times that are $O(1)$ on the slow time scale, they remain exponentially close to the unstable manifold of S as they leave S. Thus, the boundary conditions at b need to allow the solver to find points that lie close to the unstable manifold of S. This condition will be satisfied if the boundary conditions at b define a manifold B_r that is transverse to the unstable manifold of S. See Figure 4.1.

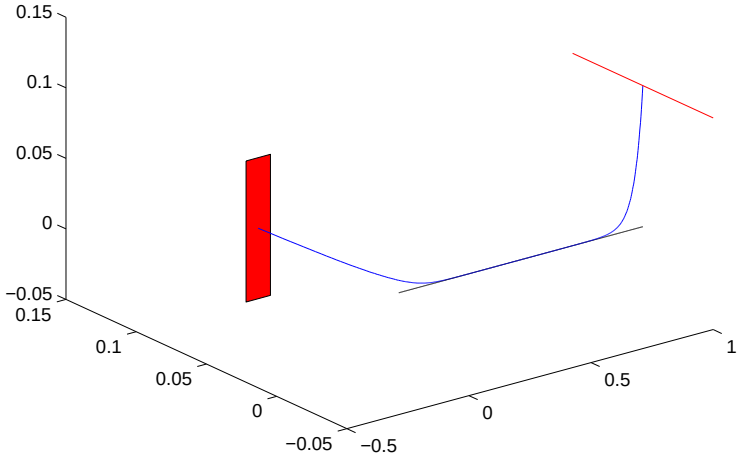

Figure 4.1: Boundary conditions for the SMST algorithm are illustrated with a three dimensional example with one slow and two fast variables. The slow manifold of saddle type is drawn black and labeled S. A trajectory that approaches the slow manifold along a strong stable direction and departs along a strong unstable manifold is drawn blue. The initial point of this trajectory lies in a two dimensional manifold B_l transverse to the stable manifold of S, and the final point lies in a one dimensional manifold B_r transverse to the unstable manifold of S.

To make the requirements on B_r and B_l more concrete, let u be the dimension of the strong unstable manifolds of S and let $E^u(p)$ and $E^s(p)$ be the strong unstable and stable subspaces in R^m at a point p in the critical manifold S_0 of system (4.1). Normal hyperbolicity asserts $s+u=m$. Fenichel Theory states that the stable manifold of S_ϵ will be close to $E^s(p) \times T_p S_0$ at a nearby point q of S_ϵ with the same slow coordinates as p and the unstable manifold of S_ϵ at q will be close to $E^u(p) \times T_p S_0$. To formulate a well posed boundary value problem, we want B_l to have dimension at least u and be transverse to the stable manifold of S_0, while B_r needs to have dimension at least s and be transverse to the unstable

manifold of S_0. The dimensions of B_l and B_r are complementary to the number of boundary conditions: we can have no more than $n + s$ boundary conditions at a and no more than $n + u$ boundary conditions at b. A trajectory segment on the time interval $[a, b]$ is determined by $m + n$ boundary conditions, so we can specify $s \leq k \leq s + n$ boundary conditions at a and $u \leq m + n - k \leq n + u$ boundary conditions at b. The n boundary conditions associated with the slow variables can be split between a and b in an arbitrary manner. As an alternative, the time length of the trajectory can be allowed to vary, and one more boundary condition can be imposed at one of the endpoints while maintaining transversality to the stable and unstable manifolds of S_0.

In our tests of the SMST algorithm, we chose boundary conditions aligned with the stable and unstable manifolds of the critical manifold S_0. We used boundary conditions at a that define a manifold passing through a point $p \in S_0$ and containing $E^u(p)$, while at b the boundary conditions define a manifold passing through a point $q \in S_0$ and containing $E^u(p)$. Normal hyperbolicity implies that the transversality conditions are satisfied for small ϵ. We know that p and q will be located at a distance $O(\epsilon)$ from the slow manifold, so the initial and final segments of our computed trajectory that diverge from S_ϵ will have length $O(\epsilon)$. In addition to the boundary conditions, the algorithm takes a (discretized) trajectory $\gamma_0 : [a, b] \to S_0$ of the slow flow with $\gamma_0(a) = p$, $\gamma_0(a) = q$ as input. With this input, we form a system of collocation equations whose solution yields a better approximation to the desired trajectory that follows S_ϵ.

Denote the mesh points in the discretization of $[a, b]$ by $a = t_0 < t_1 < \cdots < t_N = b$. There are a total of $(N + 1)(m + n)$ variables, so we need that many equations to determine an approximate trajectory that satisfies the boundary conditions

from the input data. (If $b - a$ is allowed to vary, then the number of boundary conditions is increased by one.) From points $z_j = z(t_j) \in R^{m+n}$, a C^1 cubic spline σ is constructed with the z_j as knot points and tangent vectors $F(z_j)$ at these points. On the mesh interval $[t_{j-1}, t_j]$, σ is a cubic curve whose coefficients are linear combinations of $z_{j-1}, z_j, F(z_{j-1}), F(z_j)$ that are readily determined. Each of the N mesh intervals $[t_{j-1}, t_j]$ contributes $(m + n)$ equations to the system of collocation equations by requiring that $F(\sigma((t_{j-1} + t_j)/2)) = \sigma'((t_{j-1} + t_j)/2)$. The values of σ and σ' in these equations can be expressed as

$$\begin{aligned} \sigma(\frac{t_{j-1} + t_j}{2}) &= \frac{z_{j-1} + z_j}{2} - \frac{(t_j - t_{j-1})(F(z_j) - F(z_{j-1}))}{8} \\ \sigma'(\frac{t_{j-1} + t_j}{2}) &= \frac{3(z_j - z_{j-1})}{2(t_j - t_{j-1})} - \frac{F(z_j) + F(z_{j-1})}{4} \end{aligned} \tag{4.2}$$

The boundary conditions constitute the remaining $m+n$ equations of the system. The system of $(N + 1)(m + n)$ equations is solved with Newton's method starting with the data in γ_0. The Jacobian of this system is computed explicitly, using the derivatives of the equations (4.2) with respect to z_{j-1}, z_j. The solution of the system gives a spline that satisfies the boundary conditions and satisfies the differential equation $\dot{z} = F(z)$ at the endpoints and midpoint of each mesh interval.

Two types of error estimates are of interest for this algorithm. On each mesh interval, there is a local error estimate for how much the spline σ differs from a trajectory of the vector field. The spline satisfies $\sigma'(t) = F(\sigma(t))$ at the collocation points t_{j-1}, t_j and $(t_j + t_{j-1})/2$. If γ is the trajectory of the vector field through one these points, this implies that $\sigma - \gamma = O(|t_j - t_{j-1}|^4)$. Since this classical estimate is based upon the assumption that the norm of the vector field is $O(1)$, it is only likely to hold for intervals that are short on the fast time scale and trajectory segments that lie close to the slow manifold. Globally, the trajecto-

ries of the flow display a strong separation due to the normal hyperbolicity. In Fenichel coordinates [71], stable coordinates converge rapidly to the slow manifold while unstable coordinates diverge rapidly from the slow manifold. In the case of a one-dimensional slow manifold, shadowing [12] implies that any pseudo-trajectory pieced together from local approximations to the flow will lie close to a unique trajectory of the flow. Moreover, in this case, different choices of boundary conditions that lie in the same strong stable manifold at a and the same strong unstable manifold at b yield trajectories that are exponentially close to each other and to the slow manifold outside of small subintervals near the ends of the time interval $[a, b]$. Consequently, the value of F will be $O(1)$ on the slow time scale and the middle of the spline is expected to give an excellent approximation to a trajectory on the slow manifold. Rather than pursuing more careful theoretical analysis of the algorithm here, we calculate the errors for a linear example in which the slow manifold and its numerical approximation can be computed explicitly.

4.3.1 Slow manifolds of a linear system

Consider the linear vector field

$$\begin{aligned} \epsilon \dot{x}_1 &= y - x_1 \\ \epsilon \dot{x}_2 &= x_2 \\ \dot{y} &= 1 \end{aligned} \tag{4.3}$$

Its general solution is

$$(x_1, x_2, y)(t) = (y(0) - \epsilon + t + (x_1(0) - y(0) + \epsilon) \exp(-t/\epsilon), x_2(0) \exp(t/\epsilon), y(0) + t)$$

This explicit solution provides a benchmark for evaluating the accuracy of the algorithm described above. The slow manifold of the system is the line $\{y = x_1 + \epsilon, x_2 = 0\}$ containing the trajectories $(x_1, x_2, y)(t) = (y(0) - \epsilon + t, 0, y(0) + t)$.

The discretized equations of the algorithm can also be solved explicitly for system (4.3). The first step in doing so is to observe that the equations for x_1 and y are separable from those for x_2, and this remains the case for the discretized equations of the boundary value solver. Substituting the equations for the y-variable into the boundary value equations produces the equation $y_{j+1} - y_j = t_{j+1} - t_j$ on each mesh interval. If a boundary condition is imposed on one end of the time interval $[a, b]$, these equations yield a solution that is a discretization of an exact solution of the differential equation. Convergence occurs in a single step.

Assume now that $y_{j+1} - y_j = t_{j+1} - t_j$ and set $w_j = y_j - (x_1)_j - \epsilon$ to be the difference between the x_1 coordinate of a point and a point of the slow manifold. The boundary value equations become

$$\frac{\delta^2 - 6\delta\epsilon + 12\epsilon^2}{8\delta\epsilon^2} w_j - \frac{\delta^2 + 6\delta\epsilon + 12\epsilon^2}{8\delta\epsilon^2} w_{j+1} = 0 \tag{4.4}$$

for a uniform mesh with $\delta = y_{j+1} - y_j = t_{j+1} - t_j$. The boundary conditions at $t_0 = a$ must be transverse to the x_1 coordinate axis which is E^s. Therefore, we choose to fix the value of x_1 as the boundary condition at $t_0 = a$. Note that these equations are satisfied when the w_j vanish, so if the value of x_1 is $y - \epsilon$ at $t_0 = a$, the w_j yield a discretization of the exact solution along the slow manifold. Solving the equation (4.4) for w_{j+1} in terms of w_j yields

$$w_{j+1} = \frac{\delta^2 - 6\delta\epsilon + 12\epsilon^2}{\delta^2 + 6\delta\epsilon + 12\epsilon^2} w_j$$

Like the solutions of the differential equation, the values w_j decrease exponentially as a function of time. The ratio $\rho_j = w_{j+1}/w_j$ is a function of (δ/ϵ) whose

Taylor expansion agrees with that of $\exp(-\delta/\epsilon)$ through terms of degree 4, and its value always lies in the interval $(0, 1)$. Thus the solutions of the boundary value equation converge geometrically toward the slow manifold along its stable manifold with increasing time. If the mesh intervals have length $\delta \leq \epsilon$, then the relative error of the decrease satisfies

$$0 < \frac{\rho_j(\frac{\delta}{\epsilon}) - \exp(\frac{\delta}{\epsilon})}{\exp(\frac{\delta}{\epsilon})} < 0.0015$$

For large values of δ/ϵ, the solution is no longer accurate near $t = a$ if the boundary conditions do not satisfy $y_0 = (x_1)_0 + \epsilon$. A similar, but simpler argument establishes that the solution of the discretized problem converges to the slow manifold at an exponential rate with decreasing time from $t = b$. Thus, the boundary value solver is stable and yields solutions that qualitatively resemble the exact solution for all meshes when applied to this linear problem. In particular, the solution of the discretized problem is exponentially close to the slow manifold away from the ends of the time interval $[a, b]$. As the mesh size decreases to zero, the algorithm has fourth-order convergence to the exact solution.

4.4 Numerical Examples

4.4.1 Bursting Neurons

This section on the Terman modification of the Morris-Lecar model appeared in the original paper [55] but has been omitted here for brevity.

4.4.2 Traveling Waves of the FitzHugh-Nagumo Model

The FitzHugh-Nagumo equation is a model for the electric potential $u = u(x, \tau)$ of a nerve axon interacting with an auxiliary variable $v = v(x, \tau)$ (see [43],[94]):

$$\begin{cases} \frac{\partial u}{\partial \tau} = \delta \frac{\partial^2 u}{\partial x^2} + f_a(u) - w + p \\ \frac{\partial w}{\partial \tau} = \epsilon(u - \gamma w), \end{cases} \tag{4.5}$$

where $f_a(u) = u(u-a)(1-u)$ and p, γ, δ and a are parameters. Assuming a traveling wave solution with $t = x + s\tau$ to (4.5) we get:

$$\begin{aligned} u' &= v \\ v' &= \frac{1}{\delta}(sv - f_a(u) + w - p) \\ w' &= \frac{\epsilon}{s}(u - \gamma w). \end{aligned} \tag{4.6}$$

A homoclinic orbit of (4.6) corresponds to a traveling pulse solution in (4.5). An analysis of (4.6) using numerical continuation has been carried out by Champneys et al. [18]. They fixed the parameters $a = \frac{1}{10}$, $\delta = 5$, $\gamma = 1$ and investigated bifurcations in (p, s)-parameter space. We shall fix the same values and hence write $f_{1/10}(u) =: f(u)$. To bring (4.6) into the standard form (4.1) set $x_1 := u$, $x_2 := v$, $y := w$ and change to the slow time scale:

$$\begin{aligned} \epsilon \dot{x}_1 &= x_2 \\ \epsilon \dot{x}_2 &= \frac{1}{5}(sx_2 - x_1(x_1 - 1)(\frac{1}{10} - x_1) + y - p) = \frac{1}{5}(sx_2 - f(x_1) + y - p), \\ \dot{y} &= \frac{1}{s}(x_1 - y) \end{aligned} \tag{4.7}$$

We refer to (4.7) as "the" FitzHugh-Nagumo equation. Our goal is to use the fast slow structure of (4.7) and the SMST algorithm to compute its homoclinic orbits. The critical manifold S of the FitzHugh-Nagumo equation is the cubic curve:

$$S = \{(x_1, x_2, y) \in \mathbb{R}^3 : \quad x_2 = 0, \quad y = f(x_1) + p =: c(x_1)\}. \tag{4.8}$$

The two local non-degenerate extrema of $c(x_1)$ yield the fold points of S. Denote the local minimum by $x_{1,-}$ and the local maximum by $x_{1,+}$. The critical manifold S has three normally hyperbolic components:

$$S_l = \{x_1 < x_{1,-}\} \cap S, \quad S_m = \{x_{1,-} < x_1 < x_{1,+}\} \cap S, \quad S_r = \{x_{1,+} < x_1\} \cap S.$$

Fenichel's theorem provides associated slow manifolds $S_{l,\epsilon}$, $S_{m,\epsilon}$ and $S_{r,\epsilon}$ outside neighborhoods of the fold points. The manifolds $S_{l,\epsilon}$ and $S_{r,\epsilon}$ are of saddle-type for ϵ sufficiently small. The middle branch $S_{m,\epsilon}$ is completely unstable in the fast directions. Denote the unique equilibrium point of (3.6) by $q = (x_1^*, 0, x_1^*)$. The location of q depends on the parameter p, and q moves along the cubic S. For the analysis of homoclinic orbits we shall assume that $q \in S_{l,0}$. In this case, the unstable manifold $W^u(q)$ is one-dimensional and the stable manifold $W^s(q)$ is two-dimensional. This also covers the case $q \in S_r$ by a symmetry in the FitzHugh-Nagumo equation and avoids the region where q is completely unstable [18, 56]. Homoclinic orbits exist if $W^u(q) \subset W^s(q)$.

We focus first on the case of relatively large wave speeds s ("fast waves"). Existence of these homoclinic orbits has been proved for small enough ϵ, viewing them as perturbations of a singular trajectory consisting of four segments: a fast subsystem heteroclinic connection from q to C_r at $y = x_1^*$, a slow segment on C_r, a fast subsystem heteroclinic from C_r to C_l at $y = x_1^* + c$ for some constant $c = c(p, s) > 0$ and a slow segment on C_l connecting back to q [69]. We aim to compute homoclinic orbits by a similar procedure for a given small $\epsilon > 0$ in several steps:

1. Find parameter values (p_0, s_0) such that a homoclinic orbit exists very close or exactly at (p_0, s_0). This can be achieved by a splitting algorithm without

computing the homoclinic orbit, even for very small values of ϵ [56]. Carry out all the following computations for $(p, s) = (p_0, s_0)$.

2. Compute the slow manifolds $S_{\epsilon,l}$ and $S_{\epsilon,r}$ using the SMST algorithm.

3. Compute the unstable manifold of the equilibrium $W^u(q)$ by forward integration.

4. Define a section $\Sigma = \{x_1 = c\}$ where the constant c is chosen between $x_{1,-}$ and $x_{1,+}$ e.g. $c = (x_{1,-} + x_{1,+})/2$. Compute the transversal intersection of $W^s(S_{l,\epsilon})$ and $W^u(S_{r,\epsilon})$ on Σ, call the intersection point $x_{su} = (c, x_{2,su}, y_{su})$ (see Figure 4.2). Integrate forward and backward starting at x_{su} to obtain trajectories γ_{fw} and γ_{bw}.

5. The homoclinic orbit is approximated by a concatenation of the trajectory segments on $W^u(q)$, $S_{r,\epsilon}$, $W^u(S_{r,\epsilon}) \cap W^s(S_{l,\epsilon})$ and $S_{l,\epsilon}$ computed in steps 1.-4. The endpoints of these trajectory segments are exponentially close to one another and therefore indistinguishable numerically.

All our figures for the fast wave case have been computed for $\epsilon = 10^{-3}$, $p_0 = 0$ and $s_0 \approx 1.2463$. Jones et al. [69] proved the existence of homoclinic orbits in this region for small ϵ. In Figure 4.3(a) we show the result from the SMST algorithm and the unstable manifold of the equilibrium $W^u(q)$, i.e. the output of steps 2 and 3. Due to the exponential separation along $S_{r,\epsilon}$ the trajectory $W^u(q)$ obtained from numerical integration cannot track the slow manifold for an O(1) distance and escapes after following the slow manifold for a very short time. This happens despite the fact that we have computed parameter values (p_0, s_0) with maximal accuracy in double precision arithmetic at which we expect $W^u(q)$ to follow $S_{r,\epsilon}$ almost up to the fold point $x_{1,+}$. This observation is relevant to Figure 4.3(b) where the result of step 5 is shown. All the fast segments (red)

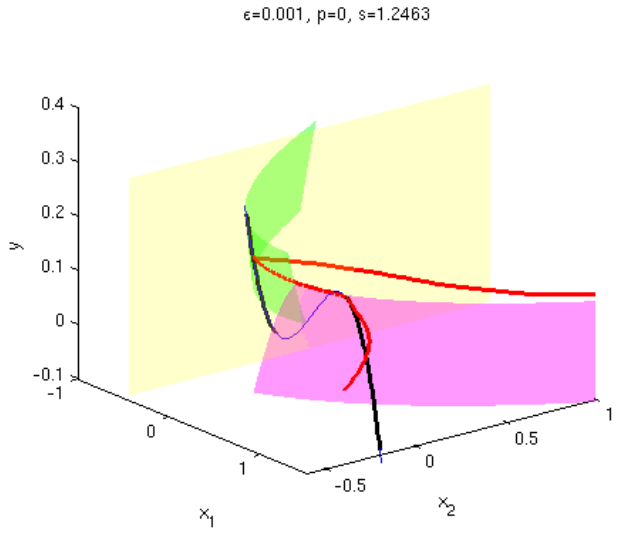

Figure 4.2: Illustration of transversal intersection of stable and unstable manifolds of the slow manifolds $W^s(S_{l,\epsilon})$ (green) and $W^u(S_{r,\epsilon})$ (magenta). The manifolds are truncated at the yellow section Σ and the trajectory $\gamma_{fw} \cup \gamma_{bw}$ started on Σ at the transversal intersection point x_{su} is shown in red.

had to be truncated almost immediately after they entered a neighborhood of a slow manifold. The final output of the algorithm after interpolation near the truncation points is shown in Figure 4.4.

Now we consider the case of "slow waves" and work with smaller wave speeds s. Homoclinic orbits representing slow waves should be thought of as perturbations of singular limit orbits for the FitzHugh-Nagumo equation (3.6) with $s = 0$. In this case the fast subsystem

$$\begin{aligned} x_1' &= x_2 \\ x_2' &= \frac{1}{5}(-f(x_1) + y - p) \end{aligned} \tag{4.9}$$

is Hamiltonian. Singular homoclinic orbits exist in a single fast subsystem with the y-coordinate of the equilibrium $y = x_1^*$. A direct application of Fenichel the-

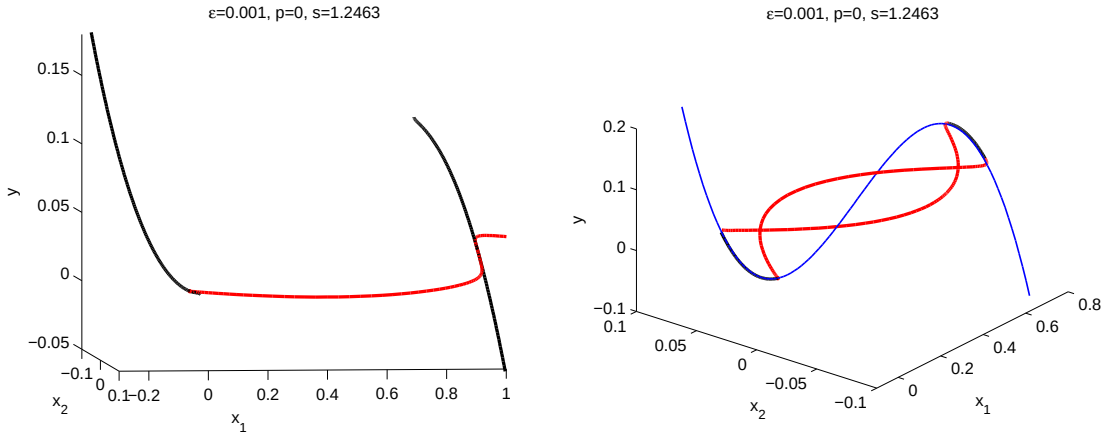

Figure 4.3: Illustration of the algorithm for computing homoclinic orbits in the FitzHugh-Nagumo equation. (a)Slow manifolds $S_{l,\epsilon}$ and $S_{r,\epsilon}$ are shown in black and the unstable manifold of the equilibrium $W^u(q)$ is displayed in red. (b) Pieces of the homoclinic orbit; slow segments in black, fast segments in red and S shown in blue.

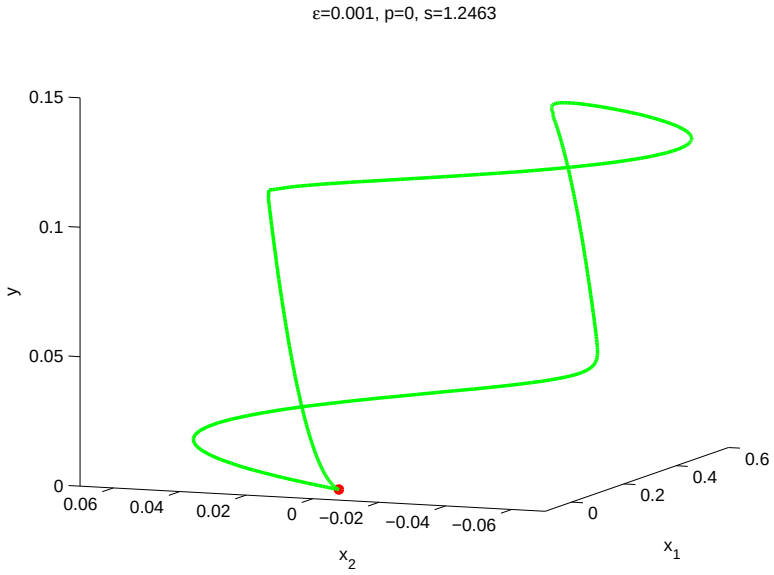

Figure 4.4: Homoclinic orbit (green) of the FitzHugh-Nagumo equation representing a fast wave. The equilibrium point q is shown in red.

ory implies that a perturbed singular "slow" homoclinic orbit persists for $\epsilon > 0$ [103]. Again it is possible to compute parameter values (p_1, s_1) at which homoclinic orbits for $\epsilon > 0$ exist [56]. To compute the orbits themselves a similar approach as described above can be used. We have to track when $W^u(q)$ enters a small neighborhood of $W^s(S_{l,\epsilon})$ respectively of $S_{l,\epsilon}$. Figure 4.5 shows two computed homoclinic orbits for $p_1 = 0$ and $s_1 \approx 0.29491$.

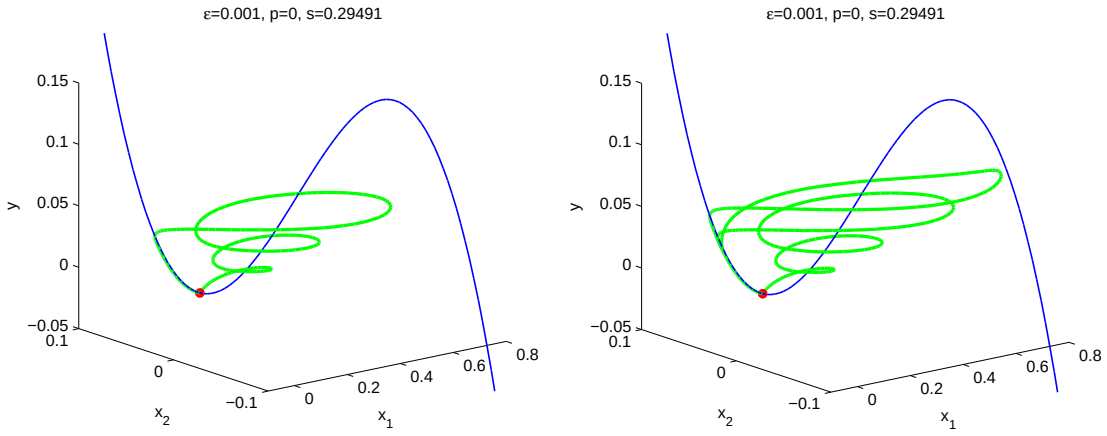

(a) (a) (b) (b)

Figure 4.5: Homoclinic orbits (green) representing slow waves in the FitzHugh-Nagumo equation. The slow manifold S is shown in blue and the equilibrium q in red. (a) "Single pulse" homoclinic orbit. (b) "Double pulse" homoclinic orbit. This trajectory returns to $S_{l,\epsilon}$ before approaching $S_{r,\epsilon}$, then leaves $S_{l,\epsilon}$ along its repelling manifold, approaches $S_{r,\epsilon}$ briefly and then returns to $S_{l,\epsilon}$ a second time, finally flowing along $S_{l,\epsilon}$ back to q.

The orbits spiral around the middle branch and do not enter the vicinity of $S_{r,\epsilon}$. This is expected as the middle branch S_m of the critical manifold consists of unstable spiral equilibria for the fast subsystems. The Hamiltonian analysis for the case $s = 0$ shows that the singular slow homoclinic orbits do not come close to S_r for values of p approximately between -0.24 and 0.05 (see [56]). In Figure 4.5(a) a homoclinic orbit enters the vicinity of the slow manifold $S_{l,\epsilon}$ and

returns directly to q. Figure 4.5(b) shows a homoclinic orbit that makes one additional large excursion around $S_{m,\epsilon}$ after it was close to $S_{r,\epsilon}$ and then returns to q; hence we refer to the orbit in 4.5(b) as a double-pulse homoclinic orbit. The same double-pulse phenomenon exists for fast waves as well. In this case the double-pulse orbit has no additional interaction with the middle branch S_m and therefore it is difficult to distinguish between different pulse types for fast waves numerically and graphically as the second loop follows the first one very closely.

4.4.3 A Model of Reciprocal Inhibition

This section on a 4D fast-slow model of coupled neurons appeared in the original paper [55] but has been omitted here for brevity.

4.5 Conclusion

We have illustrated how slow manifolds of saddle type appear in the bifurcation analysis of slow-fast systems. From the perspective of simulation via initial value solvers, these manifolds are ephemeral objects. Different methods are needed to compute them accurately. Heretofore, collocation and continuation methods incorporated into the program AUTO [34] have been used to compute periodic and homoclinic orbits in multiple time scale systems, but this approach becomes increasingly difficult as one approaches the singular limit. Our experience [53] in using AUTO has been that increasingly fine meshes are required to analyze stiff systems as the ratio of time scales becomes more extreme, es-

pecially when the solutions of interest contain canards. Our investigations of the FitzHugh-Nagumo model agree with this observation: AUTO appears to have difficulty computing homoclinic or periodic orbits that contain a lengthy segment along the slow manifold $S_{r,\epsilon}$ like the one shown in Figure 4.4. There has been little investigation of the limitations of boundary value methods in computing trajectories that contain canards, but one possible reason might be that trajectory segments which follow a slow manifold for different distances are almost impossible to distinguish numerically. This paper approaches this difficulty by introducing a two point boundary value solver that computes the slow manifolds themselves. The solver is based upon a different collocation scheme than the one used in AUTO. Though our method has worked better for us than a few attempts to solve these problems with AUTO, we have performed neither theoretical analysis or comparative numerical studies of stability and convergence of different collocation methods in computing slow manifolds of saddle-type. Such studies are interesting topics for further research. Here, we only present evidence that the SMST algorithm is an effective, fast and accurate method for computing slow manifolds in the systems that we studied. Our solver works effectively with the examples presented in this paper, yielding modest sized systems of equations that are solved with a few iterations of Newton's method. Attracting and repelling manifolds of a slow manifold S with the method are computed by numerical integration. In these numerical integrations, we start with initial points that lie in the directions of eigenvectors of the layer equations. Since these directions are almost tangent to the invariant manifolds of S that we seek and nearby trajectories converge to the manifolds, we think that the resulting surfaces are very good approximations to the manifolds. Asymptotic expansions for trajectories in the attracting and repelling manifolds

are complicated [107]: we expect that theoretical improvements in this part of the computations would require great effort for marginal gains in accuracy.

The SMST algorithm can be incorporated into multiple shooting methods for computing periodic and homoclinic orbits along the lines of those introduced in Guckenheimer and Lamar [58]. The strategy used in these methods is to define surfaces that separate the desired trajectory into segments that can be stably computed by forward or backward numerical integration, or here with the SMST algorithm. Computations of the homoclinic orbits in the FitzHugh-Nagumo model are very complex. The decomposition of these homoclinic orbits into segments that can be computed with the SMST algorithm and with numerical integration changes as one moves along the homoclinic curve in parameter space. Nonetheless, we can compute good approximations to the homoclinic orbits along the entire curve with our methods.

Theoretical analysis of the SMST algorithm and exploration of variants have hardly begun. As one possible variation, automatic differentiation methods that compute Taylor polynomials of the vector field at mesh points could be used to obtain discretized equations based upon Hermite interpolation with higher degree splines, similar to the methods used by Guckenheimer and Meloon to compute periodic orbits [59].

4.6 Additions

In addition to the boundary value solver described in Section 4.3 other approaches were tested. Several observations were made:

(a) In the case when the slow flow is one-dimensional ($y \in \mathbb{R}$) it seems to be very helpful (possibly essential) to rescale the vector field:

$$\begin{aligned} x' &= f(x, y, \epsilon) \\ y' &= \epsilon g(x, y, \epsilon) \end{aligned}$$

The slow flow will be normalized to unit speed $\epsilon t g(x, y, \epsilon) \mapsto \tilde{t}$ so that:

$$\begin{aligned} \frac{dx}{d\tilde{t}} &= \frac{f(x, y, \epsilon)}{\epsilon g(x, y, \epsilon)} \\ \frac{dy}{d\tilde{t}} &= 1 \end{aligned}$$

Note that it remains a question for future work how to access the influence of the re-scaling on the numerical method including the case of higher-dimensional slow manifolds ($y \in \mathbb{R}^n, n > 1$).

(b) The standard boundary value solvers in MatLab `bvp4c` and `bvp5c` [101] do not seem to be able to solve the problem, although the same boundary conditions and initial guess as for our scheme presented above were used. Note that it is unclear whether this is a problem on the implementation, user or algorithmic side. In fact, for moderate values of $\epsilon = O(10^{-2})$ we would expect that almost any standard 2-point boundary value solver should be able to solve for a trajectory in the slow manifold manifold.

Furthermore a different strategy for the linear test problem (4.3) was implemented in `AUTO` [34]. First we re-write the fast-slow system as $z' = F(z)$ where $z = (x, y) \in \mathbb{R}^N$ and $F = (f, \epsilon g)$. Let T denote the final time of a trajectory and re-scale $t \mapsto tT$. Then we consider the following boundary value problem for

$t \in [0,1]$:

$$\begin{aligned} z' &= TF(z) \\ H_0(z(0)) &= h_0 \\ H_1(z(1)) &= h_1 \end{aligned} \tag{4.10}$$

with $(h_0, h_1) \in \mathbb{R}^N$. The boundary conditions can be chosen as described in Section 4.3. The problem (4.10) is in the standard form for computations with `AUTO` using 2-parameter continuation with `NICP=2` as `NICP=NBC+NINT-NDIM+2`; see the `AUTO` manual for details [34]. Note that for (4.10) the final time T has become a parameter. As a second parameter we parametrize the endpoint boundary condition $h_1 = h_1(\alpha)$ with $\alpha \in \mathbb{R}$. The main idea of the method is illustrated in Figure 4.6.

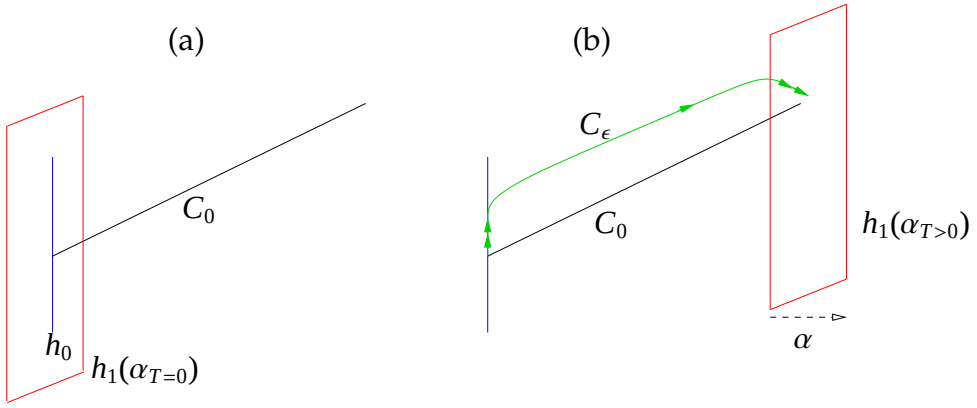

Figure 4.6: Boundary conditions are blue and red, the critical manifold C_0 is black and the trajectory that lies (disregarding transients) in the slow manifold is green. (a) The initialization step is shown. The solution is identically constant for all $t \in [0,1]$. (b) The primary continuation parameter α has been moved, T will increase and a slow manifold piece is computed.

1. Initialize the constant solution $z(0) = z(1)$ with $T = 0$ and $\alpha_{T=0}$ satisfying the terminal boundary conditions.

2. Use α as a primary continuation parameter moving the boundary conditions.

3. Via 2-parameter continuation "grow" a solution segment in C_ϵ.

4. The final value of α is chosen so that we get the boundary conditions as described in Section 4.3.

One difference between the SMST algorithm presented previously and the continuation approach is that for the latter we do not need to know an initial solution (i.e. the critical manifold). On the other hand we still need to know enough about the geometry of the critical manifold to define $h_1(\alpha)$ correctly which makes the two methods basically equivalent in terms of starting conditions.

CHAPTER 5

PAPER III: "HOMOCLINIC ORBITS OF THE FITZHUGH-NAGUMO EQUATION: BIFURCATIONS IN THE FULL SYSTEM"

5.1 Abstract

This paper investigates traveling wave solutions of the FitzHugh-Nagumo equation from the viewpoint of fast-slow dynamical systems. These solutions are homoclinic orbits of a three dimensional vector field depending upon system parameters of the FitzHugh-Nagumo model and the wave speed. Champneys et al. [A.R. Champneys, V. Kirk, E. Knobloch, B.E. Oldeman, and J. Sneyd, When Shil'nikov meets Hopf in excitable systems, *SIAM Journal of Applied Dynamical Systems*, 6(4), 2007] observed sharp turns in the curves of homoclinic bifurcations in a two dimensional parameter space. This paper demonstrates numerically that these turns are located close to the intersection of two curves in the parameter space that locate non-transversal intersections of invariant manifolds of the three dimensional vector field. The relevant invariant manifolds in phase space are visualized. A geometrical model inspired by the numerical studies displays the sharp turns of the homoclinic bifurcations curves and yields quantitative predictions about multi-pulse and homoclinic orbits and periodic orbits that have not been resolved in the FitzHugh-Nagumo model. Further observations address the existence of canard explosions and mixed-mode oscillations.

5.2 Introduction

This paper investigates the three dimensional FitzHugh-Nagumo vector field defined by:

$$\begin{aligned} \epsilon \dot{x}_1 &= x_2 \\ \epsilon \dot{x}_2 &= \frac{1}{\Delta}\left(s x_2 - x_1(x_1-1)(\alpha - x_1) + y - p\right) =: \frac{1}{\Delta}\left(s x_2 - f(x_1) + y - p\right) \\ \dot{y} &= \frac{1}{s}(x_1 - y) \end{aligned} \tag{5.1}$$

where p, s, Δ, α and ϵ are parameters. Our analysis views equations (5.1) as a fast-slow system with two fast variables and one slow variable. The dynamics of system (5.1) were studied extensively by Champneys et al. [18] with an emphasis on homoclinic orbits that represent traveling wave profiles of a partial differential equation [2]. Champneys et al. [18] used numerical continuation implemented in AUTO [34] to analyze the bifurcations of (5.1) for $\epsilon = 0.01$ with varying p and s. As in their studies, we choose $\Delta = 5$, $\alpha = 1/10$ for the numerical investigations in this paper. The main structure of the bifurcation diagram is shown in Figure 5.1.

Figure 5.1 shows a curve of Hopf bifurcations which is U-shaped and a curve of Shil'nikov homoclinic bifurcations which is C-shaped. Champneys et al. [18] observed that the C-curve is a closed curve which folds back onto itself before it reaches the U-curve, and they discussed bifurcations that can "terminate" a curve of homoclinic bifurcations. Their analysis does not take into account the multiple-time scales of the vector field (5.1). This paper demonstrates that fast-slow analysis of the homoclinic curve yields deeper insight into the events that occur at the sharp turn of the homoclinic curve. We shall focus on the turning

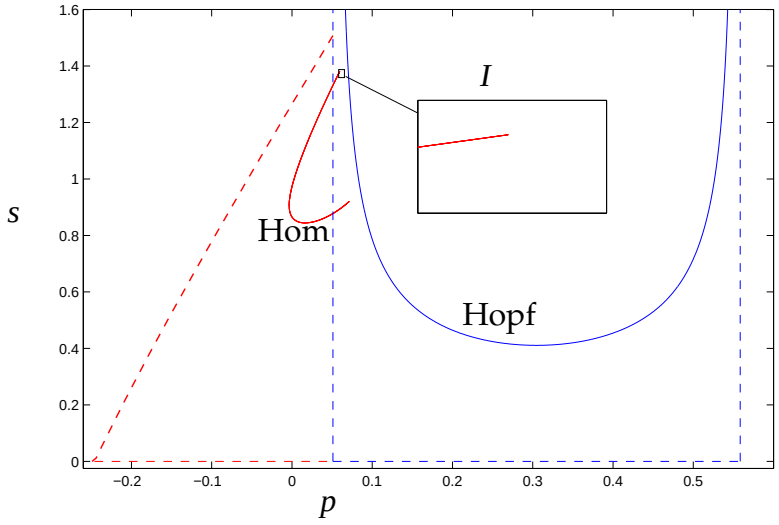

Figure 5.1: Bifurcation diagram for the FitzHugh-Nagumo equation (3.6). Shil'nikov homoclinic bifurcations (solid red) and Hopf bifurcations (solid blue) are shown for $\epsilon = 0.01$. The dashed curves show the singular limit ($\epsilon = 0$) bifurcation curves for the homoclinic and Hopf bifurcations; see [56] and Section 5.3 for details on the singular limit part of the diagram.

point at the top end of the C-curve and denote this region by I.

We regard ϵ in the FitzHugh-Nagumo equation (5.1) as a small parameter. In [56], we derived a singular bifurcation diagram which represents several important bifurcation curves in (p, s)-parameter space in the singular limit $\epsilon = 0$. The singular limits of the Hopf and homoclinic curves are shown in Figure 5.1 as dotted lines.[1] In the singular limit, there is no gap between the Hopf and homoclinic curves. We demonstrate below in Proposition 2.1 that a gap must appear for $\epsilon > 0$. The main point of this paper is that the termination point of the C-curve at the end of the gap is due to a fast-slow "bifurcation" where

[1] In Section 5.3 we recall the precise meaning of the singular limit bifurcation from [56] and how they these bifurcations arise when $\epsilon = 0$.

the two dimensional stable manifold of an equilibrium is tangent to the two dimensional unstable manifold of a one dimensional slow manifold.[2] Since the analysis of [18] does not explicitly consider slow manifolds of the system, this tangency does not appear in their list of possibilities for the termination of a C-curve. Note that the slow manifolds of the system are unique only up to "exponentially small" quantities of the form $\exp(-c/\epsilon), c > 0$, so our analysis only identifies the termination point up to exponentially small values of the parameters.

Fast-slow dynamical systems can be written in the form

$$\begin{aligned} \epsilon\dot{x} &= \epsilon\frac{dx}{d\tau} = f(x,y,\epsilon) \\ \dot{y} &= \frac{dy}{d\tau} = g(x,y,\epsilon) \end{aligned} \tag{5.2}$$

where $(x,y) \in \mathbb{R}^m \times \mathbb{R}^n$ and ϵ is a small parameter $0 < \epsilon \ll 1$. The functions $f : \mathbb{R}^m \times \mathbb{R}^n \times \mathbb{R} \to \mathbb{R}^m$ and $g : \mathbb{R}^m \times \mathbb{R}^n \times \mathbb{R} \to \mathbb{R}^n$ are analytic in the systems studied in this paper. The variables x are fast and the variables y are slow. We can change (5.2) from the slow time scale τ to the fast time scale $t = \tau/\epsilon$, yielding

$$\begin{aligned} x' &= \frac{dx}{dt} = f(x,y,\epsilon) \\ y' &= \frac{dy}{dt} = \epsilon g(x,y,\epsilon) \end{aligned} \tag{5.3}$$

In the singular limit $\epsilon \to 0$ the system (5.2) becomes a differential-algebraic equation. The algebraic constraint defines the critical manifold:

$$C_0 = \{(x,y) \in \mathbb{R}^m \times \mathbb{R}^n : f(x,y,0) = 0\}$$

[2] An analogous tangency plays an important role in the formation of mixed mode oscillations associated with singular Hopf bifurcations in fast-slow systems with one fast and two slow variables [52].

For a point $p \in C_0$ we say that C_0 is normally hyperbolic at p if the all the eigenvalues of the $m \times m$ matrix $D_x f(p)$ have non-zero real parts. A normally hyperbolic subset of C_0 is an actual manifold and we can locally parametrize it by a function $h(y) = x$. This yields the slow subsystem (or reduced flow) $\dot{y} = g(h(y), y)$ defined on C_0. Taking the singular limit $\epsilon \to 0$ in (5.3) gives the fast subsystem (or layer equations) $x' = f(x, y)$ with the slow variables y acting as parameters. Fenichel's Theorem [42] states that normally hyperbolic critical manifolds perturb to invariant slow manifolds C_ϵ. A slow manifold C_ϵ is $O(\epsilon)$ distance away from C_0. The flow on the (locally) invariant manifold C_ϵ converges to the slow subsystem on the critical manifold as $\epsilon \to 0$. Slow manifolds are usually not unique for a fixed value of $\epsilon = \epsilon_0$ but lie at a distance $O(e^{-K/\epsilon_0})$ away from each other for some $K > 0$; nevertheless we shall refer to "the slow manifold" for a fast-slow system with the possibility of an exponentially small error being understood.

Section 5.3 discusses the fast-slow decomposition of the homoclinic orbits of the FitzHugh-Nagumo equation in the region I. This decomposition has been used to prove the existence of homoclinic orbits in the system for ϵ sufficiently small [15, 63, 70, 69, 82], but previous work only applies to a situation where the equilibrium point for the homoclinic orbit is not close to a fold point. At a fold point the critical manifold of a fast-slow system is locally quadratic and not normally hyperbolic. This new aspect of the decomposition is key to understanding the sharp turn of the homoclinic curve. Section 5.4 presents a numerical study that highlights the geometric mechanism for the turning of the C-curve. We visualize relevant aspects of the phase portraits near the turns of the C-curve. In Section 5.5 we show that exponential contraction of the Shil'nikov return map

in the FitzHugh-Nagumo equation explains why n-homoclinic and n-periodic orbits are expected to be found at parameter values very close to a primary 1-homoclinic orbit. Section 5.6 presents two further observations. We identify where a canard explosion [86] occurs and we note the existence of two different types of mixed-mode oscillations in the system.

5.3 Fast-Slow Decomposition of Homoclinic Orbits

We introduce notation used in our earlier work [56]. The critical manifold of (5.1) is given by:

$$C_0 = \{(x_1, x_2, y) \in \mathbb{R}^3 : x_2 = 0 \text{ and } y = f(x_1) + p\}$$

It is normally hyperbolic away from the two fold points $x_{1,\pm}$ with $x_{1,-} < x_{1,+}$ which are found by solving $f'(x_1) = 0$ as the local minimum and maximum of the cubic f. Hence C_0 splits into three parts:

$$C_l = \{x_1 < x_{1,-}\} \cap C_0, \quad C_m = \{x_{1,-} \leq x_1 \leq x_{1,+}\} \cap C_0, \quad C_r = \{x_{1,+}\} \cap C_0$$

We are mostly interested in the two branches C_l and C_r which are of saddle-type, i.e. points in C_l and C_r are saddle equilibria of the fast subsystem. The middle branch $C_m - \{x_{1,\pm}\}$ consists of unstable foci for the fast subsystem. The slow manifolds provided by Fenichel's Theorem will be denoted by $C_{l,\epsilon}$ and $C_{r,\epsilon}$. The notation for the two-dimensional stable and unstable manifolds of $C_{l,\epsilon}$ is $W^s(C_{l,\epsilon})$ and $W^u(C_{r,\epsilon})$ with similar notation for $C_{r,\epsilon}$; the notation for the associated linear eigenspaces is e.g. $E^s(C_{l,\epsilon})$. The full system (5.1) has a unique equilibrium point which we denote by q. For $(p, s) \in I$ and $\epsilon = 0.01$ the dimensions of the stable and unstable manifolds are $\dim(W^u(q)) = 1$ and $\dim(W^s(q)) = 2$ with a complex

conjugate pair of eigenvalues for the linearization at q. The equilibrium q is completely unstable inside the U-curve and the Hopf bifurcations we are interested in near I are all subcritical [56, 18].

As $\epsilon \to 0$ the Hopf bifurcation curve converges to a region in (p, s) parameter space bounded by two vertical lines $p = p_{\pm}$ and the segment $\{s = 0, p_- \leq p \leq p_+\}$; see Figure 5.1. The parameter values $p_{\pm}$ are precisely the values when the equilibrium point q coincides with the fold points $x_{1,\pm}$ [56]. This analysis gives one part of the singular limit bifurcation diagram showing what happens to the Hopf bifurcation curves for $\epsilon = 0$.

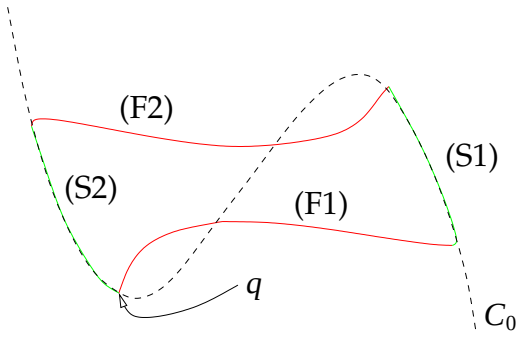

Figure 5.2: Sketch of a homoclinic orbit to the unique equilibrium q. Fast (red) and slow (green) segments decompose the orbit into segments.

When ϵ is small, the homoclinic orbit in $W^u(q) \cap W^s(q)$ can be partitioned into fast and slow segments. The singular limit of this fast-slow decomposition has four segments: a fast subsystem heteroclinic connection from q to C_r, a slow segment on C_r, a heteroclinic connection from C_r to C_l and a slow segment back to q on C_l; see Figure 5.2. Existence proofs for the homoclinic orbits [69, 63, 15] are based upon analysis of the transitions between these segments. Trajecto-

ries that remain close to a normally hyperbolic slow manifold must be "exponentially close" to the manifold except for short segments where the trajectory approaches the slow manifold along its stable manifold and departs along its unstable manifold. Existence of the homoclinic orbit depends upon how the four segments of its fast-slow decomposition fit together:

(F1) The one dimensional $W^u(q)$ approaches C_r along its two dimensional stable manifold $W^s(C_{r,\epsilon})$. Intersection of these manifolds cannot be transverse and occurs only for parameter values that lie along a curve in the (p, s) parameter plane.

(S1) The Exchange Lemma [68] was developed to analyze the flow map for trajectories that approach $C_{r,\epsilon}$ along its stable manifold and depart $C_{r,\epsilon}$ along its unstable manifold.

(F2) The fast jump from a neighborhood of $C_{r,\epsilon}$ to a neighborhood of $C_{l,\epsilon}$ occurs along a transversal intersection of the two dimensional $W^s(C_{l,\epsilon})$ and two dimensional $W^u(C_{r,\epsilon})$.

(S2) The connection from $C_{l,\epsilon}$ to q lies close to an intersection of the two dimensional $W^u(C_{l,\epsilon})$ and the two dimensional $W^s(q)$. Previous analysis has dealt with parameter regions where the connection (S2) exists and is transversal, but it *cannot* persist up to the Hopf curve in the (p, s)-plane.

Proposition 5.3.1. *There exists a region in (p, s)-parameter space near the Hopf U-curve where no trajectories close to $C_{l,\epsilon}$ lie in $W^s(q)$.*

Proof. (Sketch) The Lyapunov coefficients of the Hopf bifurcations near I are positive [56], so the periodic orbits emanating from these bifurcations occur in the parameter region to the left of the Hopf curve. The periodic orbits are completely unstable. By calculating the eigenvalues of the linearization at the equilibrium we find that there is no Fold-Hopf bifurcation on the Hopf curve near I. Hence center manifold reduction implies that there will be a region of parameters near the Hopf curve where $W^s(q)$ is a topological disk whose boundary is the periodic orbit. Close enough to the Hopf curve, $W^s(q)$ and the periodic orbit lie at a finite distance from $C_{l,\epsilon}$ and there is no connection from $C_{l,\epsilon}$ to q. □

This proposition implies that the parameter region in which there is a connection from $C_{l,\epsilon}$ to q is bounded away from the Hopf curve. The next section shows that the boundary of this parameter region is very close to a curve along which there are tangential intersections of $W^u(C_{l,\epsilon})$ and $W^s(q)$.

Remark: As $\epsilon \to 0$, the C-curve converges to two lines (dashed red in Figure 5.1) defined by homoclinic and heteroclinic orbits of the fast subsystem [56]. The horizontal segment of the C-curve to homoclinic orbits of the equilibrium point, and the sloped segment to heteroclinic orbits from the equilibrium point to the right branch of the critical manifold. Note that the C-curve terminates on the Hopf curve in the singular limit. The singular limit analysis does not explain the sharp turning of the C-curve for $\epsilon > 0$ which is the focus of the next section.

5.4 Interaction of Invariant Manifolds

The slow manifold $C_{l,\epsilon}$ is normally hyperbolic away from the fold point $x_{1,-}$, with one attracting direction and one repelling direction. We recently introduced a method [55] for computing slow manifolds of saddle type. This algorithm is used here to help determine whether there are connecting orbits from a neighborhood of $C_{l,\epsilon}$ to the equilibrium point q. Our numerical strategy for finding connecting orbits has three steps:

1. Choose the cross section

$$\Sigma_{0.09} = \{(x_1, x_2, y) \in \mathbb{R}^3 : y = 0.09\}$$

   transverse to $C_{l,\epsilon}$,

2. Compute intersections of trajectories in $W^s(q)$ with $\Sigma_{0.09}$. These points are found either by backward integration from initial conditions that lie in a small disk D containing q in $W^s(q)$ or by solving a boundary value problem for trajectories that have one end in $\Sigma_{0.09}$ and one end on the boundary of D.

3. Compute the intersection $p_l \in C_{l,\epsilon} \cap \Sigma_{0.09}$ with the algorithm described in Guckenheimer and Kuehn [55] and determine the directions of the positive and negative eigenvectors of the Jacobian of the fast subsystem at p_l.

Figure 5.3 shows the result of these computations for $\epsilon = 0.01$, $s = 1.37$ and three values of p.[3] The intersections of $W^s(q)$ with $\Sigma_{0.09}$ lies close to $W^s(C_{l,\epsilon})$.

[3]The second step above was carried out with two different initial value solvers, *ode15s* in MatLab [100] and dop853 [61], and with AUTO [34] producing similar results.

Table 5.1: Euclidean distance in (p,s)-parameter space between the Hopf curve and the location of the tangency point between $W^s(q)$ and $W^u(C_{l,\epsilon})$.

ϵ	D=d(tangency,Hopf)
10^{-2}	$\approx 1.07\epsilon$
10^{-3}	$\approx 1.00\epsilon$
10^{-4}	$\approx 0.98\epsilon$

Backward trajectories flowing along $C_{l,\epsilon}$ converge to its stable manifold at a fast exponential rate. This fact also explains the observation that $W^s(q) \cap \Sigma_{0.09}$ makes a sharp turn. In Figure 5.3(a), it is apparent that the turn lies to the left of $W^u(C_{l,\epsilon}) \cap \Sigma_{0.09}$ and that $W^s(q) \cap W^u(C_{l,\epsilon})$ is non-empty. In Figure 5.3(c), the turn lies to the right of $W^u(C_{l,\epsilon}) \cap \Sigma_{0.09}$. We have also computed the distance from the Hopf curve of the parameters at which $W^s(q)$ and $W^u(C_{l,\epsilon})$ appear to have a tangential intersection for several different values of ϵ; see Table 5.1 from which we observe that the distance is $O(\epsilon)$.

In Figure 5.3(d) the C-curve of homoclinic bifurcations (solid red) has been computed using continuation in AUTO [34] as carried out by Champneys et al. [18]. Despite the fact that no homoclinic orbit exists in part of the region I it is possible to check whether the unstable manifold $W^u(q)$ reaches a small neighborhood of $W^s(C_{r,\epsilon})$. This idea has been used in a splitting algorithm [56] to calculate where homoclinic orbits would occur if $W^s(q)$ would not move away from $C_{l,\epsilon}$ as shown in Figures 5.3(a)-5.3(c). This yields the dashed red curve in

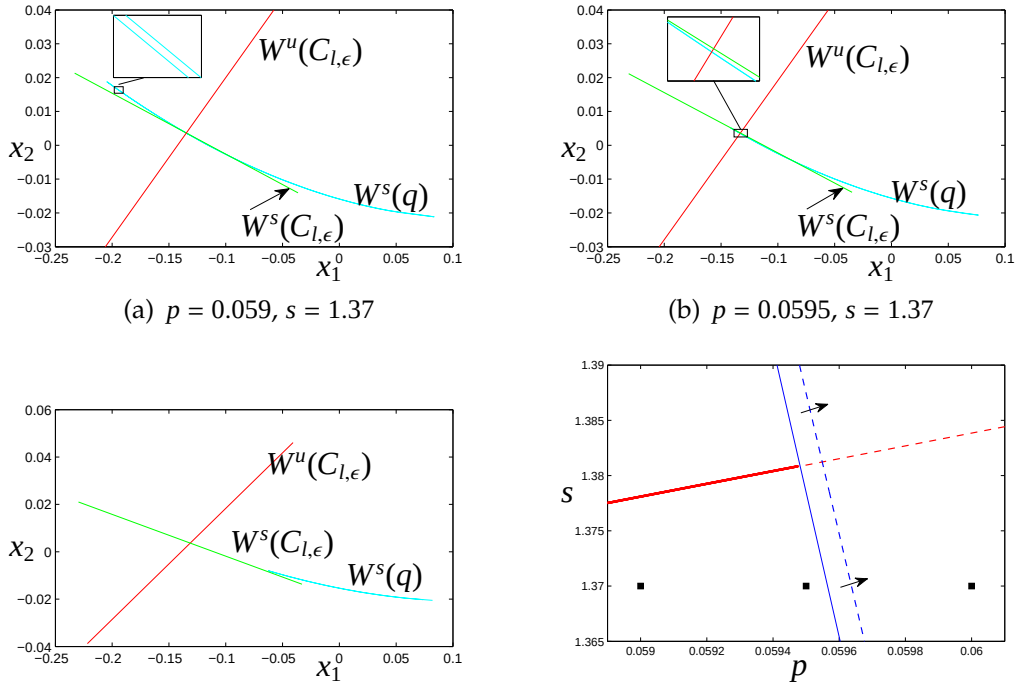

(a) $p = 0.059$, $s = 1.37$

(b) $p = 0.0595$, $s = 1.37$

(c) $p = 0.06$, $s = 1.37$

(d) Parameter space, region I.

Figure 5.3: Figures (a)-(c) show the movement of the stable manifold $W^s(q)$ (cyan) with respect to $E^u(C_{l,\epsilon})$ (red) and $E^s(C_{l,\epsilon})$ (green) in phase space on the section $y = 0.09$ for $\epsilon = 0.01$. The parameter space diagram (d) shows the homoclinic C-curve (solid red), an extension of the C-curve of parameters where $W^u(q) \cap W^s(C_{r,\epsilon})$ is nonempty, a curve that marks the tangency of $W^s(q)$ to $E^u(C_{l,\epsilon})$ (blue) and a curve that marks a distance between $C_{l,\epsilon}$ and $W^s(q)$ (dashed blue) of 0.01 where the arrows indicate the direction in which the distance is bigger than 0.01. The solid black squares in (d) show the parameter values for (a)-(c).

Figure 5.3(d). On this curve we verified that $W^s(C_{l,\epsilon})$ and $W^u(C_{r,\epsilon})$ still intersect transversally by computing those manifolds; see [56, 55] for details.

The blue curves in Figure 5.3(d) have been obtained by measuring the Euclidean distances between $W^s(q)$ and $C_{l,\epsilon}$ in the section $\Sigma_{0.09}$. Along the dashed blue curve the distance between $C_{l,\epsilon}$ and $W^s(q)$ is 0.01. The arrows indicate the direction in which this distance increases. The solid blue curve marks a tan-

gency of $W^s(q)$ with $E^u(C_{l,\epsilon})$. These calculations demonstrate that the sharp turn in the C-curve of homoclinic bifurcations occurs very close to the curve where there is a tangential intersection of $W^s(q)$ and $W^u(C_{l,\epsilon})$. Therefore, we state the following conjecture.

Conjecture 5.4.1. *The C-curve of homoclinic bifurcations of the FitzHugh-Nagumo system turns exponentially close to the boundary of the region where $W^u(C_{l,\epsilon}) \cap W^s(q)$ is nonempty.*

Note that trajectory segments of types (F1), (S1) and (F2) are still present along the dashed red curve in Figure 5.3(d). Only the last slow connection (S2) no longer exists. Existence proofs for homoclinic orbits that use Fenichel's Theorem for C_l to conclude that trajectories entering a small neighborhood of $C_{l,\epsilon}$ must intersect $W^s(q)$ break down in this region. The equilibrium q has already moved past the fold point $x_{1,-}$ in I as seen from the singular bifurcation diagram in Figure 5.1 where the blue dashed vertical lines mark the parameter values where q passes through $x_{1,\pm}$. Therefore Fenichel's Theorem does not provide the required perturbation of $C_{l,\epsilon}$. Previous proofs [69, 63, 15] assumed $p = 0$ and the connecting orbits of type (S2) do exist in this case.

Shil'nikov proved that there are chaotic invariant sets in the neighborhood of homoclinic orbits to a saddle-focus in three dimensional vector fields when the magnitude of the real eigenvalue is larger than the magnitude of the real part of the complex pair of eigenvalues [102]. The homoclinic orbits of the FitzHugh-

Nagumo vector field satisfy this condition in the parameter region I. Therefore, we expect to find many periodic orbits close to the homoclinic orbits and parameters in I with "multi-pulse" homoclinic orbits that have several jumps connecting the left and right branches of the slow manifold [38]. Without making use of concepts from fast-slow systems, Champneys et al. [18] described interactions of homoclinic and periodic orbits that can serve to terminate curves of homoclinic bifurcations. This provides an alternate perspective on identifying phenomena that occur near the sharp turn of the C-curve in I. AUTO can be used to locate families of periodic orbits that come close to a homoclinic orbit as their periods grow.

Figure 5.4 shows several significant objects in phase space for parameters lying on the C-curve. The homoclinic orbit and the two periodic orbits were calculated using AUTO. The periodic orbits were continued in p starting from a Hopf bifurcation for fixed $s \approx 1.3254$. Note that the periodic orbit undergoes several fold bifurcations [18]. We show two of the periodic orbits arising at $p = 0.05$; see [18]. The trajectories in $W^s(C_{l,\epsilon})$ have been calculated using a mesh on $C_{l,\epsilon}$ and using backward integration at each mesh point and initial conditions in the linear approximation $E^s(C_{l,\epsilon})$.

We observe from Figure 5.4 that part of $W^s(q)$ lies near $C_{l,\epsilon}$ as expected for (S2) to be satisfied. This is in contrast to the situation beyond the turning of the C-curve shown in Figure 5.5 for $p = 0.06$ and $s = 1.38$. We observe that $W^s(q)$ is bounded. Figure 5.5(a) shows two periodic orbits P_1 and P_2 obtained from a Hopf bifurcation continuation starting for $s = 1.38$ fixed. P_2 is of large

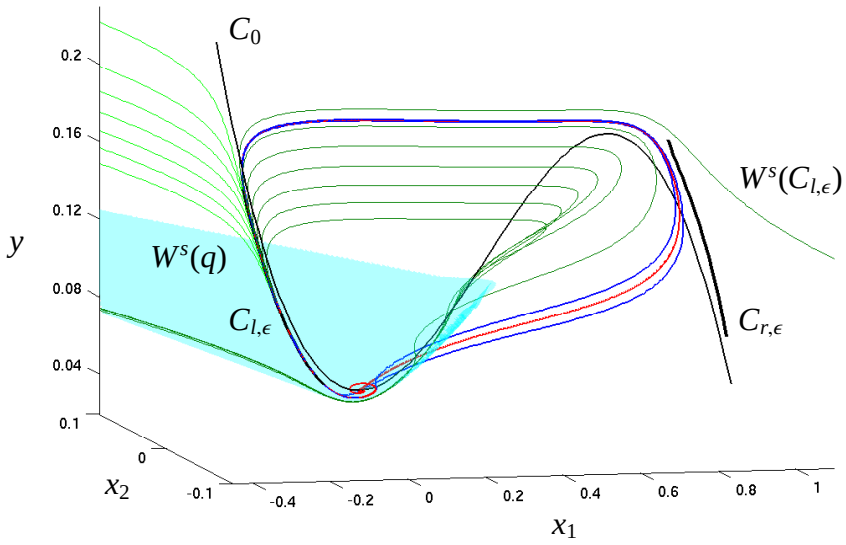

Figure 5.4: Phase space along the C-curve near its sharp turn: the parameter values $\epsilon = 0.01$, $p = 0.05$ and $s \approx 1.3254$ lie on the C-curve. The homoclinic orbit (red), two periodic orbits born in the subcritical Hopf (blue), C_0 (thin black), $C_{l,\epsilon}$ and $C_{r,\epsilon}$ (thick black) are shown. The manifold $W^s(q)$ (cyan) has been truncated at a fixed coordinate of y. Furthermore $W^s(C_{l,\epsilon})$ (green) is separated by $C_{l,\epsilon}$ into two components shown here by dark green trajectories interacting with $C_{m,\epsilon}$ and by light green trajectories that flow left from $C_{l,\epsilon}$.

amplitude and is obtained after the first fold bifurcation occurred. P_1 is of small amplitude and is completely unstable. A zoom near P_1 in Figure 5.5(b) and a time series comparison of a trajectory in $W^s(q)$ and P_1 in Figure 5.5(c) show that

$$\lim_{\alpha}\{p : p \in W^s(q) \text{ and } p \neq q\} = P_1 \tag{5.4}$$

where $\lim_\alpha U$ denotes the α-limit set of some set $U \subset \mathbb{R}^m \times \mathbb{R}^n$. From (5.4) we can also conclude that there is no heteroclinic connection from q to P_1 and only a connection from P_1 to q in a large part of the region I beyond the turning of the C-curve. Since P_1 is completely unstable, there can be no heteroclinic connections from q to P_1. Therefore, double heteroclinic connections between a

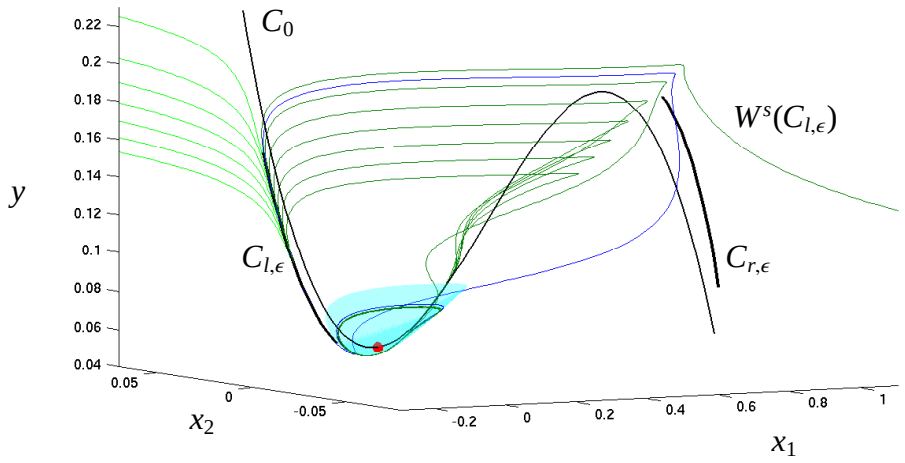

(a) Sample phase space plot between the end of the C-curve and the U-curve.

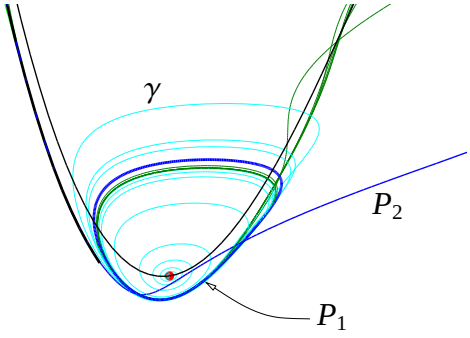

(b) Zoom for (a) near q.

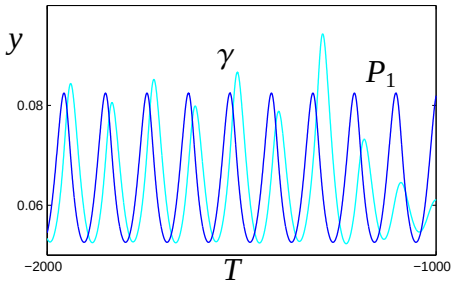

(c) Time series.

Figure 5.5: The parameter values are $\epsilon = 0.01$, $p = 0.06$ and $s = 1.38$. For (a) we display two periodic orbits (blue), one with a single large excursion P_2 and one consisting of a small loop P_1. We also show q (red dot), trajectories in $W^s(C_{l,\epsilon})$ (green) and $W^s(q)$ (cyan). In (b) a zoom near q is shown and we made plotted a single trajectory $\gamma \in W^s(q)$ (cyan). The plot (c) gives a time series of this trajectory γ in comparison to the periodic orbit P_1. Note that the trajectories are computed backward in time, so the final points of the trajectories are on the left of the figure. A phase shift of time along the periodic orbit would bring the two time series closer.

periodic orbit and q are restricted to periodic orbits that lie closer to the homoclinic orbit than P_1. These can be expected to exist for parameter values near the end of the C-curve in accord with the conjecture of Champneys et al. [18] and the "Shilnikov"-model presented in the next section.

Remark: The recent manuscript [17] extends the results of [18] that motivated this paper. A partial unfolding of a heteroclinic cycle between a hyperbolic equilibrium point and a hyperbolic periodic orbit is developed in [17]. Champneys et al. call this codimension two bifurcation an EP1t-cycle and the point where it occurs in a two dimensional parameter space an EP1t-point. The manuscript [17] does not conclude whether the EP1t-scenario occurs in the FitzHugh-Nagumo equation. The relationship between the results of this paper and those of [17] have not yet been clarified.

5.5 Homoclinic Bifurcations in Fast-Slow Systems

It is evident from Figure 5.3 that the homoclinic orbits in the FitzHugh-Nagumo equation exist in a very thin region in (p, s)-parameter space along the C-curve. We develop a geometric model for homoclinic orbits that resemble those in the FitzHugh-Nagumo equation containing segments of types (S1), (F1), (S2) and (F2). The model will be seen to be an exponentially distorted version of the Shilnikov model for a homoclinic orbit to a saddle-focus [54]. Throughout this section we assume that the parameters lie in a region I the region of the (p, s)-plane close to the upper turn of the C-curve.

The return map of the Shilnikov model is constructed from two components: the flow map past an equilibrium point, approximated by the flow map of a linear vector field, composed with a regular map that gives a "global return" of the unstable manifold of the equilibrium to its stable manifold [54]. Place two cross-sections Σ_1 and Σ_2 moderately close to the equilibrium point and model the flow map from Σ_1 to Σ_2 via the linearization of the vector field at the equilibrium.

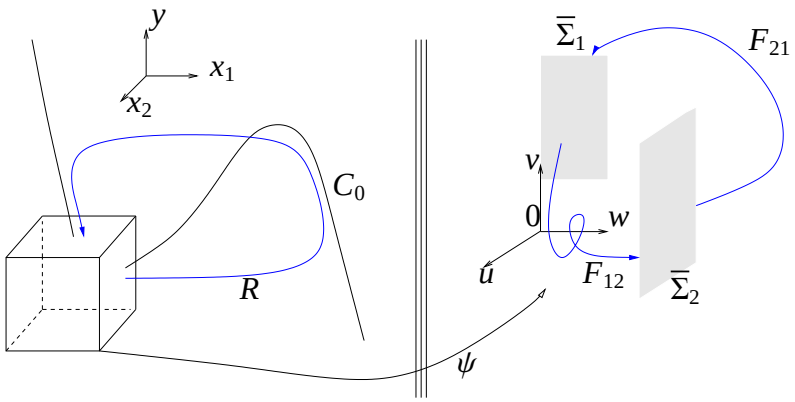

Figure 5.6: Sketch of the geometric model for the homoclinic bifurcations. Only parts of the sections $\overline{\Sigma}_i$ for $i = 1, 2$ are shown.

The degree one coefficient of the characteristic polynomial at the equilibrium has order $O(\epsilon)$, so the imaginary eigenvalues at the Hopf bifurcation point have magnitude $O(\epsilon^{1/2})$. The real part of these eigenvalues scales linearly with the distance from the Hopf curve. Furthermore we note that the real eigenvalue of the equilibrium point remains bounded away from 0 as $\epsilon \to 0$.

Let $\psi(x_1, x_2, y) = (u, v, w)$ be a coordinate change near q so that $\psi(q) = 0$ and the vector field is in Jordan normal form up to higher order terms. We denote the sections obtained from the coordinate change into Jordan form coordinates

by $\overline{\Sigma}_1 = \psi(\Sigma_1)$ and $\overline{\Sigma}_2 = \psi(\Sigma_2)$; see Figure 5.6. Then the vector field is

$$\begin{aligned} u' &= -\beta u - \alpha v \\ v' &= \alpha u - \beta v \qquad + \text{h.o.t.} \\ w' &= \gamma \end{aligned} \tag{5.5}$$

with α, β, γ positive. We can choose ψ so that the cross-sections are $\overline{\Sigma}_1 = \{u = 0, w > 0\}$ and $\overline{\Sigma}_2 = \{w = 1\}$. The flow map $F_{12} : \overline{\Sigma}_1 \to \overline{\Sigma}_2$ of the (linear) vector field (5.5) without higher-order terms is given by

$$F_{12}(v, w) = v w^{\beta/\gamma} \left(\cos\left(-\frac{\alpha}{\gamma} \ln(w) \right), \sin\left(-\frac{\alpha}{\gamma} \ln(w) \right) \right) \tag{5.6}$$

Here β and α tend to 0 as $\epsilon \to 0$. The domain for F_{12} is restricted to the interval $v \in [\exp(-2\pi\beta/\alpha), 1]$ bounded by two successive intersections of a trajectory in $W^s(0)$ with the cross-section $u = 0$.

The global return map $R : \Sigma_2 \to \Sigma_1$ of the FitzHugh-Nagumo system is obtained by following trajectories that have successive segments that are near $W^s(C_{r,\epsilon})$ (fast), $C_{r,\epsilon}$ (slow), $W^u(C_{r,\epsilon}) \cap W^s(C_{l,\epsilon})$ (fast), $C_{l,\epsilon}$ (slow) and $W^u(C_{l,\epsilon})$ (fast). The Exchange Lemma [68] implies that the size of the domain of R in Σ_2 is a strip whose width is exponentially small. As the parameter p is varied, we found numerically that the image of R has a point of quadratic tangency with $W^s(q)$ at a particular value of p. We also noted that $W^u(q)$ crosses $W^s(C_{r,\epsilon})$ as the parameter s varies [56]. Thus, we choose to model R by the map

$$(w, v) = F_{21}(u, v) = (\sigma v + \lambda_2 - \rho^2 (u - \lambda_1)^2, \rho(u - \lambda_1) + \lambda_3) \tag{5.7}$$

for F_{21} where λ_1 represents the distance of $W^u(q) \cap \Sigma_2$ from the domain of F_{21}, λ_2 represents how far the image of F_{21} extends in the direction normal to $W^s(q)$,

λ_3 is the v coordinate of $F_{21}(\lambda_1, 0)$ and ρ^{-1}, σ are $O(e^{-K/\epsilon})$ for suitable $K > 0$. We assume further that the domain of F_{21} is $[\lambda_1, \lambda_1 + \rho^{-1}] \times [-1, 1]$. Figure 5.7 depicts F_{21}. With these choices, we observe two properties of the C-curve of homoclinic orbits in the geometric model:

1. If $\sigma v + \lambda_2 - \rho^2(u - \lambda_1)^2$ is negative on the domain of F_{21}, then the image of F_{21} is disjoint from the domain of F_{12} and there are no recurrent orbits passing near the saddle point. Thus, recurrence implies that $\lambda_2 > -\sigma$.
2. If $\lambda_2 > 0$, then there are two values of λ_1 for which the saddle-point has a single pulse homoclinic orbit. These points occur for values of λ_1 for which the w-component of $F_{21}(0, 0)$ vanishes: $\lambda_1 = \pm\rho^{-1}|\lambda_2|^{1/2}$. The magnitude of these values of λ_2 is exponentially small.

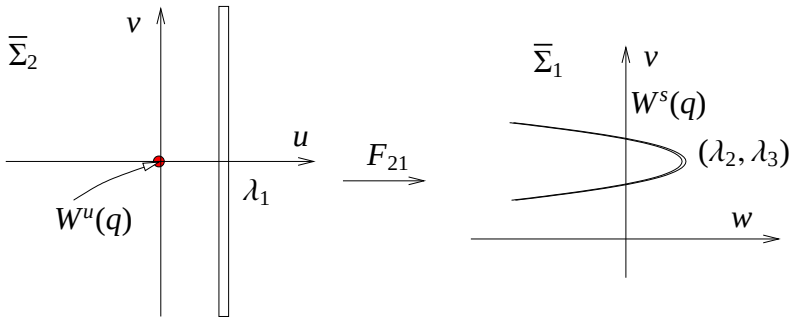

Figure 5.7: Sketch of the map $F_{21} : \overline{\Sigma}_2 \to \overline{\Sigma}_1$. The (u, v) coordinates are centered at $W^u(q)$ and the domain of F_{21} is in the thin rectangle at distance λ_1 from the origin. The image of this rectangle is the parabolic strip in $\overline{\Sigma}_2$.

When a vector field has a single pulse homoclinic orbit to a saddle-focus whose real eigenvalue has larger magnitude than the real part of the complex

eigenvalues, Shilnikov [102] proved that a neighborhood of this homoclinic orbit contains chaotic invariant sets. This conclusion applies to our geometric model when it has a single pulse homoclinic orbit. Consequently, there will be a plethora of bifurcations that occur in the parameter interval $\lambda_2 \in [0, \sigma]$, creating the invariant sets as λ_2 decreases from σ to 0.

The numerical results in the previous section suggest that in the FitzHugh-Nagumo system, some of the periodic orbits in the invariant sets near the homoclinic orbit can be continued to the Hopf bifurcation of the equilibrium point. Note that saddle-node bifurcations that create periodic orbits in the invariant sets of the geometric model lie exponentially close to the curve $\lambda_2 = 0$ that models tangency of $W^s(q)$ and $W^u(C_{l,\epsilon})$ in the FitzHugh-Nagumo model. This observation explains why the right most curve of saddle-node bifurcations in Figure 7 of Champneys et al. [18] lies close to the sharp turn of the C-curve.

There will also be curves of heteroclinic orbits between the equilibrium point and periodic orbits close to the C-curve. At least some of these form codimension two EP1t bifurcations near the turn of the C-curve as discussed by Champneys et al. [18]. Thus, the tangency between $W^s(q)$ and $W^u(C_{l,\epsilon})$ implies that there are several types of bifurcation curves that pass exponentially close to the sharp turn of the C-curve in the FitzHugh-Nagumo model. Numerically, any of these can be used to approximately locate the sharp turn of the C-curve.

5.6 Canards and Mixed Mode Oscillations

This section reports two additional observations about the FitzHugh-Nagumo model resulting from our numerical investigations and analysis of the turning of the C-curve.

5.6.1 Canard Explosion

The previous sections draw attention to the intersections of $W^s(q)$ and $W^u(C_{l,\epsilon})$ as a necessary component for the existence of homoclinic orbits in the FitzHugh-Nagumo system. Canards for the backward flow of this system occur along intersections of $W^u(C_{l,\epsilon})$ and $C_{m,\epsilon}$. These intersections form where trajectories that track $C_{l,\epsilon}$ have continuations that lie along $C_{m,\epsilon}$ which has two unstable fast directions. We observed from Figures 5.4 and 5.5 that a completely unstable periodic orbit born in the Hopf bifurcation on the U-curve undergoes a canard explosion, increasing its amplitude to the size of a relaxation oscillation orbit upon decreasing p. This canard explosion happens very close to the intersections of $W^u(C_{l,\epsilon})$ and $C_{m,\epsilon}$.

To understand where this transition starts and ends we computed the middle branch $C_{m,\epsilon}$ of the slow manifold by integrating backwards from points between the fold points $x_{1,-}$ and $x_{1,+}$ starting close to $C_{m,0}$ and determined which side of $W^u(C_{l,\epsilon})$ these trajectories came from. The results are shown in Figure 5.8. The dashed green curve divides the (p, s) plane into regions where the trajectory that flows into $C_{m,\epsilon}$ lies to the left of $W^u(C_{l,\epsilon})$ and is unbounded from the region

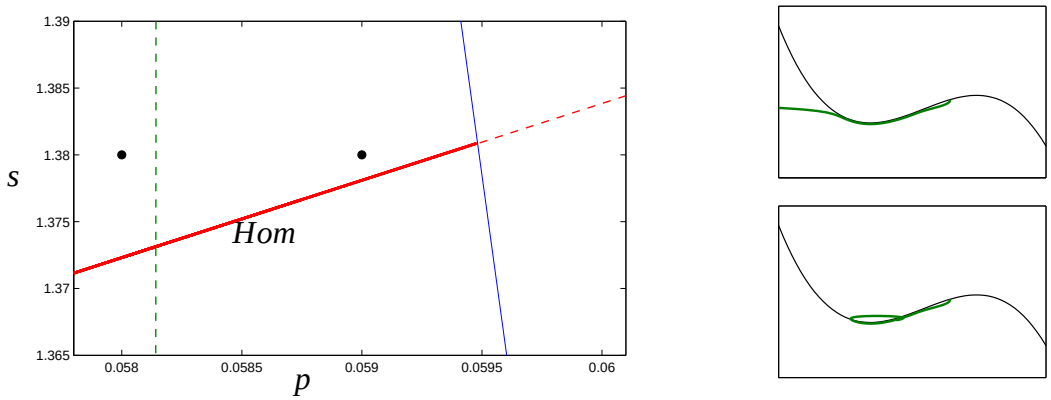

(a) (p, s)-space: Black circles correspond to two portraits in (b).

(b) (x_1, y)-projection.

Figure 5.8: The dashed green curve indicates where canard orbits start to occur along $C_{m,\epsilon}$. For values of p to the left of the dashed green curve we observe that orbits near the middle branch escape in backward time (upper panel in (b)). For values of p to the right of the dotted green curve trajectories near $C_{m,\epsilon}$ stay bounded in backward time.

where the trajectory that flows into $C_{m,\epsilon}$ lies to the right of $W^u(C_{l,\epsilon})$ and comes from the periodic orbit or another bounded invariant set. This boundary was found by computing trajectories starting on $C_{m,0}$ backward in time. In backward time the middle branch of the slow manifold is attracting, so the trajectory first approaches $C_{m,\epsilon}$ and then continues beyond its end when x_1 decreases below $x_{1,-}$. Figure 5.8(b) illustrates the difference in the behavior of these trajectories on the two sides of the dashed green curve. Figure 5.8 shows that the parameters with canard orbits for the backward flow have smaller values of p than those for which $W^s(q)$ and $W^u(C_{l,\epsilon})$ have a tangential intersection. The turns of the C-curve do not occur at parameters where the backward flow has canards.

5.6.2 Mixed-Mode Oscillations

Mixed-mode oscillations (MMOs) have been observed in many fast-slow systems; see e.g. [92, 98, 99, 52]. MMOs are periodic orbits which consist of sequences of small and large amplitude oscillations. The notation L^s is used to indicate an MMO with L large and s small oscillations.

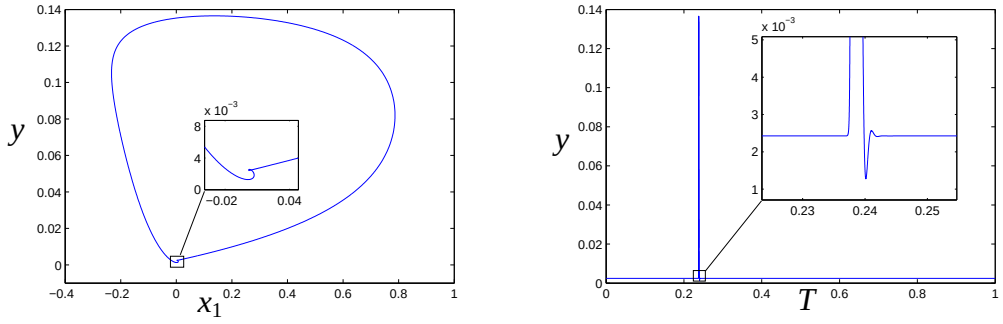

(a) (x_1, y)-space, $p = 0.00266172$.

(b) Time series for (a).

(c) (x_1, y)-space, $p = 0.0628718$.

(d) Time Series for (c).

Figure 5.9: Some examples of mixed-mode oscillations in the FitzHugh-Nagumo equation. Fixed parameter values are $\epsilon = 0.01$ and $s = 1$. Note that the period of the orbits has been rescaled to 1 in (*b*) and (*d*).

The FitzHugh-Nagumo equation (5.1) exhibits MMOs: the periodic orbits close to the homoclinic orbit make small oscillations near the equilibrium point in addition to large amplitude relaxation oscillations. A 1^1 MMO is shown in

Figure 5.9(a)-(b). It was obtained by switching from the homoclinic C-curve to a nearby curve of periodic orbits in a continuation framework. Note that the existence of multi-pulse homoclinic orbits near a Shilnikov homoclinic orbit [45, 38] implies that much more complicated patterns of MMOs also exist near the homoclinic C-curve. L^s MMOs with very large L and s near the homoclinic C-curve are theoretically possible although observing them will be very difficult due to the exponential contraction described in Section 5.5.

In addition to the MMOs induced by the Shilnikov bifurcation we also find MMOs which exist due to orbits containing canard segments near the completely unstable slow manifold $C_{m,\epsilon}$. An example of a 4^1 MMO is shown in Figure 5.9(c)-(d) obtained by continuation. In this case the small oscillations arise due to small excursions reminiscent to MMOs in three-time scale systems [67, 81]. MMOs of type L^1 with $L = 1, 2, 3, \ldots, O(10^2)$ can easily be observed from continuation and we expect that L^1 MMOs exist for any $L \in \mathbb{N}$. It is likely that these MMOs can be analyzed using a version of the FitzHugh-Nagumo equation containing $O(1)$, $O(\epsilon)$ and $O(\epsilon^2)$ terms similar to the one introduced in [56] but we leave this analysis for future work.

Figure 5.9 was obtained by varying p for fixed values of $\epsilon = 0.01$ and $s = 1$. Thus, varying a single parameter suffices to switch between MMOs whose small amplitude oscillations have a different character. In the first case, the small amplitude oscillations occur when the orbit comes close to a saddle focus rotating around its stable manifold, while in the second case, the trajectory never approaches the equilibrium and its small amplitude oscillations occur when the

trajectory flows along the completely unstable slow manifold $C_{m,\epsilon}$. Different types of MMOs seem to occur very frequently in single- and multi-parameter bifurcation problems; see [27] for a recent example. This contrasts with most work on the analysis of MMOs [76, 98] that focuses on identifying *the* mechanism for generating MMOs in an example. The MMOs in the FitzHugh-Nagumo equation show that a fast-slow system with three or more variables can exhibit MMOs of different types and that one should not expect a priori that a single mechanism suffices to explain all the MMO dynamics.

5.7 Additions

We will give some additional details of the computations for the invariant manifolds. The slow manifold $C_{l,\epsilon}$ is of saddle type. Hence a special algorithm is needed to compute it. We used the boundary value approach (BVP) described in [55] with boundary conditions well-away from the section

$$\Sigma_{0.09} = \{(x_1, x_2, y) \in \mathbb{R}^3 : y = 0.09\}$$

near C_l. The computed piece of $C_{l,\epsilon}$ was then intersected with $\Sigma_{0.09}$. At the intersection point the linearization of (5.1) is used to compute the eigenspaces $E^s(C_{l,\epsilon})$ and $E^u(C_{l,\epsilon})$. The stable manifold $W^s(q)$ was computed by considering a line segment $L \subset E^s(q)$ close to q such that

$$\{\phi_t(L), t \to \infty\} \cup \{\phi_t(L), t \to -\infty\} \approx W^s(q)$$

where ϕ_t denotes the flow of (5.1). Choosing a mesh on L we can use backward integration to trace out trajectories in $W^s(q)$ that intersect $\Sigma_{0.09}$. These intersections have been recorded and give $W^s(q)$ in Figure 5.3(a)-5.3(c). The integration

was carried out with the stiff solver *ode15s* in MatLab [100]. Since the distance between $y = 0.09$ and the equilibrium point q is moderate and trajectories do not travel a long time near a slow manifold this approach works but we also used a BVP calculation in AUTO [34] to verify the calculations. For the BVP calculation the integration time T is a free parameter and we consider the BVP

$$u'(t) = TF(u(t)) \qquad \text{with } t \in [0,1] \tag{5.8}$$

$$u(0) = \mu v \qquad \text{with } v \in E^s(q) \tag{5.9}$$

$$(u(1))_3 = y_{end} \qquad \text{with } y_{end} \in \mathbb{R} \tag{5.10}$$

where μ and y_{end} are a free parameters. The four boundary conditions (5.9)-(5.10) describe a trajectory that starts in the eigenspace $E^s(q)$ and ends in a plane $y = y_{end}$. We start with μ sufficiently small and a constant solution μv with $T = 0$. Varying y_{end} as the main continuation parameter with second free parameter T and keeping μ fixed we stop at $y_{end} = 0.09$; see also [26]. Then we can free μ and continue in μ and T to trace out the intersection $W^s(q) \cap \Sigma_{0.09}$. This method confirmed the direct integration calculations; note that this type of BVP approach is well-known and works well for small pieces of stable and unstable invariant manifolds. More elaborate methods for complicated invariant manifolds exist [77]. This completes the calculations for Figures 5.3(a)-5.3(c).

CHAPTER 6

PAPER IV: "FROM FIRST LYAPUNOV COEFFICIENTS TO MAXIMAL CANARDS"

6.1 Abstract

Hopf bifurcations in fast-slow systems of ordinary differential equations can be associated with surprising rapid growth of periodic orbits. This process is referred to as canard explosion. The key step in locating a canard explosion is to calculate the location of a special trajectory, called a maximal canard, in parameter space. A first-order asymptotic expansion of this location was found by Krupa and Szmolyan [86, 85, 83] in the framework of a "canard point"-normal-form for systems with one fast and one slow variable. We show how to compute the coefficient in this expansion using the first Lyapunov coefficient at the Hopf bifurcation thereby avoiding use of this normal form. Our results connect the theory of canard explosions with existing numerical software, enabling easier calculations of where canard explosions occur.

6.2 Introduction

Our framework in this paper is the theory of fast-slow ordinary differential equations (ODEs):

$$\begin{aligned} \epsilon\dot{x} &= \epsilon\frac{dx}{d\tau} = f(x,y,\lambda,\epsilon) \\ \dot{y} &= \frac{dy}{d\tau} = g(x,y,\lambda,\epsilon) \end{aligned} \tag{6.1}$$

where $(x,y) \in \mathbb{R}^m \times \mathbb{R}^n$, $\lambda \in \mathbb{R}$ is viewed as a parameter and ϵ is sufficiently small, i.e. $0 < \epsilon \ll 1$. The functions $f : \mathbb{R}^m \times \mathbb{R}^n \times \mathbb{R} \times \mathbb{R} \to \mathbb{R}^m$ and $g : \mathbb{R}^m \times \mathbb{R}^n \times \mathbb{R} \times \mathbb{R} \to \mathbb{R}^n$ are assumed to be at least C^3 in this paper. The variables x are fast and the variables y are slow. An introduction to the theory of fast-slow systems from the geometric viewpoint can be found in [1, 71, 49], asymptotic methods are developed in [93, 47] and ideas from nonstandard analysis are considered in [28]. We will only use geometric and asymptotic methods here.

In the singular limit $\epsilon \to 0$ the system (6.1) becomes a differential-algebraic equation. The algebraic constraint defines the critical manifold:

$$C_0 = \{(x,y) \in \mathbb{R}^m \times \mathbb{R}^n : f(x,y,\lambda,0) = 0\}$$

For a point $p \in C_0$ we say that C_0 is normally hyperbolic at p if all the eigenvalues of the $m \times m$ matrix $D_x f(p)$ have non-zero real parts. A normally hyperbolic subset of C_0 is an actual manifold and we can locally parametrize it by a map $\psi(y) = x$. This yields the slow subsystem (or reduced flow) $\dot{y} = g(\psi(y), y, \lambda, 0)$ defined on C_0.

Changing in (6.1) from the slow time scale τ to the fast time scale $t = \tau/\epsilon$

yields:

$$\begin{aligned} x' &= \frac{dx}{dt} = f(x, y, \lambda, \epsilon) \\ y' &= \frac{dy}{dt} = \epsilon g(x, y, \lambda, \epsilon) \end{aligned} \tag{6.2}$$

Taking the singular limit $\epsilon \to 0$ in (6.2) gives the fast subsystem (or layer equations) $x' = f(x, y, \lambda, 0)$ with the slow variables y acting as parameters. A point $p \in C_0$ is an equilibrium of the fast subsystem. We call a subset $S \subset C_0$ an attracting critical manifold if all points p on it are stable equilibria of the fast subsystem i.e. all eigenvalues of $D_x f(p)$ have negative real parts. The subset $S \subset C_0$ is called a repelling critical manifold if for all $p \in S$ at least one eigenvalue of $D_x f(p)$ has positive real part.

Fenichel's Theorem [42] states that normally hyperbolic critical manifolds perturb to invariant slow manifolds C_ϵ. A slow manifold C_ϵ is $O(\epsilon)$ distance away from C_0. The flow on the (locally) invariant manifold C_ϵ converges to the slow subsystem on the critical manifold as $\epsilon \to 0$. Slow manifolds are usually not unique for a fixed value of $\epsilon = \epsilon_0$ but lie at a distance $O(e^{-k/\epsilon_0})$ away from each other for some $k > 0$; nevertheless we shall refer to "the slow manifold" associated to subset of the a critical manifold with the possibility of an exponentially small error being understood.

Suppose the critical manifold can be divided into two subsets S_a and S_r where S_a is attracting and S_r is repelling so that $C_0 = S_a \cup L \cup S_r$. Here L denotes the part of C_0 that is not normally hyperbolic. We assume that for $p \in L$ the matrix $D_x f(p)$ has a single zero eigenvalue with right and left eigenvectors v and w and that $w \cdot D_{xx}(p)(v, v)$ and $w \cdot D_y f(p)$ are non-zero. In this case points in L

are called fold points. We can use the flow of (6.2) to extend the associated slow manifolds $S_{a,\epsilon}$ and $S_{r,\epsilon}$ but the extensions might not be normally hyperbolic. The key definition used in this paper is that a trajectory γ in the intersection of $S_{a,\epsilon}$ and $S_{r,\epsilon}$ is called a maximal canard; note that this definition requires the extensions of the slow manifolds under the flow. Observe that $\gamma \subset S_{r,\epsilon}$ despite the fact that $S_{r,\epsilon}$ is repelling in the fast directions.

We are interested in the case when a fast-slow system undergoes a Hopf bifurcation and a maximal canard is formed close to this bifurcation. The periodic orbits resulting from the Hopf bifurcation grow rapidly in a λ-interval of width $O(e^{-K/\epsilon})$ for some $k > 0$. The rapid orbit growth is usually referred to as canard explosion and the bifurcation scenario is called singular Hopf bifurcation.

The paper is organized as follows. In Section 6.3 we describe results on singular Hopf bifurcation and canard explosion obtained by Krupa and Szmolyan [86]. In Section 6.4 we clarify the different definitions of the first Lyapunov coefficient of a Hopf bifurcation. In Section 6.5 we present the main results on the relation between the location of the maximal canard and the first Lyapunov coefficient. We describe which terms will contribute to the first order approximation using a rescaled Hopf bifurcation normal form. Then we show explicitly how to compute a first order approximation to the location of the maximal canard avoiding additional center manifold reduction and normal form transformations. In Section 6.6 we locate the maximal canards in two examples: a two-dimensional version of van der Pol's equation and a three-dimensional version of the FitzHugh-Nagumo equation.

Note that we do not give a detailed description of dynamics associated to a singular Hopf bifurcation and refer the reader to the previous extensive literature e.g. [4, 5, 13, 86, 52].

6.3 Canard Explosion

We describe the main results about canard explosion in fast-slow systems with one fast and one slow variable from [86]. Consider a planar fast-slow system of the form

$$\begin{aligned} x' &= f(x, y, \lambda, \epsilon) \\ y' &= \epsilon g(x, y, \lambda, \epsilon) \end{aligned} \tag{6.3}$$

where $f, g \in C^k(\mathbb{R}^4, \mathbb{R})$ for $k \geq 3$, $\lambda \in \mathbb{R}$ is a parameter and $0 < \epsilon \ll 1$. Denote the critical manifold of (6.3) by C_0. We assume that C_0 is locally parabolic with a minimum at the origin $(x, y) = (0, 0)$ independent of λ so that $(0, 0)$ is a fold point; more precisely

$$f(0, 0, \lambda, 0) = 0, \quad f_x(0, 0, \lambda, 0) = 0, \quad f_{xx}(0, 0, \lambda, 0) \neq 0, \quad f_y(0, 0, \lambda, 0) \neq 0 \tag{6.4}$$

In addition, we assume that $g(0, 0, \lambda \neq 0, 0) \neq 0$; under these conditions the fold point at the origin is generic for $\lambda \neq 0$. We assume without loss of generality that $f_{xx}(0, 0, \lambda, 0) > 0$ so that C_0 is locally a parabola with a minimum at the origin. Using (6.4) and the implicit function theorem we have that C_0 is the graph of a function $y = \phi(x)$ for $\phi : U \to \mathbb{R}$ where U is a sufficiently small neighborhood of $x = 0$. Assume that C_0 splits into an attracting and a repelling

curve $C = C_l \cup \{(0,0)\} \cup C_r$ where

$$C_l = \{x < 0,\, f_x < 0\} \cap C_0, \quad C_r = \{x > 0,\, f_x > 0\} \cap C_0$$

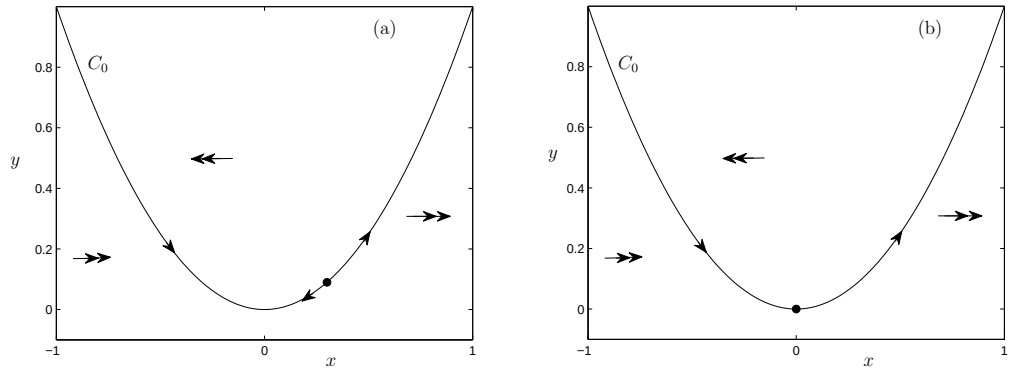

Figure 6.1: (a) A generic fold for $\lambda \neq 0$. (b) A nondegenerate canard point for $\lambda = 0$. The slow flow is indicated by single and the fast flow by double arrows.

The situation is shown in Figure 6.1(a). Differentiating $y = \phi(x)$ with respect to $\tau = t\epsilon$ we get that the slow flow on C_0 is defined by

$$\frac{dx}{d\tau} = \dot{x} = \frac{g(x, \phi(x), \lambda, 0)}{\phi'(x)}$$

Note that the slow flow is singular for $\lambda \neq 0$ at $(0,0)$ since $\phi'(0) = 0$ and $g(0,0,\lambda,0) \neq 0$. Assume that at $\lambda = 0$ we have a non-degenerate canard point (see Figure 6.1(b)) so that in addition to the fold conditions we have

$$g(0,0,0,0) = 0, \quad g_x(0,0,0,0) \neq 0, \quad g_\lambda(0,0,0,0) \neq 0$$

Therefore the slow flow is well-defined at $(0,0)$ for $\lambda = 0$ and we assume without loss of generality that $\dot{x} > 0$ in this case. Near a non-degenerate canard point (6.3) can be transformed into a normal form [83]:

$$\begin{aligned} x' &= -yh_1(x,y,\lambda,\epsilon) + x^2 h_2(x,y,\lambda,\epsilon) + \epsilon h_3(x,y,\lambda,\epsilon) \\ y' &= \epsilon(xh_4(x,y,\lambda,\epsilon) - \lambda h_5(x,y,\lambda,\epsilon) + yh_6(x,y,\lambda,\epsilon)) \end{aligned} \tag{6.5}$$

where the functions h_i are given by:

$$\begin{aligned} h_3(x,y,\lambda,\epsilon) &= O(x,y,\lambda,\epsilon) \\ h_j(x,y,\lambda,\epsilon) &= 1 + O(x,y,\lambda,\epsilon), \qquad j = 1,2,4,5 \end{aligned}$$

We define several computable constants, abbreviating $(0,0,0,0) = 0$ in the definitions:

$$a_1 = (h_3)_x(0), \quad a_2 = (h_1)_x(0), \quad a_3 = (h_2)_x(0), \quad a_4 = (h_4)_x(0), \quad a_5 = (h_6)_x(0)$$

Note that all a_i for $i = 1,2,3,4,5$ only depend on partial derivatives with respect to x. Next we define another constant:

$$A = -a_2 + 3a_3 - 2a_4 - 2a_5$$

Theorem 6.3.1. *(Krupa and Szmolyan [86]) For $0 < \epsilon < \epsilon_0$, $|\lambda| < \lambda_0$ and $\epsilon_0 > 0$, $\lambda_0 > 0$ sufficiently small and under the previous assumptions in this section there exists a unique equilibrium point p for (6.5) in a neighborhood of $(x,y) = (0,0)$. The equilibrium p undergoes a Hopf bifurcation at λ_H with*

$$\lambda_H = -\frac{a_1 + a_5}{2}\epsilon + O(\epsilon^{3/2}) \tag{6.6}$$

The slow manifolds $C_{\epsilon,l}$ and $C_{\epsilon,r}$ intersect/coincide in a maximal canard at λ_c for

$$\lambda_c = -\left(\frac{a_1 + a_5}{2} + \frac{A}{8}\right)\epsilon + O(\epsilon^{3/2}) \tag{6.7}$$

The equilibrium p is stable for $\lambda < \lambda_H$ and unstable for $\lambda > \lambda_H$. The Hopf bifurcation is non-degenerate for $A \neq 0$, supercritical for $A < 0$ and subcritical for $A > 0$.

Remark: The asymptotic expansions for λ_H and λ_c are asymptotic series with asymptotic sequence $\{\epsilon^{k/2}\}_{k=0}^{\infty}$ and Theorem 6.3.1 implies that the first two coefficients of the expansion are zero and the third coefficient can be computed

explicitly.

Note that currently no standard bifurcation software such as AUTO [34] or MatCont [46] computes the constants a_i and A automatically. Nevertheless bifurcation software can detect Hopf bifurcations so that given a fixed ϵ we can approximate λ_H numerically. Hence the numerical problem that remains is to compute A since

$$\lambda_H - \lambda_c = \frac{A}{8}\epsilon + O(\epsilon^{3/2})$$

To simplify the notation we define $K = A/8$. If we know K we can easily approximate the location of the maximal canard by $\lambda_c = \lambda_H - K\epsilon + O(\epsilon^{3/2})$. The maximal canard organizes the canard explosion [86] and indicates where the rapid amplitude growth of the small orbits generated in the Hopf bifurcation occurs. Our goal is to avoid any additional normal form transformations and center manifold reductions to compute K. The key point to achieve this is to observe that K is just a rescaled version of "the" first Lyapunov coefficient of the Hopf bifurcation at λ_H.

6.4 The First Lyapunov Coefficient

We review and clarify the interpretation, computation and conventions associated with the first Lyapunov coefficient of a Hopf bifurcation. Consider a general N-dimensional ODE at a non-degenerate Hopf bifurcation point. We assume that the equilibrium has been translated to the origin so that

$$z' = Mz + F(z), \qquad \text{for } z \in \mathbb{R}^N \tag{6.8}$$

with $F(z) = O(\|z\|^2)$ and $M = (m_{ij})$. Taylor expanding F yields

$$z' = Mz + \frac{1}{2}B(z,z) + \frac{1}{6}C(z,z,z)$$

where the multilinear functions B and C are given by:

$$\begin{aligned} B_i(u,v) &= \sum_{j,k=1}^{N} \left.\frac{\partial^2 F_i(\xi)}{\partial\xi_j\partial\xi_k}\right|_{\xi=0} u_j v_k \\ C_i(u,v,w) &= \sum_{j,k,l=1}^{N} \left.\frac{\partial^3 F_i(\xi)}{\partial\xi_j\partial\xi_k\partial\xi_l}\right|_{\xi=0} u_j v_k w_l \end{aligned}$$

The matrix M has eigenvalues $\lambda_{1,2} = \pm i\omega_0$ for $\omega_0 > 0$. Let $q \in \mathbb{C}^N$ be the eigenvector of λ_1 and $p \in \mathbb{C}^N$ the corresponding eigenvector of the transpose M^T i.e.

$$Mq = i\omega_0 q, \quad M\bar{q} = -i\omega_0\bar{q}, \quad M^T p = -i\omega_0 p, \quad M\bar{p} = i\omega_0\bar{p}$$

where the the overbar denotes componentwise complex conjugation. We can always normalize p so that the standard complex inner product with q satisfies $\bar{p}^T q = \sum_{j=1}^{N} \bar{p}_j q_j = 1$. The first Lyapunov coefficient of the Hopf bifurcation can then be defined by (Kuznetsov [88], p.180):

$$l_1^{Ku} = \frac{1}{2\omega_0}\left(\bar{p}^T C(q,q,\bar{q}) - 2\bar{p}^T B(q, L^{-1}B(q,\bar{q})) + \bar{p}^T B(\bar{q}, (2i\omega_0 I_N - M)^{-1}B(q,q))\right) \quad (6.9)$$

In the case of a two-dimensional vector field $F = (F^1, F^2)$ the formula (6.9) can be expressed in the simpler form (Kuznetsov [88], p.98):

$$l_1^{Ku} = \frac{1}{2\omega_0^2}\mathrm{Re}(ig_{20}g_{11} + \omega_0 g_{21}) \quad (6.10)$$

where

$$g_{20} = \bar{p}^T B(q,q), \quad g_{11} = \bar{p}^T B(q,\bar{q}), \quad g_{21} = \bar{p}^T C(q,q,\bar{q})$$

It is important to note that l_1^{Ku} is not uniquely defined until we choose a normalization of the eigenvector q. We adopt the convention using unit norm $\bar{q}^T q = 1$.

A slight modification of the formula (6.9) is used to evaluate the Lyapunov coefficient l_1^{MC} numerically in the bifurcation software MatCont [46]. Using the current MatCont convention[1] we note that

$$\omega_0 l_1^{Ku} = l_1^{MC}$$

Other expressions for the first Lyapunov coefficient can be found in the literature. We consider only the planar case using simpler notation $(z_1, z_2) = (x, y)$:

$$\begin{pmatrix} x' \\ y' \end{pmatrix} = \begin{pmatrix} F^1(x,y) \\ F^2(x,y) \end{pmatrix} =: M \begin{pmatrix} x \\ y \end{pmatrix} + \begin{pmatrix} f(x,y) \\ g(x,y) \end{pmatrix} \tag{6.11}$$

Then another convention for l_1 is (Chow, Li and Wang [19], p.211):

$$\begin{aligned} l_1^{CLW} = \quad & \frac{m_{12}}{16\omega_0^4}[\omega_0^2[(f_{xxx} + g_{xxy}) + 2m_{22}(f_{xxy} + g_{xyy}) - m_{21}(f_{xyy} + g_{yyy})] \\ & -m_{12}m_{22}(f_{xx}^2 - f_{xx}g_{xy} - f_{xy}g_{xx} - g_{xx}g_{yy} - 2g_{xy}) \\ & -m_{21}m_{22}(g_{yy}^2 - g_{yy}f_{xy} - g_{xy}f_{yy} - f_{xx}f_{yy} - 2f_{xy}^2) \\ & +m_{12}^2(f_{xx}g_{xx} + g_{xx}g_{xy}) - m_{21}^2(f_{yy}g_{yy} + f_{xy}f_{yy}) \\ & -(\omega_0^2 + 3m_{22}^2)(f_{xx}f_{xy} - g_{xy}g_{yy})] \end{aligned} \tag{6.12}$$

where all evaluations in (6.12) are at $(x, y) = (0, 0)$. Next, assume that we have applied a preliminary linear coordinate change

$$\begin{pmatrix} x \\ y \end{pmatrix} = N \begin{pmatrix} u \\ v \end{pmatrix} \qquad \text{where } N : \mathbb{R}^2 \to \mathbb{R}^2$$

to the system (6.11) to transform M into Jordan normal form. Then we look at:

$$\begin{aligned} \begin{pmatrix} u' \\ v' \end{pmatrix} &= \begin{pmatrix} 0 & -\omega_0 \\ \omega_0 & 0 \end{pmatrix} \begin{pmatrix} u \\ v \end{pmatrix} + N^{-1} \begin{pmatrix} f(u,v) \\ g(u,v) \end{pmatrix} \\ &= \begin{pmatrix} 0 & -\omega_0 \\ \omega_0 & 0 \end{pmatrix} \begin{pmatrix} u \\ v \end{pmatrix} + \begin{pmatrix} f^*(u,v) \\ g^*(u,v) \end{pmatrix} \end{aligned} \tag{6.13}$$

[1] MatCont version 2.5.1 - December 2008

In this case the Lyapunov coefficient formula simplifies (Guckenheimer and Holmes [54], p.152):

$$l_1^{GH} = \frac{1}{16}[f^*_{xxx} + f^*_{xyy} + g^*_{xxy} + g^*_{yyy}] + \frac{1}{16\omega_0}[f^*_{xy}(f^*_{xx} + f^*_{yy}) - g^*_{xy}(g^*_{xx} + g^*_{yy}) - f^*_{xx}g^*_{xx} + f^*_{yy}g^*_{yy}] \tag{6.14}$$

Note that the linear transformation N is not unique. We adopt the convention that

$$N = \begin{pmatrix} 2\mathrm{Re}(q_1) & -2\mathrm{Im}(q_1) \\ 2\mathrm{Re}(q_2) & -2\mathrm{Im}(q_2) \end{pmatrix}$$

where $q = (q_1, q_2)$ is the normalized eigenvector of the linearization L that satisfies $Lq = i\omega_0 q$. Another common definition for (6.13) is (Perko [96], p.353):

$$l_1^{Pe} = \frac{3\pi}{4\omega_0^2}([f^*_{xy}f^*_{yy} + f^*_{yy}g^*_{yy} - f^*_{xx}g^*_{xx} - g^*_{xy}g^*_{xx} - g^*_{xy}g^*_{yy} + f^*_{xy}f^*_{xx}] + \omega_0[g^*_{yyy} + f^*_{xxx} + f^*_{xyy} + g^*_{xxy}]) \tag{6.15}$$

The Hopf bifurcation theorem holds for any version of l_1 as only the sign is relevant in this case:

Theorem 6.4.1. *(see e.g. [54, 88]) A non-degenerate Hopf bifurcation of* (6.8) *is supercritical if* $l_1 < 0$ *and subcritical if* $l_1 > 0$.

Since we need not only a qualitative result such as Theorem 6.4.1, but a quantitative one relating the Lyapunov coefficient to canard explosion, it is necessary to distinguish between the different conventions we reviewed above.

6.5 Relating l_1 and K

Krupa and Szmolyan consider a blow-up [86, 83, 85] of (6.5) given by $\Phi : S^3 \times I \to \mathbb{R}^4$ in a particular chart K_2:

$$x = rx_2, \qquad y = r^2 y_2, \qquad \lambda = r\lambda_2, \qquad \epsilon = r^2 \epsilon_2 \tag{6.16}$$

where $r \in I \subset \mathbb{R}$ and $(x_2, y_2, \lambda_2, \epsilon_2) \in S^3$. Using (6.16) the resulting vector field can be desingularized by dividing it by $\sqrt{\epsilon}$. We shall not discuss the details of the blow-up approach and just note that this transformation and the following desingularization are simply a rescaling of the vector field given by:

$$x_2 = \epsilon^{-1/2} x, \qquad y_2 = \epsilon^{-1} y, \qquad \lambda_2 = \epsilon^{-1/2} \lambda, \qquad t_2 = \epsilon^{1/2} t \tag{6.17}$$

Using the formula from Chow, Li and Wang [19] in the rescaled version of (6.5) Krupa and Szmolyan get the following result:

Proposition 6.5.1. *In the coordinates* (6.17) *the first Lyapunov coefficient* l_1 *has asymptotic expansion:*

$$\overline{l}_1^{CLW} = K\sqrt{\epsilon} + O(\epsilon) \tag{6.18}$$

where the overbar indicates the first Lyapunov coefficient in coordinates given by (6.17)*.*

First, we want to explain in more detail which terms in the vector field (6.5) contribute to the leading order coefficient K. The main problem is that the Lyapunov coefficient is often calculated after an ϵ-dependent rescaling, such as (6.17), has been carried out. This can lead to rather unexpected effects in which terms contribute to the Lyapunov coefficient, as pointed out by Guckenheimer [52] in the context of singular Hopf bifurcation in $\mathbb{R}^3$.

To understand how the rescaling (6.17) affects the Lyapunov coefficient we consider the Hopf normal form case. We start with a planar vector field with linear part in Jordan form (6.13). Assume that the equilibrium is at the origin $(x, y) = 0$ and Hopf bifurcation occurs for $\lambda = 0$. Applying the rescaling (6.17) we get:

$$\begin{pmatrix} dx_2/dt_2 \\ dy_2/dt_2 \end{pmatrix} = \begin{pmatrix} 0 & -\omega_0/\sqrt{\epsilon} \\ \omega_0/\sqrt{\epsilon} & 0 \end{pmatrix} \begin{pmatrix} x_2 \\ y_2 \end{pmatrix} + \begin{pmatrix} \frac{1}{\epsilon} f^*(\sqrt{\epsilon}x_2, \epsilon y_2) \\ \frac{1}{\epsilon^{3/2}} g^*(\sqrt{\epsilon}x_2, \epsilon y_2) \end{pmatrix} \tag{6.19}$$

In a fast-slow system with singular Hoof bifurcation we know that $g^*(.,.) = \epsilon(\ldots)$ and that $\omega_0 = O(\sqrt{\epsilon})$. Setting $k_\omega = \omega_0/\sqrt{\epsilon}$ the Lyapunov coefficient can be computed to leading order by (6.14):

$$\overline{l}_1^{GH} = \frac{1}{k_\omega} \left(f^*_{x_2x_2}(0,0)[g^*_{x_2x_2}(0,0) + f^*_{x_2y_2}(0,0)] + k_\omega f_{x_2x_2x_2}(0,0) \right) \sqrt{\epsilon} + O(\epsilon) \tag{6.20}$$

Equation (6.20) explains the leading-order behavior more clearly and shows that due to the rescaling certain derivative terms in the Lyapunov coefficient for a singular Hopf bifurcation are non-leading terms with respect to $\epsilon \to 0$. The point is that the rescaling modifies the order with respect to ϵ of the linear and nonlinear terms. Also, applying the chain rule to the nonlinear terms to calculate the necessary derivatives can affect which terms contribute.

To make Proposition (6.5.1) more useful in an applied framework we have computed all the different versions of the Lyapunov coefficient defined in Section (6.4) up to leading order for equation (6.5) in original non-rescaled coordi-

nates. The computer algebra system Maple [66] was used in this case:

$$\begin{aligned} l_1^{Ku} &= \frac{4K}{\sqrt{\epsilon}} + O(\sqrt{\epsilon}) \\ l_1^{MC} &= \frac{4K\omega_0}{\sqrt{\epsilon}} + O(\omega_0\sqrt{\epsilon}) \\ l_1^{GH} &= K + O(\epsilon) \\ l_1^{CLW} &= K + O(\epsilon) \\ l_1^{Pe} &= \frac{3\pi K}{64\omega_0} + O(\epsilon/\omega_0) \end{aligned} \tag{6.21}$$

Using the results (6.21) we now have a direct strategy how to analyze a canard explosion generated in a singular Hopf bifurcation.

1. Compute the location of the Hopf bifurcation. This gives λ_H.
2. Find the first Lyapunov coefficient at the Hopf bifurcation, e.g. we get $l_1^{MC} \approx 4K\omega_0/\sqrt{\epsilon}$.
3. Compute the location of the maximal canard, and hence the canard explosion, by $\lambda_c \approx \lambda_H - K\epsilon$. For example, using MatCont we would get

$$\lambda_c \approx \lambda_H - \frac{l_1^{MC}}{4\omega_0}\epsilon^{3/2} \tag{6.22}$$

Observe that the previous calculation may require calculating the eigenvalues at the Hopf bifurcation to determine ω_0 but does not require any center manifold calculations nor additional normal form transformations; these have basically been encoded in the calculation of the Lyapunov coefficient.

6.6 Examples

The first example is a version of van der Pol's equation [23, 24, 86] given by:

$$\begin{aligned} x' &= y - x^2 - \frac{x^3}{3} \\ y' &= \epsilon(\lambda - x) \end{aligned}$$

We have to reverse time $t \to -t$ to satisfy the assumptions of Section (6.3). This gives:

$$\begin{aligned} x' &= x^2 + \frac{x^3}{3} - y \\ y' &= \epsilon(x - \lambda) \end{aligned} \tag{6.23}$$

The critical manifold is given by $C_0 = \{y = x^2 + x^3/3\}$ with two fold points at $(0, 0)$ and $(-2, 4/3)$. The fold points split the critical manifold into three normally hyperbolic parts:

$$C_l = C_0 \cap \{x < -2\}, \quad C_m = C_0 \cap \{-2 < x < 0\}, \quad C_r = C_0 \cap \{0 < x\}$$

We only study the fold point at the origin which becomes a canard point for $\lambda = 0$. The unique equilibrium point $p = (x_e(\lambda), y_e(\lambda))$ of (6.23) lies on C_0 and satisfies $x_e(\lambda) = \lambda$. It is easy to check that subcritical Hopf bifurcation occurs for $\lambda = \lambda_H = 0$. Matching terms in (6.23) and the normal form (6.5) we find:

$$h_1 = h_4 = h_5 = 1, \qquad h_2 = 1 + \frac{1}{3}x, \quad h_6 = 0$$

Therefore $K = 1/8$ and we find analytically that the location of the maximal canard representing the intersection of $C_{m,\epsilon}$ and $C_{r,\epsilon}$ is

$$\lambda_c = -(1/8)\epsilon + O(\epsilon^{3/2}) \tag{6.24}$$

A numerical continuation calculation using a bifurcation software tool - we used MatCont [46] - gives that the first Lyapunov coefficient for the Hopf bifurcation

at $\lambda = \lambda_H = 0$ for $\epsilon = 0.05$ is

$$l_1^{MC} \approx 0.4762$$

An easy calculation[2] yields that $\omega_0 \approx 0.2236$. Using (6.22) we compare this to the result in equation (6.24) with $\epsilon = 0.05$. Dropping higher-order terms we have:

$$\lambda_c(\text{analytical}) = -0.0063, \qquad \lambda_c(\text{numerical using } l_1) = -0.0060 \tag{6.25}$$

The coincidence of the values of the location of the maximal canard is already quite good but this is expected since we have only compared the asymptotic formula to the Lyapunov coefficient formula derived from it which was evaluated numerically using continuation. A simple direct test to compare (6.25) to the location of the maximal canard is to use continuation of periodic orbits from the Hopf bifurcation point. The results are shown in Figure 6.2.

Remark: Depending on the bifurcation software used, direct continuation of periodic orbits can fail for small values of ϵ. In this case special methods are needed to continue periodic orbits having canard segments; see e.g. [58, 55, 27]. Note that locating Hopf bifurcations and calculating Lyapunov coefficients works well even for very small values of ϵ as we require only local algebraic calculations.

We conclude from Figure 6.2 that our estimates in (6.25) are very good indicators to determine where the canard explosion exists since they are already decent for a relatively large $\epsilon = 0.05$. In many standard fast-slow systems values of $\epsilon \leq 0.01$ are commonly considered.

[2]Using MatCont 2.5.1. we can modify the file `/matcont2.5.1/MultilinearForms/nf_H.m` to return the variable `omega`= ω_0 or to return $l_1^K = l_1^{MC}/\omega_0$.

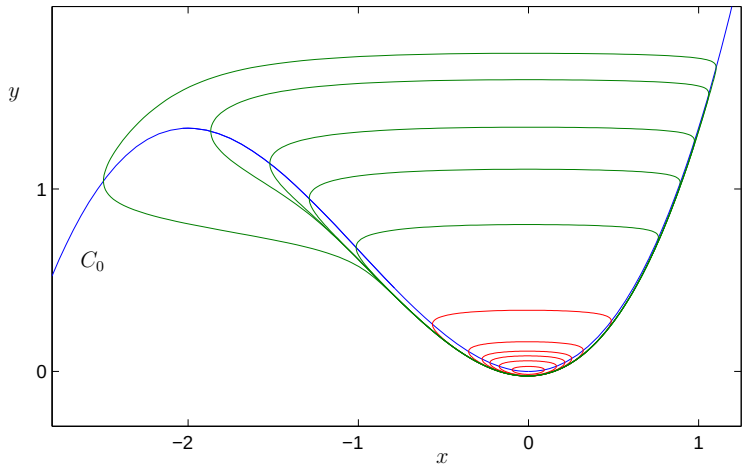

Figure 6.2: Continuation of periodic orbits emanating from the Hopf bifurcation at $\lambda = 0$. The parameter values for the red orbits are $\lambda = -0.001, -0.0025, -0.004, -0.005, -0.006, -0.0065$ and for all the green orbits the parameter value is $\lambda \approx -0.006509$ indicating a canard explosion near this parameter value.

In higher dimensions the analytical calculations will be very difficult to carry out. As a second example consider a version of the FitzHugh-Nagumo equation [18, 56, 57]:

$$\begin{aligned} x_1' &= x_2 \\ x_2' &= \frac{1}{5}\left(sx_2 - x_1(x_1-1)(0.1-x_1) + y - I\right) \\ y' &= \frac{\epsilon}{s}(x_1 - y) \end{aligned} \tag{6.26}$$

where I and s are parameters. Equation (6.26) has two fast and one slow variable and a unique equilibrium point $p(I) = p$. For a detailed fast-slow system analysis describing the bifurcations we refer the reader to [56, 57]. We only note that the critical manifold is cubic curve given by

$$C_0 = \{(x_1, x_2, y) \in \mathbb{R}^3 : x_2 = 0 \text{ and } y = x_1(x_1-1)(0.1-x_1) + I\}$$

It is normally hyperbolic away from two fold points $x_{1,\pm}$ given by the local min-

imum and maximum of the cubic. The equilibrium p passes through the fold points under parameter variation; $O(\epsilon)$ away from these points the equilibrium undergoes Hopf bifurcation [56, 57]. We shall just compute a particular case applying our result (6.21). We fix $s = 1.37$ and observe that I plays the same role as λ in our previous calculations. We calculated the location of the maximal canard for several values of ϵ. The results are shown in Table 6.1.

Table 6.1: Comparison between the actual location of the maximal canard (canard explosion) I_c and the first-order approximation $I_c(Lyapunov)$ computed using the first Lyapunov coefficient at the Hopf bifurcation.

ϵ	I_c	$I_c(Lyapunov)$
10^{-2}	≈ 0.0582046	≈ 0.06308
$5 \cdot 10^{-3}$	≈ 0.0545535	≈ 0.05629
10^{-3}	≈ 0.0517585	≈ 0.05196
$5 \cdot 10^{-4}$	≈ 0.0514108	≈ 0.05150

The second column of Table 6.1 shows the actual location I_c of the maximal canard (canard explosion) obtained from continuation of periodic orbits using AUTO [34]. The third column shows the approximation obtained by using the first Lyapunov coefficient. The Lyapunov coefficient has been computed using MatCont [46]. The error $E(\epsilon)$ of this calculation is of order $O(\epsilon^{3/2})$ as expected from (6.18). Obviously the approximation improves for smaller values of ϵ.

In the case of $\epsilon = 0.01$ it has been shown in [56, 57] that there is an intricate bifurcation scenario involving homoclinic orbits in a parameter interval near I_c.

The first order approximation of the maximal canard is not sufficient to relate it to the homoclinic bifurcation. This shows that the magnitude of ϵ and other relevant bifurcations in the system have to be taken into account carefully when applying the results we presented here.

6.7 Discussion

We have investigated the relation between the first Lyapunov coefficient at a singular Hopf bifurcation and the associated maximal canard orbit. The major result is that no additional algorithms are needed to compute a first order approximation to the location of the maximal canard. Standard bifurcation software packages compute the Lyapunov coefficient and our results can be used to approximate the maximal canard location from this numerical calculation.

We also pointed out that there is no "standard definition" of the first Lyapunov coefficient of a Hopf bifurcation. This is not surprising since classical qualitative bifurcation theory only requires the sign of the Lyapunov coefficient. We hope that the comparison in Section 6.4 will help the reader to adapt their own numerical algorithms and software packages to support the calculation of maximal canard locations.

Open questions which we leave for future work include the extensions to multiple slow variables, higher-order asymptotic expansions and the relation between the Lyapunov coefficient and blow-up transformations.

6.8 Additions

It is important to note that the idea presented here to find the maximal canard via the first Lyapunov coefficient at the singular Hopf bifurcation can potentially be very useful for analyzing mixed-mode oscillations (MMOs). This was actually one of the motivations to find an explicit/computable formula as presented in Section 6.5. We shall consider a particular example to illustrate this point.

Koper [76] studied a three-dimensional model of Van der Pol-Duffing-type as a prototypical example for MMOs:

$$\begin{aligned} \epsilon\dot{x} &= ky - x^3 + 3x - \lambda \\ \dot{y} &= x - 2y + z \\ \dot{z} &= (y - z) \end{aligned} \tag{6.27}$$

where λ, k are parameters and we always assume $0 \leq \epsilon \ll 1$. We note that a two-dimensional version of (6.27) was first studied by Boissonade and De Kepper [10]. The first analysis of MMOs in the three-dimensional extended model was carried out by Koper. Observe that the critical manifold obtained by setting $\epsilon = 0$ depends on k and λ. Usually it is more convenient to work with a fixed critical manifold so we propose the coordinate change:

$$x \to x, \qquad y \to \frac{y + \lambda}{k}, \qquad z \to \frac{z}{k} \tag{6.28}$$

Applying (6.28) to (6.27) we obtain:

$$\begin{aligned} \epsilon\dot{x} &= y - x^3 + 3x \\ \dot{y} &= kx - 2(y + \lambda) + z \\ \dot{z} &= (\lambda + y - z) \end{aligned} \tag{6.29}$$

We start with the standard fast-slow analysis assuming $\epsilon_2 = 1$. The critical manifold is

$$C_0 = \{(x, y, z) \in \mathbb{R}^3 | y = x^3 - 3x =: c(x)\}$$

The two fold curves are $L_\pm = \{(x, y, z) \in \mathbb{R}^3 | x = \pm 1, y = \mp 2\}$. This gives a decomposition of C^{Kop}:

$$C_0 = S^{a,-} \cup L_- \cup S^r \cup L_+ \cup S^{a,+}$$

where $S^{a,-} = C_0 \cap \{x < -1\}$, $S^r = C_0 \cap \{-1 < x < 1\}$ and $S^{a,+} = C_0 \cap \{1 < x\}$ are normally hyperbolic. Note that $S^{a,\pm}$ are attracting and S^r is repelling.

Figure 6.3 shows a region in parameter space near a singular Hopf bifurcation curve and some of the associated stable MMOs that can be detected by numerical integration. To understand the relation to the fast-slow structure and the MMOs we also show the singular bifurcation curves of folded saddle-nodes [104, 108] in Figure 6.3(a). The key observation from Figures 6.3(b)-(c) is that the tangency between the slow manifold S^r_ϵ and the unstable manifold manifold of the unique equilibrium $W^u(q)$ marks the boundary of the MMO regime in parameter space [52] i.e. the transition from small oscillations to MMOs.

The small-amplitude oscillations (SAOs) near the singular Hopf bifurcation are generated by the saddle-focus q as discussed in [52]. The key point is that

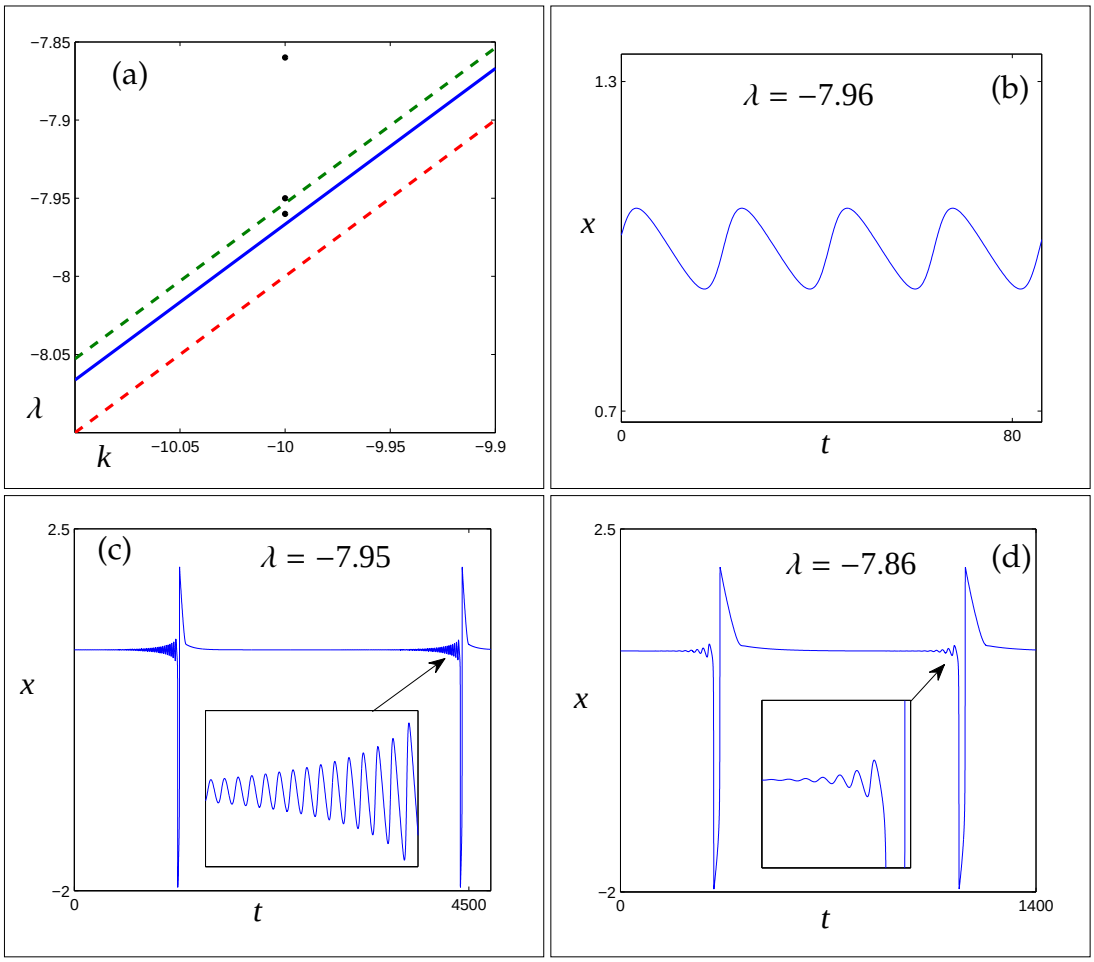

Figure 6.3: For all computations of the full system we have $\epsilon = 0.01$ and for all time series we fixed $k = -10$. (a) Parameter space showing curves of Hopf bifurcations (blue), folded saddle-nodes of type II (red) and tangencies between S^r_ϵ and $W^u(q)$ (green). Note that the distances between the curves are $O(\epsilon)$. The three black circles mark the parameter values for the time series in (b)-(d). (b) Small amplitude oscillation of the limit cycle generated in the Hopf bifurcation $\lambda = -7.96$. (c) MMO of type 1^s with a very large value of s near the tangency of invariant manifolds. (d) MMO of type 1^s with much smaller s.

the location of the tangency between the manifolds S^r_ϵ and $W^u(q)$ can be derived from the Lyapunov coefficient.

Conjecture 6.8.1. *Proposition 6.5.1 also applies for systems with more than one slow variable and the onset of MMOs can be calculated from the first Lyapunov coefficient at the Hopf bifurcation. For example, formula* (6.22) *- or a minor modification of it - is expected to hold.*

BIBLIOGRAPHY

[1] V.I. Arnold. *Encyclopedia of Mathematical Sciences: Dynamical Systems V*. Springer, 1994.

[2] D.G. Aronson and H.F. Weinberger. Nonlinear diffusion in population genetics, combustion, and nerve pulse propagation. *in: Partial Differential Equations and Related Topics (Lecture Notes in Mathematics)*, 446:5–49, 1974.

[3] U.M. Ascher, R.M.M. Mattheij, and R.D. Russell. *Numerical Solution of Boundary Value Problems for Ordinary Differential Equations*. SIAM, 1987.

[4] S.M. Baer and T. Erneux. Singular Hopf bifurcation to relaxation oscillations I. *SIAM J. Appl. Math.*, 46(5):721–739, 1986.

[5] S.M. Baer and T. Erneux. Singular Hopf bifurcation to relaxation oscillations II. *SIAM J. Appl. Math.*, 52(6):1651–1664, 1992.

[6] E. Benoit. Systems lents-rapides dans $\mathbb{R}^3$ et leurs canards. In *Third Snepfenried geometry conference*, volume 2, pages 159–191. Soc. Math. France, 1982.

[7] E. Benoit. Enlacements de canards. *C.R. Acad. Sc. Paris*, 300(8):225–230, 1985.

[8] E. Benoit, J.L. Callot, F. Diener, and M. Diener. Chasse au canards. *Collect. Math.*, 31:37–119, 1981.

[9] E. Benoit and C. Lobry. Les canards de $\mathbb{R}^3$. *C.R. Acad. Sc. Paris*, 294:483–488, 1982.

[10] J. Boissonade and P. DeKepper. Transitions from bistability to limit cycle oscillations. Theoretical analysis and experimental evidence in an open chemical system. *J. Phys. Chem.*, 84:501–506, 1980.

[11] K. Bold, C. Edwards, J. Guckenheimer, S. Guharay, K. Hoffman, Judith Hubbard, Ricardo Oliva, and Waren Weckesser. The forced van der pol equation 2: Canards in the reduced system. *SIAM Journal of Applied Dynamical Systems*, 2(4):570–608, 2003.

[12] R. Bowen. *Equilibrium states and the ergodic theory of Anosov diffeomorphisms*, volume 470 of *Lecture Notes in Mathematics*. Springer, 1975.

[13] B. Braaksma. Singular Hopf bifurcation in systems with fast and slow variables. *Journal of Nonlinear Science*, 8(5):457–490, 1998.

[14] P. Brunovsky. Tracking invariant manifolds without differential forms. *Acta Math. Univ. Comenianae*, LXV(1):23–32, 1996.

[15] G.A. Carpenter. A geometric approach to singular perturbation problems with applications to nerve impulse equations. *Journal of Differential Equations*, 23:335–367, 1977.

[16] J. Carr. *Applications of Centre Manifold Theory*. Springer, 1981.

[17] A.R. Champneys, V. Kirk, E. Knobloch, B.E. Oldeman, and J.D.M. Rademacher. Unfolding a tangent equilibrium-to-periodic heteroclinic cycle. *SIAM J. Appl. Dyn. Sys.*, 8(3):1261–1304, 2009.

[18] A.R. Champneys, V. Kirk, E. Knobloch, B.E. Oldeman, and J. Sneyd. When Shil'nikov meets Hopf in excitable systems. *SIAM J. Appl. Dyn. Syst.*, 6(4):663–693, 2007.

[19] S.-N. Chow, C. Li, and D. Wang. *Normal forms and bifurcation of planar vector fields*. CUP, 1994.

[20] E.A. Coddington and N. Levinson. *Theory of Ordinary Differential Equations*. McGraw-Hill, 1955.

[21] C. de Boor and B. Swartz. Collocation at Gaussian points. *SIAM J. Numer. Anal. 10*, 10:582–606, 1973.

[22] B. Deng. The existence of infinitely many traveling front and back waves in the fitzhugh-nagumo equations. *SIAM J. Appl. Math.*, 22(6):1631–1650, 1991.

[23] B. Van der Pol. A theory of the amplitude of free and forced triode vibrations. *Radio Review*, 1:701–710, 1920.

[24] B. Van der Pol. On relaxation oscillations. *Philosophical Magazine*, 7:978–992, 1926.

[25] B. Van der Pol. The nonlinear theory of electric oscillations. *Proc. IRE*, 22:1051–1086, 1934.

[26] M. Desroches, B. Krauskopf, and H.M. Osinga. Mixed-mode oscillations and slow manifolds in the self-coupled FitzHugh-Nagumo system. *Chaos*, 18, 2008.

[27] M. Desroches, B. Krauskopf, and H.M. Osinga. Numerical continuation of canard orbits in slow-fast dynamical systems. *Nonlinearity*, 23(3):739–765, 2010.

[28] F. Diener and M. Diener. *Nonstandard Analysis in Practice*. Springer, 1995.

[29] M. Diener. The canard unchained or how fast/slow dynamical systems bifurcate. *The Mathematical Intelligencer*, 6:38–48, 1984.

[30] E. Doedel, H.B. Keller, and J.-P. Kernevez. Numerical analysis and control of bifurcation problems. I. Bifurcation in finite dimensions. *Internat. J. Bifur. Chaos Appl. Sci. Engrg.*, 1(3):493–520, 1991.

[31] E. Doedel, H.B. Keller, and J.-P. Kernevez. Numerical analysis and control of bifurcation problems. II. Bifurcation in infinite dimensions. *Internat. J. Bifur. Chaos Appl. Sci. Engrg.*, 1(4):745–772, 1991.

[32] E.J. Doedel. Auto 97: Continuation and bifurcation software for ordinary differential equations. *http://indy.cs.concordia.ca/auto*, 1997.

[33] E.J. Doedel. Auto 2000: Continuation and bifurcation software for ordinary differential equations (with homcont). *http://cmvl.cs.concordia.ca/auto*, 2000.

[34] E.J. Doedel, A. Champneys, F. Dercole, T. Fairgrieve, Y. Kuznetsov, B. Oldeman, R. Paffenroth, B. Sandstede, X. Wang, and C. Zhang. Auto 2007p: Continuation and bifurcation software for ordinary differential equations (with homcont). *http://cmvl.cs.concordia.ca/auto*, 2007.

[35] F. Dumortier. Techniques in the theory of local bifurcations: Blow-up, normal forms, nilpotent bifurcations, singular perturbations. *in: Bifurcations and Periodic Orbits of Vector Fields [D. Schlomiuk (ed.)]*, pages 19–73, 1993.

[36] F. Dumortier and R. Roussarie. Canard cycles and center manifolds. *Memoirs of the American Mathematical Society*, 121(577), 1996.

[37] W. Eckhaus. Relaxation oscillations including a standard chase on french ducks. *Lecture Notes in Mathematics*, 985:449–494, 1983.

[38] J.W. Evans, N. Fenichel, and J.A. Feroe. Double impulse solutions in nerve axon equations. *SIAM J. Appl. Math.*, 42(2):219–234, 1982.

[39] N. Fenichel. Persistence and smoothness of invariant manifolds for flows. *Indiana University Mathematical Journal*, 21:193–225, 1971.

[40] N. Fenichel. Asymptotic stability with rate conditions. *Indiana University Mathematical Journal*, 23:1109–1137, 1974.

[41] N. Fenichel. Asymptotic stability with rate conditions II. *Indiana University Mathematical Journal*, 26:81–93, 1977.

[42] N. Fenichel. Geometric singular perturbation theory for ordinary differential equations. *Journal of Differential Equations*, 31:53–98, 1979.

[43] R. FitzHugh. Mathematical models of threshold phenomena in the nerve membrane. *Bull. Math. Biophysics*, 17:257–269, 1955.

[44] G. Flores. Stability analysis for the slow traveling pulse of the fitzhugh-nagumo system. *SIAM J. Math. Anal.*, 22(2):392–399, 1991.

[45] S.V. Gonchenko, D.V. Turaev, P. Gaspard, and G. Nicolis. Complexity in the bifurcation structure of homoclinic loops to a saddle-focus. *Nonlinearity*, 10:409–423, 1997.

[46] W. Govaerts and Yu.A. Kuznetsov. Matcont. *http://www.matcont.ugent.be/*, 2008.

[47] J. Grasman. *Asymptotic Methods for Relaxation Oscillations and Applications*. Springer, 1987.

[48] A. Griewank. ODE solving via automatic differentiation and rational prediction. In *Numerical analysis 1995 (Dundee, 1995) - Res. Notes Math. Ser., 344*, pages 36–56. Pitman, 1996.

[49] J. Guckenheimer. Bifurcation and degenerate decomposition in multiple time scale dynamical systems. *in: Nonlinear Dynamics and Chaos: Where do we go from here? Eds.: John Hogan, Alan Champneys and Bernd Krauskopf*, pages 1–20, 2002.

[50] J. Guckenheimer. Global bifurcations of periodic orbits in the forced van der pol equation. *in: Global Analysis of Dynamical Systems - Festschrift ded-*

icated to Floris Takens. Eds.: Henk W. Broer, Bernd Krauskopf and Gert Vegter, pages 1–16, 2003.

[51] J. Guckenheimer. Bifurcations of relaxation oscillations. *Normal forms, bifurcations and finiteness problems in differential equations, NATO Sci. Ser. II Math. Phys. Chem.*, 137:295–316, 2004.

[52] J. Guckenheimer. Singular Hopf bifurcation in systems with two slow variables. *SIAM J. Appl. Dyn. Syst.*, 7(4):1355–1377, 2008.

[53] J. Guckenheimer, K. Hoffman, and W. Weckesser. Numerical computation of canards. *Internat. J. Bifur. Chaos Appl. Sci. Engrg.*, 10(12):2669–2687, 2000.

[54] J. Guckenheimer and P. Holmes. *Nonlinear Oscillations, Dynamical Systems, and Bifurcations of Vector Fields*. Springer, 1983.

[55] J. Guckenheimer and C. Kuehn. Computing slow manifolds of saddle-type. *SIAM J. Appl. Dyn. Syst.*, 8(3):854–879, 2009.

[56] J. Guckenheimer and C. Kuehn. Homoclinic orbits of the FitzHugh-Nagumo equation: The singular limit. *DCDS-S*, 2(4):851–872, 2009.

[57] J. Guckenheimer and C. Kuehn. Homoclinic orbits of the FitzHugh-Nagumo equation: Bifurcations in the full system. *SIAM J. Appl. Dyn. Syst.*, 9:138–153, 2010.

[58] J. Guckenheimer and D. LaMar. Periodic orbit continuation in multiple time scale systems. In *Understanding Complex Systems: Numerical continuation methods for dynamical systems*, pages 253–267. Springer, 2007.

[59] J. Guckenheimer and B. Meloon. Computing periodic orbits and their bifurcations with automatic differentiation. *SIAM J. Sci. Comp.*, 22:951–985, 2000.

[60] John Guckenheimer, Kathleen Hoffman, and Warren Weckesser. The forced van der pol equation 1: The slow flow and its bifurcations. *SIAM Journal of Applied Dynamical Systems*, 2(1):1–35, 2003.

[61] E. Hairer and G. Wanner. *Solving Ordinary Differential Equations II*. Springer, 1991.

[62] S.P. Hastings. Some mathematical problems from neurobiology. *The American Mathematical Monthly*, 82(9):881–895, 1975.

[63] S.P. Hastings. On the existence of homoclinic and periodic orbits in the fitzhugh-nagumo equations. *Quart. J. Math. Oxford*, 2(27):123–134, 1976.

[64] M.W. Hirsch, C.C. Pugh, and M. Shub. *Invariant Manifolds*. Springer, 1977.

[65] A.L. Hodgin and A.F. Huxley. A quantitative description of membrane current and its application to conduction and excitation in nerve. *J. Physiol.*, 117:500–505, 1952.

[66] Waterloo Maple Inc. Maple 12. *http://www.maplesoft.com/*, 2008.

[67] J. Jalics, M. Krupa, and H.G. Rotstein. A novel canard-based mechanism for mixed-mode oscillations in a neuronal model. *preprint*, 2008.

[68] C. Jones and N. Kopell. Tracking invariant manifolds with differential forms in singularly perturbed systems. *Journal of Differential Equations*, pages 64–88, 1994.

[69] C. Jones, N. Kopell, and R. Langer. Construction of the FitzHugh-Nagumo pulse using differential forms. *in: Multiple-Time-Scale Dynamical Systems*, pages 101–113, 2001.

[70] C.K.R.T. Jones. Stability of the travelling wave solution of the fitzhugh-nagumo system. *Transactions of the American Mathematical Society*, 286(2):431–469, 1984.

[71] C.K.R.T. Jones. *Geometric Singular Perturbation Theory: in Dynamical Systems (Montecatini Terme, 1994)*. Springer, 1995.

[72] C.K.R.T. Jones, T.J. Kaper, and N. Kopell. Tracking invariant manifolds up tp exponentially small errors. *SIAM Journal of Mathematical Analysis*, 27(2):558–577, 1996.

[73] T.J. Kaper. An introduction to geometric methods and dynamical systems theory for singular perturbation problems. analyzing multiscale phenomena using singular perturbation methods. *Proc. Sympos. Appl. Math.*, 56:85–131, 1999.

[74] T.J. Kaper and C.K.R.T. Jones. A primer on the exchange lemma for fast-slow systems. *in: Multiple-Time-Scale Dynamical Systems*, IMA Vol. 122:65–88, 2001.

[75] J. Kevorkian and J.D. Cole. *Multiple Scale and Singular Perturbation Methods*. Springer, 1996.

[76] M.T.M. Koper. Bifurcations of mixed-mode oscillations in a three-variable autonomous Van der Pol-Duffing model with a cross-shaped phase diagram. *Physica D*, 80:72–94, 1995.

[77] B. Krauskopf, H.M. Osinga, E.J. Doedel, M.E. Henderson, J. Guckenheimer, A. Vladimirsky, M. Dellnitz, and O. Junge. A survey of methods for computing (un)stable manifolds of vector fields. *Int. J. Bifurcation and Chaos*, 15(3):763–791, 2005.

[78] B. Krauskopf and T. Riess. A Lin's method approach to finding and continuing heteroclinic connections involving periodic orbits. *Nonlinearity*, 21(8):1655–1690, 2008.

[79] T. Krogh-Madsen, L. Glass, E. Doedel, and M. Guevara. Apparent discontinuities in the phase-setting response of cardiac pacemakers. *J. Theor. Biol.*, 230:499–519, 2004.

[80] M. Krupa, N. Popovic, and N. Kopell. Mixed-mode oscillations in three time-scale systems: A prototypical example. *SIAM J. Applied Dynamical Systems*, 7(2), 2008.

[81] M. Krupa, N. Popovic, N. Kopell, and H.G. Rotstein. Mixed-mode oscillations in a three time-scale model for the dopaminergic neuron. *Chaos*, 18, 2008.

[82] M. Krupa, B. Sandstede, and P. Szmolyan. Fast and slow waves in the FitzHugh-Nagumo equation. *Journal of Differential Equations*, 133:49–97, 1997.

[83] M. Krupa and P. Szmolyan. Extending geometric singular perturbation theory to nonhyperbolic points - fold and canard points in two dimensions. *SIAM J. Math. Anal.*, 33(2):286–314, 2001.

[84] M. Krupa and P. Szmolyan. Extending slow manifolds near transcritical and pitchfork singularities. *Nonlinearity*, 14:1473–1491, 2001.

[85] M. Krupa and P. Szmolyan. Geometric analysis of the singularly perturbed fold. *in: Multiple-Time-Scale Dynamical Systems*, IMA Vol. 122:89–116, 2001.

[86] M. Krupa and P. Szmolyan. Relaxation oscillation and canard explosion. *Journal of Differential Equations*, 174:312–368, 2001.

[87] C. Kuehn. From first Lyapunov coefficients to maximal canards. *Int. J. Bif. and Chaos*, to appear, 2010.

[88] Yu.A. Kuznetsov. *Elements of Applied Bifurcation Theory - 3^{rd} edition*. Springer, 2004.

[89] P.A. Lagerstrom. *Matched Asymptotic Expansions: Ideas and Techniques*. Springer, 1988.

[90] E. Lee and D. Terman. Uniqueness and stability of periodic bursting solutions. *J. Differential Equations*, 158:48–78, 1999.

[91] H.P. McKean. Nagumo's equation. *Adv. in Math.*, 4:209–223, 1970.

[92] A. Milik and P. Szmolyan. Multiple time scales and canards in a chemical oscillator. *in: Multiple-Time-Scale Dynamical Systems, Eds.: C.K.R.T. Jones and A.I. Khibnik*, 2001.

[93] E.F. Mishchenko and N.Kh. Rozov. *Differential Equations with Small Parameters and Relaxation Oscillations (translated from Russian)*. Plenum Press, 1980.

[94] J. Nagumo, S. Arimoto, and S. Yoshizawa. An active pulse transmission line simulating nerve axon. *Proc. IRE*, 50:2061–2070, 1962.

[95] K.J. Palmer. Exponential dichotomies and transversal homoclinic points. *J. Differential Equations*, 55:225–256, 1984.

[96] L. Perko. *Differential Equations and Dynamical Systems*. Springer, 2001.

[97] C. Rocsoreanu, A. Georgescu, and N. Giurgiteanu. *The FitzHugh-Nagumo Model - Bifurcation and Dynamics*. Kluwer, 2000.

[98] H.G. Rotstein, M. Wechselberger, and N. Kopell. Canard induced mixed-mode oscillations in a medial entorhinal cortex layer ii stellate cell model. *SIAM J. Applied Dynamical Systems*, 7(4):1582–1611, 2008.

[99] J. Rubin and M. Wechselberger. The selection of mixed-mode oscillations in a hodgin-huxley model with multiple timescales. *Chaos*, 18, 2008.

[100] L.F. Shampine and M.W. Reichelt. The matlab ode suite. *SIAM Jour. Sci. Comp.*, 18(1):1–22, 1997.

[101] L.F. Shampine, M.W. Reichelt, and J. Kierzenka. Solving boundary value problems for ordinary differential equations in MATLAB with bvp4c. *http://www.mathworks.com/bvp_tutorial*, page 27pp., 2000.

[102] L.P. Shilnikov. A case of the existence of a denumerable set of periodic motions. *Sov. Math. Dokl.*, 6:163–166, 1965.

[103] P. Szmolyan. Transversal heteroclinic and homoclinic orbits in singular perturbation problems. *Journal of Differential Equations*, 92:252–281, 1991.

[104] P. Szmolyan and M. Wechselberger. Canards in $\mathbb{R}^3$. *Journal of Differential Equations*, 177:419–453, 2001.

[105] D. Terman. Chaotic spikes arising from a model of bursting in excitable membranes. *SIAM J. Appl. Math.*, 51(5):1418–1450, 1991.

[106] A.N. Tihonov, A.B. Vasil'eva, and A.G. Sveshnikov. *Differential Equations*. Springer Series in Soviet Mathematics. Springer, 1985.

[107] A.B. Vasil'eva. Asymptotic behaviour of solutions of certain problems for ordinary non-linear differential equations with a small parameter multiplying the highest derivatives (in russian). *Russian Mathematical Surveys. Uspehi Mat. Nauk.*, 18:13–84, 1963.

[108] M. Wechselberger. Existence and bifurcation of canards in $\mathbb{R}^3$ in the case of a folded node. *SIAM J. Applied Dynamical Systems*, 4(1):101–139, 2005.